AD-A152 115 THE NONLINEAR ANALYSIS OF THICK COMPOSITE PLATES USING A CUBIC SPLINE FUNCTION(U) AIR FORCE INST OF TECH WRIGHT-PATTERSON AFB OH SCHOOL OF ENGI.. 1/2

UNCLASSIFIED R L HINRICHSEN SEP 84 AFIT/DS/AE/84-2 F/G 12/1 NL

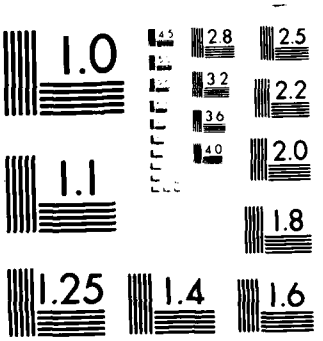

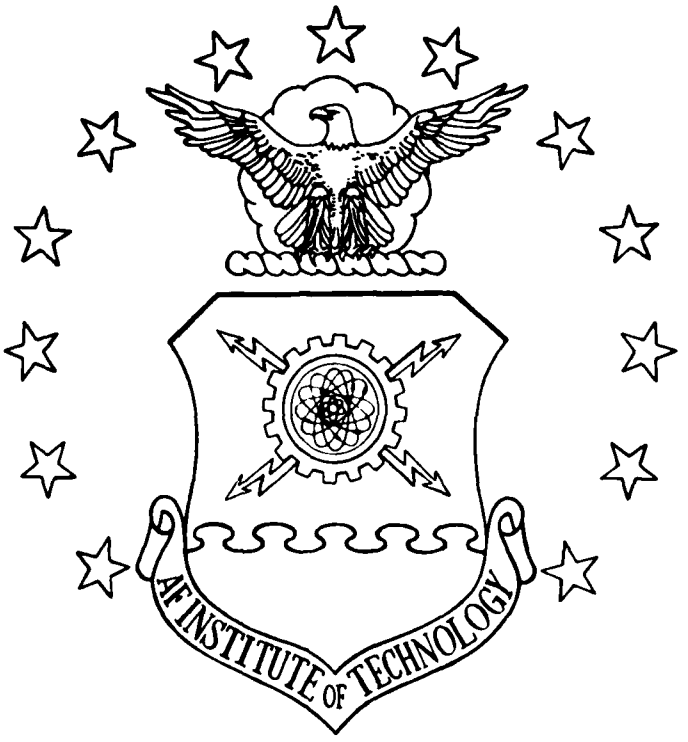

THE NONLINEAR ANALYSIS OF THICK COMPOSITE PLATES USING A CUBIC SPLINE FUNCTION

DISSERTATION

DEPARTMENT OF THE AIR FORCE
AIR UNIVERSITY
AIR FORCE INSTITUTE OF TECHNOLOGY

Wright-Patterson Air Force Base, Ohio

AFIT/DS/AE/84-2

THE NONLINEAR ANALYSIS OF THICK COMPOSITE PLATES USING A CUBIC SPLINE FUNCTION

DISSERTATION

AFIT/DS/AE/84-2 Ronald L. Hinrichsen

Captain USAF

AFIT/DS/AE/84-2

THE NONLINEAR ANALYSIS OF THICK COMPOSITE PLATES USING A CUBIC SPLINE FUNCTION

DISSERTATION

Presented to the faculty of the
School of Engineering of the Air
Force Institute of Technology in
Partial Fulfillment of the Requirements
For the Degree of Doctor of Philosophy

by

Ronald L. Hinrichsen, M.S.
Captain USAF

AFIT/DS/AE/84-2

THE NONLINEAR ANALYSIS OF

THICK COMPOSITE PLATES USING

A CUBIC SPLINE FUNCTION

by

Ronald L. Hinrichsen, B.S., M.S.

Capt USAF

A-1

Approved:

Anthony N. Palazotto 31 Aug 84

CHAIRMAN

Peter J. Torvik 31 Aug 84

Narendra S. Khot 31 Aug 84

V. B. Venkayya 31 AUG 84

John Jones Jr. 31 Aug 84

George K. Haritos 31 Aug 84

Accepted:

[signature] 12 Sep 84

for Dean, School of Engineering

CONTENTS

	PAGE
Acknowledgements	iv
List of Figures	v
List of Symbols	vii
Abstract	xii
I Introduction	1
Background	1
Problem Statement	7
II Theory	9
General Shell Equations	9
Cubic Spline Formulation	22
Finite Element Application	34
III The Finite Element Analysis Program	47
IV Applicability and Range	55
V Conclusions	112
Bibliography	117
Appendix I: Lagrangian Strain Equations	122
Appendix II: The Operator Matrix [L]	128
Appendix III: Computer Considerations	136
Vita	141

ACKNOWLEDGEMENTS

I would like to express my gratitude to Professor A.N. Palazotto for his patience, technical guidance, and encouragement during the course of this study. Thanks to the members of my committee for their patience.

My most sincere gratitude is extended to my wife and family for their love and support, without which this study could have been neither undertaken nor completed.

Ronald L. Hinrichsen

LIST OF FIGURES

Figure		Page
1.	Displacement Field	11
1a.	Deformation Terms and Geometry	12
2.	Typical Lamina Lay-up	24
3.	Two-ply Laminated Plate	29
4.	Isoparametric Quadrilateral Element	37
5.	Fiber Oriented Reference System	43
6.	Element Integration Points	54
7.	Plate Strip Problem	56
8.	Finite Element Models of Plate Strip Problem	59
9.	Convergence of 3-node Elements--Isotropic Plate.	61
10.	Convergence of 4-node Elements--Isotropic Plate.	63
11.	Convergence of 8-node Elements--Isotropic Plate.	65
12.	Multiplication Factor for G13 and G23--Isotropic	70
13.	Check of Kirchhoff's Hypothesis--Isotropic Plate	71
14.	Convergence of 3-node Elements--Orthotropic Plate.	73
15.	Convergence of 4-node Elements--Orthotropic Plate.	74
16.	Convergence of 8-node Elements--Orthotropic Plate.	75
17.	Check of Kirchhoff's Hypothesis--Orthotropic Plate	78
18.	Visualization of the Thickness Parameter S	80
19.	S vs $\bar{w}$--Fiber Orientation (0,0)	81
20.	S vs $\bar{w}$--Fiber Orientation (0,90)	82
21.	S vs $\bar{w}$--Fiber Orientation (0,90,0)	83
22.	$\bar{u}$ vs $\bar{z}$--Fiber Orientation (0,90)--(S=4)	85
23.	$\bar{u}$ vs $\bar{z}$--Fiber Orientation (0,90,0)--(S=10)	86

24. $\bar{u}$ vs $\bar{z}$--Fiber Orientation (0,90,0)--(S=4). 87

25. ($\bar{\tau}_{xz}$ vs $\bar{z}$--Fiber Orientation (0,0)--(S=4) 89

26. ($\bar{\tau}_{xz}$) vs $\bar{z}$--Fiber Orientation (0,90)--(S=4) . . . 90

27. ($\bar{\tau}_{xz}$) vs $\bar{z}$--Fiber Orientation (0,90,0)--(S=10) . 91

28. ($\bar{\tau}_{xz}$) vs $\bar{z}$--Fiber Orientation (0,90,0)--(S=4) . . 92

29. ($\bar{\sigma}_x$) vs $\bar{z}$--Fiber Orientation (0,0)--(S=10) . . . 94

30. ($\bar{\sigma}_x$) vs $\bar{z}$--Fiber Orientation (0,0)--(S=4) 95

31. ($\bar{\sigma}_x$) vs $\bar{z}$--Fiber Orientation (0,90)--(S=4) . . . 96

32. ($\bar{\sigma}_x$) vs $\bar{z}$--Fiber Orientation (0,90,0)--(S=10) . . 97

33. ($\bar{\sigma}_x$) vs $\bar{z}$--Fiber Orientation (0,90,0)--(S=4) . . 98

34. Square Orthotropic Plate Finite Element Model . . 99

35. $\bar{w}$ vs S--Square Plate (0,90,90,0) 101

36. $\bar{Q}$ vs $\bar{w}$--Nonlinear Plate Strip Problems 102

37. ($\bar{\sigma}_x$) vs $\bar{z}$ Nonlinear Plate Strip Problem (0,90) . 105

38. ($\bar{\tau}_{xz}$) vs $\bar{z}$ Nonlinear Plate Strip Problem (0,90) . 106

39. $\bar{Q}$ vs $\bar{w}$--Nonlinear Square Orthotropic Plate 107

40. ($\bar{\tau}_{yz}$) vs $\bar{z}$ Nonlinear Square Orthotropic Plate . . 109

41. ($\bar{\tau}_{xz}$) vs $\bar{z}$ Nonlinear Square Orthotropic Plate . . 110

42. 8-noded Finite Element 137

LIST OF SYMBOLS

$\vec{A}_i$	base vectors in undeformed space
$\vec{A}_i^*$	base vectors in deformed space
A_{ij}	metric tensor in undeformed space
A^*_{ij}	metric tensor in deformed space
a	distance measure in-plane
a_i	magnitudes of surface base vectors
$\vec{a}_i$	surface base vectors in undeformed surface
$\langle a \rangle$	nodal degree of freedom vector
$\langle \dot{a} \rangle$	velocity of nodal degree of freedom vector
$\langle \ddot{a} \rangle$	acceleration of nodal degree of freedom vector
$\langle B \rangle$	generalized body force vector
[B]	coefficient matrtix multiplying $\langle \phi \rangle$
$\langle b \rangle$	body force vector
[C]	coefficient matrix in spline theory [A] [B]
C_{ij}	indicial notation for [C]
[D]	constitutive matrix
$[D_l]$	constitutive matrix in fiber coordinate system
$[D_g]$	constitutive matrix in global coordinate system
D_{ij}	indicial notation for [D]
E	Young's modulus for isotropic material
E_1	longitudinal Young's modulus for orthotropic material
E_2	transverse Young's modulus for orthotropic material
$\vec{e}_i$	unit vectors in undeformed space
$\langle e \rangle$	engineering strain vector
F_u	generalized force components in the u-direction

F_{ℓ_i}	generalized force componentsin the ℓ_i -direction
FEM	finite element method
⟨F⟩	generalized surface force vector
f_u	force acting in the u-direction
⟨f⟩	surface force vector
G12	shear modulus
G23	shear modulus
[G]	constitutive matrix
H_{ij}	cubic spline shape functions
h	plate thickness
h_i	magnitudes of base vectors in undeformed space
J	Jacobian determinant
K_{ij}	indicial notation for [K]
[K]	stiffness matrix
[L]	operator matrix relating ⟨e⟩ and ⟨u⟩
[L0]	linear part of [L] (no u dependance)
[L1]	nonlinear part of [L] containing u terms
[L2]	nonlinear part of [L] containing u terms
M	number of layers in a plate
[M]	mass matrix
N_k	isoparametric shape function for the kth node
[N]	shape function matrix
n	number of nodes in an element
p(x)	loading function
p_0	magnitude of loading function
Qr,s,t	Gauss-Legendre quadrature weights

R_1	radius of curvature in the 1-direction
R_2	radius of curvature in the 2-direction
S	thickness parameter h/a
$\langle S \rangle$	2nd Piola-Kirchhoff Stress vector
$s(z)_j$	spline approximation in the jth lamina
T	kinetic energy
[T]	transformation matrix
t_j	thickness of jth layer
$\hat{t}$	time
u	displacements u
u_i	components of the displacement vector $\vec{u}$
$\tilde{u}_i$	components of the displacement vector $\vec{\tilde{u}}$
$\hat{u}_i$	components of the displacement vector $\vec{\hat{u}}$
$\vec{u}$	total displacement vector
$\vec{\tilde{u}}$	displacement vector of the reference surface
$\vec{\hat{u}}$	displacement vector through-the-thickness
$\bar{u}$	nondimensional u
$\langle u \rangle$	displacement vector
$\langle \dot{u} \rangle$	velocity vector
V	strain energy
v	displacement u_2
W	external work term
w	displacement u_3
w	nondimensional w
x	equivalent to y_1
y	equivalent to y_2

y_j	components of y
$\bar{y}$	position vector of a point in undeformed space
z	equivalent to y_3
z_j	z coordinate at the jth interface
$\bar{z}$	nondimensional z
α	angle of fiber orientation
$[B]$	$[L][N]$
δ	first variation
δ_{ij}	Kronecker's delta
Γ	surface over which integration takes place
$[\rho]$	mass density matrix
ν	Poisson's ratio for isotropic material
ν_{12}	Poisson's ratio for orthotropic material
λ_j	$t_{j+1}/(t_j+t_{j+1})$
μ_j	$1-\lambda_j$
ϕ_j	$\frac{\partial \hat{v}}{\partial z}$ evaluated at jth interface
$\langle\phi\rangle$	vector of interlaminar rotations
ϕ_{ki}	$\frac{\partial \hat{u}}{\partial z}$ evaluated at kth node ith interface
θ_{ki}	$\frac{\partial \hat{v}}{\partial z}$ evaluated at kth node ith interface
ξ	isoparametric element coordinate
η	isoparametric element coordinate
τ_{xz}	shear stress
$\bar{\tau}_{xz}$	nondimensional shear stress
σ_x	direct stress
$\bar{\sigma}_x$	nondimensional direct stress
ξ_r, η_s, γ_t	Gauss-Legendre quadrature points

ϵ_z	direct strain
ϵ_{xz}	shear strain

ABSTRACT

A non-linear thick composite shell theory is presented in which the through-the-thickness displacements are modelled using a variation of a cubic spline. The theory is developed by considering the Lagrangian strains in conjunction with the 2nd Piola-Kirchhoff stress. This formulation leads to a theory which encompasses large displacements with moderately large rotations but is restricted to small strains. The imposition of the cubic distribution through-the-thickness insures that the compatability of the displacements and their first and second derivatives and thus the shear strains are maintained from lamina to lamina. The cubic distribution is seen as a higher order approximation than has been previously employed, but because of the nature of the spline, the theory is less cumbersome and more easily implemented than the parabolic theory. In addition, there is no introduction of additional degrees of freedom with the cubic theory. A family of 2-D isoparametric elements is employed in conjunction with the theory to solve a class of 3-D thick plate problems. Results are presented showing comparisons which are in good agreement with previous work.

CHAPTER I

INTRODUCTION

BACKGROUND:

In the last fifteen to twenty years, composites, especially fiber reinforced laminates have found increasing application in aerospace structures, pressure and underwater vessels, and nuclear reactor structures. The advent of advanced fiber-reinforced composite materials has been called "the biggest technical revolution since the jet engine" (1) and has led to increasing use of laminated plates and shells.

Fiber-reinforced composites such as boron-epoxy and graphite-epoxy possess a number of desirable features. Two are their high stiffness to weight ratios and their anisotropic nature. These traits when exploited by the designer provide the means for constructing weight efficient, strong structures which respond to loads in a manner unlike isotropic materials. A good example of such an application is the forward swept wing fighter currently in the development stage. The inherent wing divergence problem of such a design is controlled by the judicious lay-up of composite laminae.

In order that full advantage be taken of these desirable traits , it is necessary to optimize the design. This optimization process requires the use of valid theories to predict structural response to a variety of load conditions.

Many of the early theories pertaining to the analysis of laminated plates and shells were based on the classical Kirchhoff hypothesis and are well established in the literature (2-6). Exact elasticity solutions for some particular plate bending problems have been obtained by Pagano (7-9) and Srinivas and Rao (10). Comparisons of results obtained from the classical theory with the exact elasticity solutions indicate the necessity of considering transverse shear deformations in the analyses of laminated structures.(11) This necessity is implied because the distortion of the deformed normal due to transverse shear strain is dependent, not only on the laminate thickness, but also on the orientation and degree of orthotropy of the individual layers (11).

One of the earliest attempts to include the shear strain effects for anisotropic laminated plates was made by Ambartsumyan (12). He assumed that the thickness shear stress was distributed as a single continuous parabolic function through the entire laminate , just as in a homogeneous shell. It was shown by Hsu and Wang (13) that

Ambartsumyan's assumption was not valid for a laminated shell (since it does not permit satisfaction of interlaminar compatibility) unless the in-plane Poisson's ratios are identical in all of the layers. Yang, Norris and Stavsky also developed a theory for heterogeneous plates (14) in which they assumed that the in-plane displacements varied linearly with the thickness coordinate. They had to use correction factors to satisfy the boundary conditions. Whitney applied the work of Ambartsumyan and Yang to specific laminated plate problems (15-17). He also presented a theory for the analysis of cylindrical shells which included both transverse shear and transverse normal strain (18). The model used was a direct extension of the Hildebrand et.al. theory (19,20) for homogeneous isotropic shells. Further extension of the Hildebrand theory was performed by Lo et.al. (21,22). In the Lo theory, in-plane and transverse displacements were assumed to be cubic and quadratic functions, respectively, of the through-the-thickness coordinate.

The next logical step following the work of Yang, Norris, and Stavsky, was to assume that the displacements varied linearly within each layer of the laminate. Such work was performed by Grot (23) and by Srinivas (24). An approach similar to that developed by Srinivas was used by Epstein to formulate the equations for the nonlinear anal-

ysis of multilayered shells (25).

The finite element method of analysis for laminated plate bending problems was presented by Pryor et.al. (26). This formulation assumed a uniform shear strain angle through the thickness of the plate and neglected local effects such as the state of stress and deformation at the layer interfaces. Perhaps the first attempt at considering these local effects was undertaken by Mawenya et.al. (26), wherein Ahmad's superparametric quadratic shell element (27) was used with independent normal rotations within each layer.

Panda et.al. (28) combined the ideas of Pryor and Mawenya by again using the Ahmad element as did Mawenya but maintaining a uniform shear strain angle as did Pryor. They later applied their theory to shell structures (29), using a doubly curved Ahmad element.

With the exception of Epstein's (25) work, each of the preceding developments was for small displacement linear theory. The work done by Witt (30) appears to have been the first attempt at satisfying the continuity of strains at layer boundaries while using a nonlinear large displacement theory. He assumed that the normal rotations varied linearly within each layer. Thus, the displacements varied quadratically. This was a direct extension of the work by

Mawenya (26), but employed a simpler triangular element and a fully nonlinear formulation.

In more recent years a number of investigators have studied various methods of including the transverse shear strain effects. Pack and Mandel (31) employed a concept whereby they derived a "connector" element which essentially linked 2-D elements in an attempt to effectively model a 3-D structure. Owen and Figueiras (32) employed a degenerate 9-noded 3-D continuum element (27) in which they assumed a constant transverse shear strain. A correction shear factor derived in cylindrical bending was used to approximate the real shear strain energy component.

The extension of Panda's work to the nonlinear theory was performed by Chang et.al. (33). He used the doubly curved Ahmad element in conjunction with the updated Lagrangian description of the virtual work equation.

The use of the so-called hybrid or mixed finite element method has been explored by a number of researchers. These applications range from linear plate theory (34-38) to non-linear shell theory employed by Noor et.al.(39). Noor has extended his work to collapse anlysis of shells (40).

During the course of this work, a number of other

authors have published papers relevant to the area of research. Reddy and Creamer's (41) work was an analytical approximation approach in which they expanded the in-plane displacements as cubic functions of the thickness coordinate and assumed the transverse deflections to be quadratic through the thickness. Solutions to the simply supported flat plate equations were obtained using Navier's method.

Epstein and Glockner (42) specialized their previous work (25) to a linear analysis of deep and multilayered beams--solving the problem using a finite difference method. Epstein and Huttelmaier (43) further specialized the Epstein theory to thick multilayered plates. In this work they employed a 4-noded isoparametric finite element to solve a linear plate bending problem.

The use of 3-D elements to model each individual lamina has been done for a number of years. The most recent works have been those of Lee (44) and Kuppusamy and Reddy (45). In these works, the 8-noded trilinear elements were used for linear as well as nonlinear analyses. The use of these elements is restricted to a class of small problems due to the large number of degrees of freedom needed to effectively model a multilayered plate.

PROBLEM STATEMENT:

In the present investigation, a family of finite elements is constructed which accounts for the following features: (most of which have not been effectively combined in previous works)

1. Nonlinear geometrical effects related to large displacements and moderately large rotations.
2. Variations of transverse shear strain through the thickness.
3. Heterogeneity through the thickness.

The transverse shear strain effects are included by assuming that there is a linear distribution of transverse curvature of each lamina, thus implying a parabolic distribution for the slope and a cubic distribution for displacements through the thickness. This choice of function is a natural extension of the previous work (in particular that of Witt).

The study is limited to a flat plate having individual laminae of equal thickness but varying material properties and fiber orientations.

The derivations that lead to the finite element stiffness formulation are discussed in Chapter II. A computer program based upon the results for a flat plate is discussed in Chapter III. The results for several problems investigating the applicability and range of the elements are discussed in Chapter IV. A number of conclusions are presented in Chapter IV as well. These conclusions are reviewed and additional conclusions are presented in Chapter V.

CHAPTER II

THEORY

GENERAL SHELL EQUATIONS:

In this section, the objective is to present the development of the general shell equations from a kinematic viewpoint, lay out the technique used to maintain strain continuity at the interlaminar boundaries, and cast the theory in finite element terms.

The derivations of the general shell equations from the Lagrangian standpoint is a straight-forward process which has been carried out in a number of previous works (for example Saada (46)) but is presented here for completeness. Also, the assumptions which are made in the derivation differ from those of Saada in that a line element which is normal to the shell reference surface is not allowed to vary in length. The equations which are finally presented will permit analysis of a class of problems which are characterized by large displacements, moderately large rotations, and small strains. One of the main reasons for choosing the Lagrangian strain for this work was that the material properties could be referenced to the undeformed configuration and not varied in the analysis. Material

nonlinearity is not considered in this work, but could be easily employed in future work.

Referring to Fig. 1, consider the displacement field defined by:

$$\vec{u} = \vec{z} - \vec{y} \tag{1}$$

and the base vectors in the undeformed space as:

$$\vec{A}_i = \frac{\partial \vec{y}}{\partial y_i} \tag{2}$$

The base vectors for the deformed space are given by:

$$\vec{A}_i^* = \frac{\partial \vec{z}}{\partial y_i} = \left(\vec{A}_i + \frac{\partial \vec{u}}{\partial y_i}\right) \tag{3}$$

The metrics for the two spaces become:

$$A_{ij} = \vec{A}_i \cdot \vec{A}_j \tag{4}$$

for the undeformed and

$$A_{ij}^* = \vec{A}_i^* \cdot \vec{A}_j^* \tag{5}$$

for the deformed space.

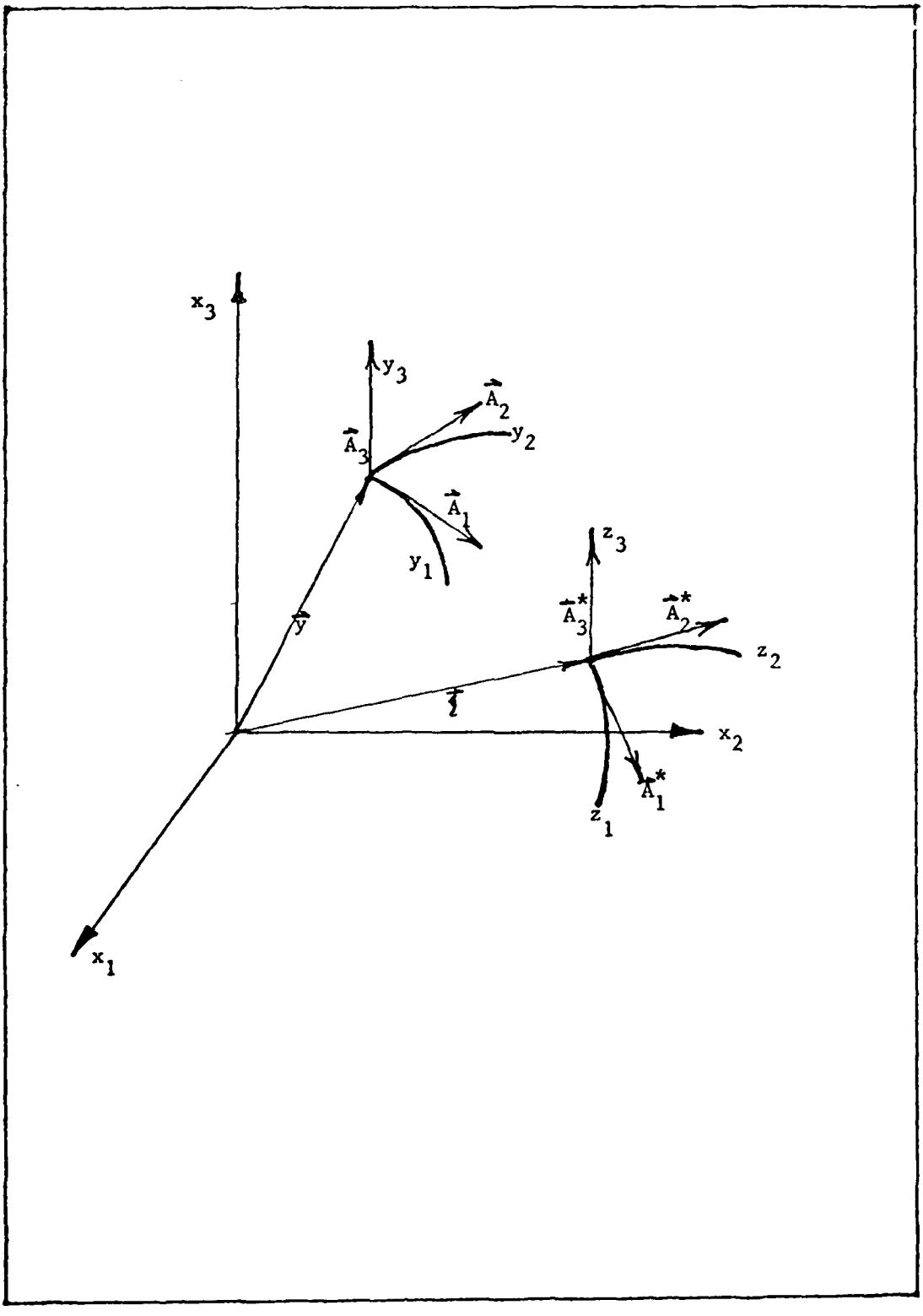

Fig. 1 Displacement Field

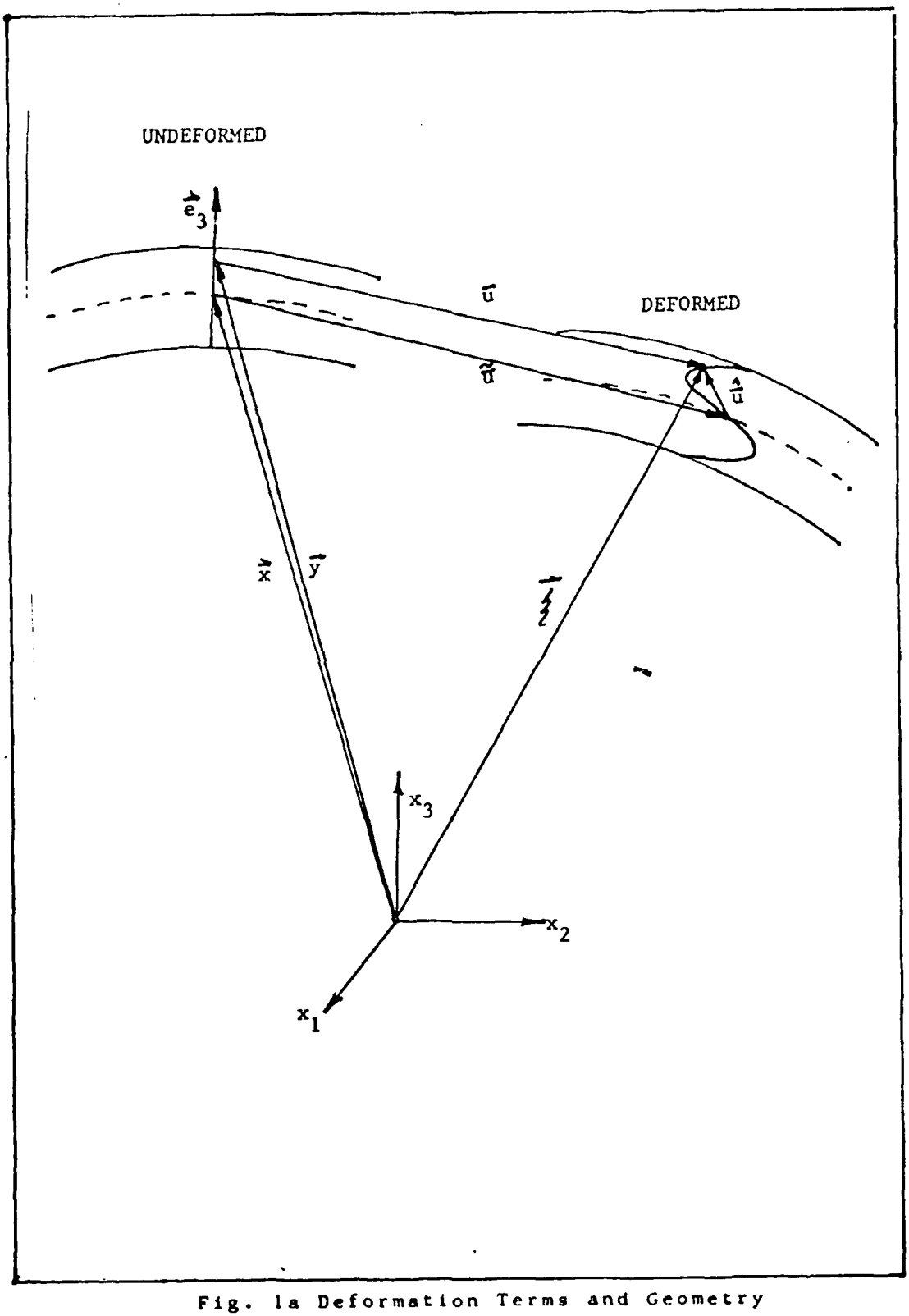

Fig. 1a Deformation Terms and Geometry

The definition of the Lagrangian strain tensor, γ_{ij}, (which is a strain measure with reference to the undeformed configuration) is given by Saada (46) as:

$$2\gamma_{ij} = A^{*}_{ij} - A_{ij} \tag{6}$$

With proper substitution of the metric tensor and simple algebraic manipulation, one obtains the expression

$$2\gamma_{ij} = \vec{A}_i \cdot \frac{\partial \vec{u}}{\partial y_j} + \vec{A}_j \cdot \frac{\partial \vec{u}}{\partial y_i} + \frac{\partial \vec{u}}{\partial y_i} \cdot \frac{\partial \vec{u}}{\partial y_j} \tag{7}$$

The unit vectors written in terms of base vectors are: (no summation)

$$\vec{e}_i = \frac{\vec{A}_i}{|\vec{A}_i|} = \frac{\vec{A}_i}{\sqrt{A_{ii}}} = \frac{\vec{A}_i}{h_i} \tag{8}$$

thus (adopting a summation convention)

$$\vec{A}_i = h_i \vec{e}_i \tag{9}$$

The displacement vector written in terms of these unit vectors becomes

$$\vec{u} = u_i \vec{e}_i \tag{10}$$

Substitution of (9) and (10) into the definition of the Lagrangian strain (7) yields

$$2\gamma_{ij} = h_i \vec{e}_i \cdot \frac{\partial}{\partial y_j}(u_k \vec{e}_k) + h_j \vec{e}_j \cdot \frac{\partial}{\partial y_i}(u_\ell \vec{e}_\ell) + \frac{\partial}{\partial y_i}(u_m \vec{e}_m) \cdot \frac{\partial}{\partial y_j}(u_n \vec{e}_n) \tag{11}$$

From the study of the theory of surfaces, one sees that any point on a shell can be located by means of three parameters, two of which vary along a reference surface while the third varies along the reference surface normal. The lines of curvature of the reference surface are chosen as parametric curves. These lines together with the normal form an orthogonal system of reference. An arbitrary point in the shell is located by means of the position vector

$$\vec{y}(y_1, y_2, y_3) = \vec{x}(y_1, y_2) + y_3 \vec{e}_3(y_1, y_2) \tag{12}$$

where $\vec{x}$ is the position vector of a corresponding point on the reference surface and y_3 is the distance of the arbitrary point from the reference surface measured along the unit normal, $\vec{e}_3$. (See Fig 1a.) The magnitude of an element of length is given by:

$$ds = (d\vec{y} \cdot d\vec{y})^{1/2} \tag{13}$$

Following manipulation $d\vec{y}$ is written as:

$$d\vec{y} = a_1\vec{e}_1 dy_1 + a_2\vec{e}_2 dy_2 + y_3\frac{\partial \vec{e}_3}{\partial y_1} dy_1 + y_3\frac{\partial \vec{e}_3}{\partial y_2} dy_2 + \vec{e}_3 dy_3 \quad (14)$$

where $a_\alpha \vec{e}_\alpha = \vec{a}_\alpha = \vec{X}_{,\alpha}$ (the base vectors for the ref. surface)

From Saada (46), one sees that the derivatives of the unit vectors are:

$$\frac{\partial \vec{e}_1}{\partial y_1} = -\frac{a_1}{R_1}\vec{e}_3 - \frac{a_{1,2}}{a_2}\vec{e}_2 \quad (15)$$

$$\frac{\partial \vec{e}_1}{\partial y_2} = \frac{a_{2,1}}{a_1}\vec{e}_2 \quad (16)$$

$$\frac{\partial \vec{e}_2}{\partial y_1} = \frac{a_{1,2}}{a_2}\vec{e}_1 \quad (17)$$

$$\frac{\partial \vec{e}_2}{\partial y_2} = -\frac{a_2}{R_2}\vec{e}_3 - \frac{a_{2,1}}{a_1}\vec{e}_1 \quad (18)$$

$$\frac{\partial \vec{e}_3}{\partial y_1} = \frac{a_1}{R_1}\vec{e}_1 \quad (19)$$

$$\frac{\partial \vec{e}_3}{\partial y_2} = \frac{a_2}{R_2}\vec{e}_2 \quad (20)$$

Where R_1 and R_2 represent the principal radii of curvature and derivatives with respect to y_3 are assumed to be zero.

Substitution of the appropriate derivatives into eqn. (14) gives:

$$d\vec{y} = \left(a_1 dy_1 + y_3 \frac{a_1}{R_1} dy_1\right)\vec{e}_1 + \left(a_2 dy_2 + y_3 \frac{a_2}{R_2} dy_2\right)\vec{e}_2 + dy_3 \vec{e}_3 \quad (21)$$

so that

$$ds^2 = a_1^2 (1 + y_3/R_1)^2 dy_1^2 + a_2^2 (1 + y_3/R_2)^2 dy_2^2 + dy_3^2 \quad (22)$$

Since by definition (Saada (46)):

$$ds^2 = h_1^2 dy_1^2 + h_2^2 dy_2^2 + h_3^2 dy_3^2 \quad (23)$$

it is seen that

$$h_1 = a_1 (1 + y_3/R_1) \quad (24)$$

$$h_2 = a_2 (1 + y_3/R_2) \quad (25)$$

$$h_3 = 1 \quad (26)$$

Substitution of (24-26) and (15-20) into the definition for Lagrangian strain yields expressions for γ_{ij}. The full derivation is given in Appendix I.

The displacement vector is divided into two parts, (see Fig. 1a) one part is $\tilde{\bar{u}}$; a function only of the surface coordinates and associated with the deformation of the reference surface. The other part is $\hat{\bar{u}}$; a function of all three coordinates and associated with the deformation through the thickness. The components of $\bar{u}$ are written as:(30)

$$u_1 = \tilde{u}_1(y_1,y_2) + \hat{u}_1(y_1,y_2,y_3) \tag{27}$$

$$u_2 = \tilde{u}_2(y_1,y_2) + \hat{u}_2(y_1,y_2,y_3) \tag{28}$$

$$u_3 = \tilde{u}_3(y_1,y_2) \tag{29}$$

so that

$$\begin{aligned}\gamma_{11} = {} & a_1(1+y_3/R_1)\left[(\tilde{u}_1+\hat{u}_1)_{,1} + (\tilde{u}_2+\hat{u}_2)\frac{a_{1,2}}{a_2} + u_3\frac{a_1}{R_1}\right] + \\ & \frac{1}{2}\left\{\left[(\tilde{u}_1+\hat{u}_1)_{,1} + (\tilde{u}_2+\hat{u}_2)\frac{a_{1,2}}{a_2} + u_3\frac{a_1}{R_1}\right]^2 + \right. \\ & \left[(\tilde{u}_2+\hat{u}_2)_{,1} - (\tilde{u}_1+\hat{u}_1)\frac{a_{1,2}}{a_2}\right]^2 + \\ & \left.\left[\tilde{u}_{3,1} - (\tilde{u}_1+\hat{u}_1)\frac{a_1}{R_1}\right]^2\right\}\end{aligned} \tag{30}$$

$$\gamma_{12} = \frac{1}{2}\Big\{ a_1\left[1 + y_3/R_1\right]\left[(\tilde{u}_1+\hat{u}_1)_{,2} - (\tilde{u}_2+\hat{u}_2)\,\frac{a_{2,1}}{a_1}\right] +$$

$$a_2\left[1 + y_3/R_2\right]\left[(\tilde{u}_2+\hat{u}_2)_{,1} - (\tilde{u}_1+\hat{u}_1)\,\frac{a_{1,2}}{a_2}\right] + \qquad (31)$$

$$\left[(\tilde{u}_1+\hat{u}_1)_{,2} - (\tilde{u}_2+\hat{u}_2)\,\frac{a_{2,1}}{a_1}\right]\left[(\tilde{u}_1+\hat{u}_1)_{,1} + (\tilde{u}_2+\hat{u}_2)\,\frac{a_{1,2}}{a_2} + \tilde{u}_3\,\frac{a_1}{R_1}\right] +$$

$$\left[(\tilde{u}_2+\hat{u}_2)_{,1} - (\tilde{u}_1+\hat{u}_1)\,\frac{a_{1,2}}{a_2}\right]\left[(\tilde{u}_2+\hat{u}_2)_{,2} + (\tilde{u}_1+\hat{u}_1)\,\frac{a_{2,1}}{a_1} + \tilde{u}_3\,\frac{a_2}{R_2}\right] +$$

$$\left[(\tilde{u}_{3,2}) - (\tilde{u}_2+\hat{u}_2)\,\frac{a_2}{R_2}\right]\left[(u_{3,1}) - (\tilde{u}_1+\hat{u}_1)\,\frac{a_1}{R_1}\right]\Big\}$$

$$\gamma_{13} = \frac{1}{2}\Big\{\left[a_1\left(1 + y_3/R_1\right)\hat{u}_{1,3}\right] + \qquad (32)$$

$$\left[\tilde{u}_{3,1} - (\tilde{u}_1+\hat{u}_1)\,\frac{a_1}{R_1}\right] +$$

$$\left[\hat{u}_{1,3}\right]\left[(\tilde{u}_1+\hat{u}_1)_{,1} + (\tilde{u}_2+\hat{u}_2)\,\frac{a_{1,2}}{a_2} + \tilde{u}_3\,\frac{a_1}{R_1}\right] +$$

$$\left[\hat{u}_{2,3}\right]\left[(\tilde{u}_2+\hat{u}_2)_{,1} - (\tilde{u}_1+\hat{u}_1)\,\frac{a_{1,2}}{a_2}\right] +$$

$$\left[\tilde{u}_{3,3}\right]\left[\tilde{u}_{3,1} - (\tilde{u}_1+\hat{u}_1)\,\frac{a_1}{R_1}\right]\Big\}$$

$$\gamma_{22} = a_2\left(1 + y_3/R_2\right)\left[(\tilde{u}_2+\hat{u}_2)_{,2} + (\tilde{u}_1+\hat{u}_1)\,\frac{a_{2,1}}{a_1} + \tilde{u}_3\,\frac{a_2}{R_2}\right] + \qquad (33)$$

$$\frac{1}{2}\Big\{\left[(\tilde{u}_1+\hat{u}_1)_{,2} - (\tilde{u}_2+\hat{u}_2)\,\frac{a_{2,1}}{a_1}\right]^2 +$$

$$\left[(\tilde{u}_2+\hat{u}_2)_{,2} + (\tilde{u}_1+\hat{u}_1)\,\frac{a_{2,1}}{a_1} + \tilde{u}_3\,\frac{a_2}{R_2}\right]^2 +$$

$$\left[\tilde{u}_{3,2} - (\tilde{u}_2+\hat{u}_2)\,\frac{a_2}{R_2}\right]^2$$

$$\gamma_{23} = \frac{1}{2}\Big\{ a_2\left(1+y_3/R_2\right)\left(\hat{u}_{2,3}\right) \; + \; \left[\tilde{u}_{3,2} - \left(\tilde{u}_2+\hat{u}_2\right)\frac{a_2}{R_2}\right] + \left[\hat{u}_{1,3}\right]\left[\left(\tilde{u}_1+\hat{u}_1\right)_{,2} - \left(\tilde{u}_2+\hat{u}_2\right)\frac{a_{2,1}}{a_1}\right] + \left[\hat{u}_{2,3}\right]\left[\left(\tilde{u}_2+\hat{u}_2\right)_{,2} + \left(\tilde{u}_1+\hat{u}_1\right)\frac{a_{2,1}}{a_1} + u_3\frac{a_2}{R_2}\right] + \left[\tilde{u}_{3,3}\right]\left[\tilde{u}_{3,2} - \left(\tilde{u}_2+\hat{u}_2\right)\frac{a_2}{R_2}\right]\Big\} \tag{34}$$

$$\gamma_{33} = \tilde{u}_{3,3} + \frac{1}{2}\left\{\hat{u}_{1,3}^{\,2} + \hat{u}_{2,3}^{\,2} + \tilde{u}_{3,3}^{\,2}\right\} \tag{35}$$

A comparison with Witt's work (30) reveals that although the method of derivation is different here, the same results are obtained.

Conversion from tensorial to physical strain is performed so that material properties can be readily found and used. This is accomplished from: (46)

$$\epsilon_{ij} = \gamma_{ij}/h_i h_j \tag{36}$$

So that

$$e_1 = \epsilon_{11} = \gamma_{11}/\left[a_1^2\left(1+y_3/R_1\right)^2\right] \tag{37}$$

$$e_2 = \epsilon_{22} = \gamma_{22} / [a_2^2 (1 + y_3/R_2)^2] \tag{38}$$

$$e_3 = \epsilon_{33} = \gamma_{33} \tag{39}$$

$$e_4 = 2\epsilon_{23} = 2\gamma_{23} / [a_2 (1 + y_3/R_2)] \tag{40}$$

$$e_5 = 2\epsilon_{13} = 2\gamma_{13} / [a_1 (1 + y_3/R_1)] \tag{41}$$

$$e_6 = 2\epsilon_{12} = 2\gamma_{12} / [a_1 a_2 [1 + y_3/R_1)(1 + y_3/R_2)] \tag{42}$$

Written in vector form, the physical strains are:

$$\{e\} = \begin{Bmatrix} e_1 \\ e_2 \\ e_3 \\ e_4 \\ e_5 \\ e_6 \end{Bmatrix} \tag{43}$$

which is expressed as the matrix product of a differential operator [L] and the displacement vector $\langle \vec{u} \rangle$

$$\{e\} = [L]\{u\} \tag{44}$$

where:

$$\{u\} = \begin{Bmatrix} \tilde{u}_1 + \hat{u}_1 \\ \tilde{u}_2 + \hat{u}_2 \\ \tilde{u}_3 \end{Bmatrix} = \begin{Bmatrix} \tilde{u} + \hat{u} \\ \tilde{v} + \hat{v} \\ w \end{Bmatrix} = \begin{Bmatrix} u \\ v \\ w \end{Bmatrix} \tag{45}$$

(Note that u,v,w are adopted here to represent the displacements u_1, u_2, and u_3. This is done to avoid confusion in subsequent derivations.)

The [L] operator matrix is further reduced to its component parts:

$$[L] = [L0] + [L1] + [L2] \tag{46}$$

where L0 contains only linear expressions, L1 contains nonlinear expressions involving only the reference surface displacements, L2 contains nonlinear expressions involving only the through the thickness displacements.

In order that the L's could be separated out, it was necessary to expand out the expressions for the strains. The full expansion was carried out and the resulting [L]

components are found in Appendix II. The expressions found in Appendix II are exactly the same as Witt's (30) but differ only in form.

CUBIC SPLINE FORMULATION:

In Witt's work (30), he considered the use of a parabolic assumption for the distribution of u through the thickness of the shell. This was done by assuming that the rotations were distributed linearly through each lamina. The parabolic nature of u was then obtained by integrating the rotations and satisfying continuity of u and the rotations at the interlaminar boundaries. With this assumption, he was able to show that strain compatibility could be maintained at the lamina interfaces. Accurate results were obtained when each lamina was modeled as two or more "pseudolayers". This modeling resulted in an increase in the number of degrees of freedom and thus increased the computer time and storage needed for solution.

In this work, an attempt was made to increase the order of the assumption for the variation of u through the thickness from parabolic to cubic. This was done to more accurately represent the real displacements without resorting to the inclusion of pseudolayers with their

inherent increase in degrees of freedom. A natural extension from Witt's work was to begin with a linear assumption for the second partial of u with respect to the thickness coordinate, integrate twice, and evaluate the constants of integration so as to insure strain compatibility through the shell. This thinking led to a variation of cubic spline theory in which the u's were represented as functions of the rotations. The following section shows how this thinking was implemented.

Concentrating our attention on the $\hat{u}$ component, we consider now the shell of concern to be made up of M layers of orthotropic laminae each having its own set of material properties which may or may not be unique within the shell (see Fig. 2). We are concerned that as we observe the interlaminar boundaries that the strains be continuous from one lamina to another.

Let the bottom of the jth layer be given the coordinate z_{j-1} and the top z_j, where $z=y_3$. At

$$z=z_{j-1} \; ; \; \frac{\partial^2 \hat{u}^1}{\partial z^2} = K_{j-1} \tag{47}$$

and at

$$z=z_j \; ; \; \frac{\partial^2 \hat{u}^1}{\partial z^2} = K_j \tag{48}$$

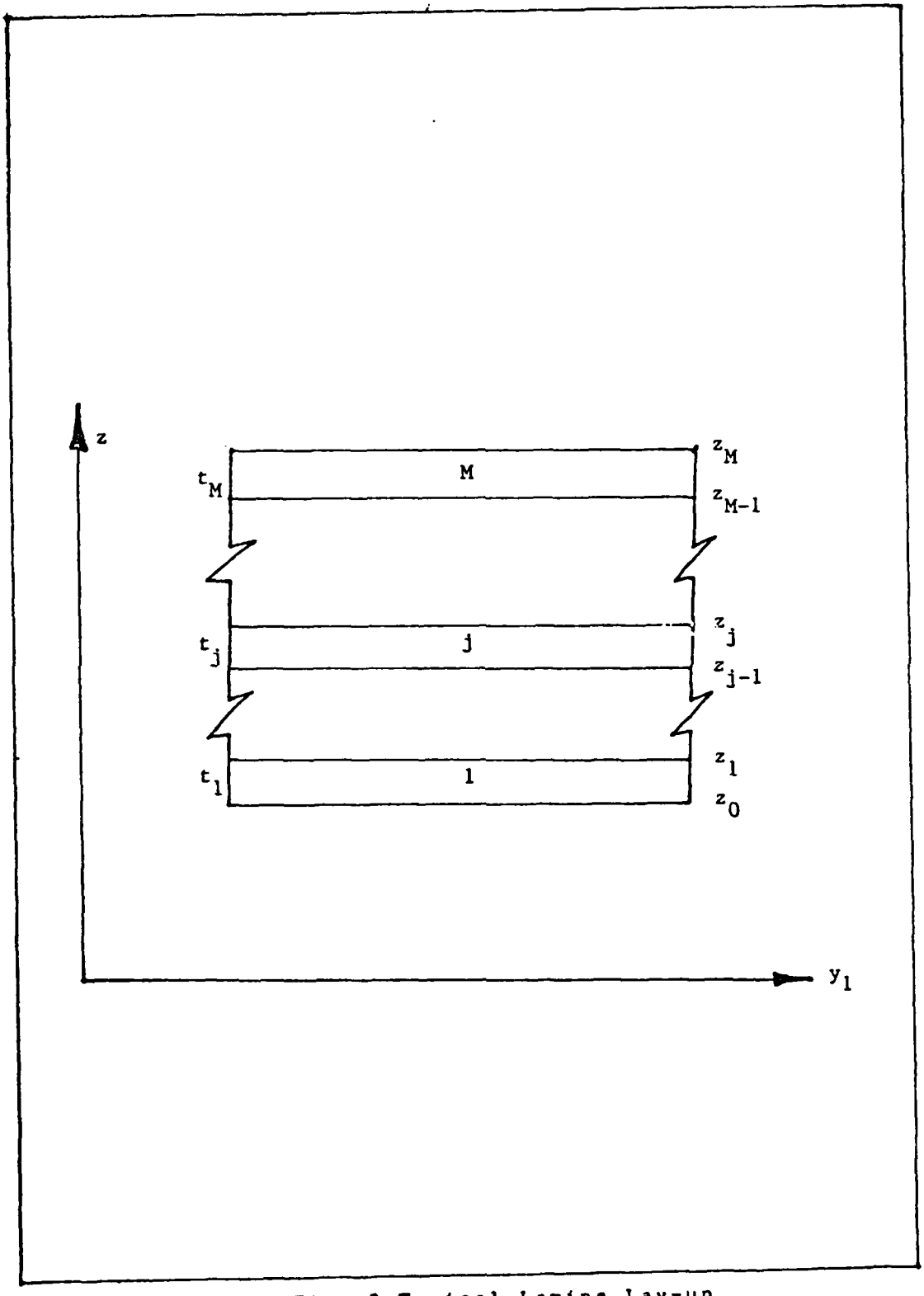

Fig. 2 Typical Lamina Lay-up

If the thickness of the jth layer is denoted by

$$t_j = z_j - z_{j-1} \tag{49}$$

and within that layer, a linear assumption is made for the distribution of the second partial of $\hat{u}$ with respect to z, then

$$\frac{\partial^2 \hat{u}}{\partial z^2} = K_{j-1} \frac{(z_j - z)}{t_j} + K_j \frac{(z - z_{j-1})}{t_j} \tag{50}$$

This assumption is recognized as the well-known starting point for the development of cubic spline theory, which is usually used in connecting graphical points with a smooth curve. A number of references are replete with documentation of this theory. One of the best treatments is found in reference (47).

If we integrate eqn (50) and evaluate the constants of integration, we obtain the equations: (see reference 47)

$$\frac{\partial \hat{u}}{\partial z} = -K_{j-1} \frac{(z_j - z)^2}{2t_j} + K_j \frac{(z - z_{j-1})^2}{2t_j} + \frac{\hat{u}_j - \hat{u}_{j-1}}{t_j} - \frac{K_j - K_{j-1}}{6} t_j \tag{51}$$

$$\hat{u} = K_{j-1} \frac{(z_j - z)^3}{6t_j} + K_j \frac{(z - z_{j-1})^3}{6t_j} + \left(\hat{u}_{j-1} - \frac{K_{j-1} t_j}{6}\right) \frac{(z_j - z)}{t_j} + \tag{52}$$

$$\left(\hat{u}_j - \frac{K_j t_j}{6}\right)^2 \frac{(z - z_{j-1})}{t_j}$$

where $\hat{u}_j$ is the value of $\hat{u}(z)$ at $z=z_j$.

The integration process yields the desired parabolic distribution for the first derivative and a cubic distribution for the displacement function.

At this juncture, we impose the continuity requirement that

$$\left.\frac{\partial \hat{u}}{\partial z}\right|_{z_j^-} = \left.\frac{\partial \hat{u}}{\partial z}\right|_{z_j^+} \tag{53}$$

(which means that the slopes are the same as one approaches the interlaminar boundary from top or bottom).

and obtain the condition:

$$\mu_j K_{j-1} + 2K_j + \lambda_j K_{j+1} = \frac{6\left[(\hat{u}_{j+1}-\hat{u}_j)/t_{j+1}\right] - \left[(\hat{u}_j-\hat{u}_{j-1})/t_j\right]}{t_j + t_{j+1}} \tag{54}$$

where:

$$\lambda_j = \frac{t_{j+1}}{t_j + t_{j+1}} \; ; \; \mu_j = 1-\lambda_j \quad (j = 1, 2, \cdots M) \tag{55}$$

Equations (52) and (54) could be used to develope an interpolation relation for $\hat{u}$. Such an interpolation would involve the second partials of $\hat{u}$ with respect to z $\left(\frac{\partial^2 \hat{u}}{\partial z^2}\right)$ at each interface and would represent a sound theory for implementation in finite elements. In other words looking ahead, some of the nodal degrees of freedom for the element would be the curvatures at the interfaces. Since Witt used

the rotations, and since rotations are easily interpreted from a physical standpoint, the foregoing development is recast in terms of the rotations or slopes as follows:

$$\text{at } z = z_{j-1} \;;\; \frac{d\hat{u}}{dz} = \phi_{j-1}$$
$$\text{at } z = z_j \;;\; \frac{d\hat{u}}{dz} = \phi_j \tag{56}$$

Equations (51,52,54) become:

$$\frac{d\hat{u}}{dz} = \phi_{j-1}\frac{(z_j - z)(2z_{j-1} + z_j - 3z)}{t_j^2} - \phi_j\frac{(z - z_{j-1})(2z_j + z_{j-1} - 3z)}{t_j^2} + \frac{\hat{u}_j - \hat{u}_{j-1}}{t_j^2}\,6(z_j - z)(z - z_{j-1}) \tag{57}$$

$$\hat{u} = \phi_{j-1}\frac{(z_j - z)^2(z - z_{j-1})}{t_j^2} - \phi_j\frac{(z - z_{j-1})^2(z_j - z)}{t_j^2} + \hat{u}_{j-1}(z_j - z)^2[2(z - z_{j-1}) + t_j]/t_j^3 + \hat{u}_j(z - z_{j-1})^2[2(z_j - z) + t_j]/t_j^3 \tag{58}$$

$$\lambda_j\phi_{j-1} + 2\phi_j + \mu_j\phi_{j+1} = 3\lambda_j\frac{\hat{u}_j - \hat{u}_{j-1}}{t_j} + 3\mu_j\frac{\hat{u}_{j+1} - \hat{u}_j}{t_{j+1}} \tag{59}$$

Equations (54 and 59) represent underdetermined systems of M-1 equations in the M+1 unknowns, $\hat{u}_j$.

One of the unknowns is eliminated by choosing the reference surface to be at the inner surface of the shell

and thus $\hat{u}_0 = 0$.

The remaining necessary condition to make the system tractable must be imposed at the outer surface of the shell. This condition was dealt with by assuming an imaginary layer to exist at the upper surface. By allowing no changes in rotation and no deformations to occur in the imaginary layer, the underdetermined system becomes tractable. A simple 2-layer example of this procedure is presented to make the process easily understood. This 2-layer case is then generalized to an M-layer case.

As an illustration of how the final condition is imposed, a two-ply laminated plate as shown in Fig. (3) is considered. Note that if a third (non-existent) layer is imagined, the following set of equations is obtained by direct substitution into eqn (59):

$$\phi_{j-1} + 4\phi_j + \phi_{j+1} = {}^{3}/_{t_j}\,(\hat{u}_{j+1} - \hat{u}_{j-1}) \qquad (60)$$

or

$$\begin{aligned} \phi_0 + 4\phi_1 + \phi_2 &= {}^{3}/_{t}\,(\hat{u}_2 - \hat{u}_0) \\ \phi_1 + 4\phi_2 + \phi_3 &= {}^{3}/_{t}\,(\hat{u}_3 - \hat{u}_1) \end{aligned} \qquad (61)$$

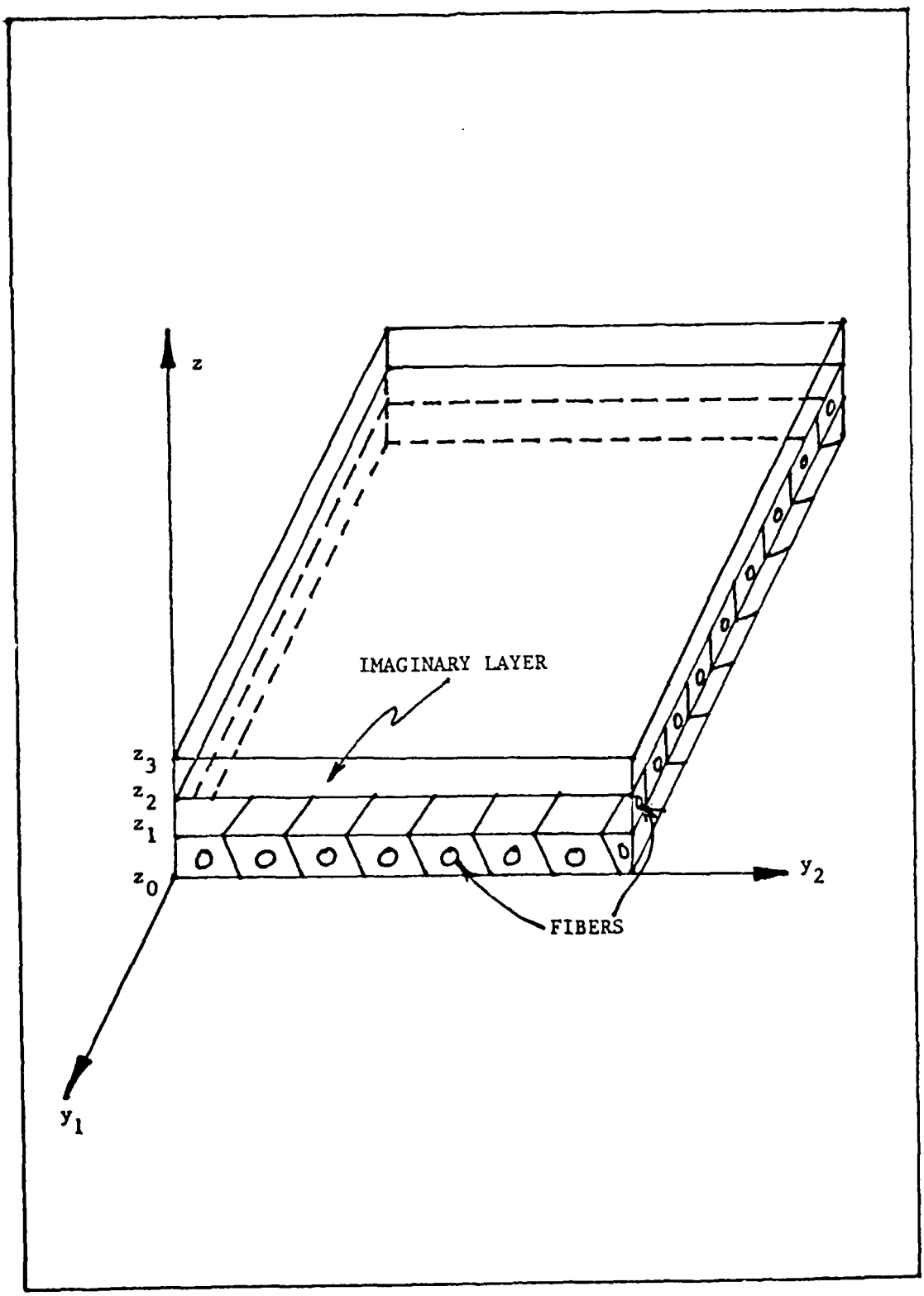

Fig. 3 Two-ply Laminated Plate

written in vector form

$$\begin{bmatrix} 1 & 4 & 1 & 0 \\ 0 & 1 & 4 & 1 \end{bmatrix} \begin{Bmatrix} \alpha_0 \\ \alpha_1 \\ \alpha_2 \\ \alpha_3 \end{Bmatrix} = \frac{3}{t} \begin{bmatrix} -1 & 0 & 1 & 0 \\ 0 & -1 & 0 & 1 \end{bmatrix} \begin{Bmatrix} \hat{u}_0 \\ \hat{u}_1 \\ \hat{u}_2 \\ \hat{u}_3 \end{Bmatrix} \tag{62}$$

Next, the reference surface boundary condition $\hat{u}_0 = 0$ is imposed. The boundary condition at the outer surface is expressed as $\alpha_3 = \alpha_2$ and $\hat{u}_3 = \hat{u}_2 + \alpha_2 t$. These conditions account for the non-existent layer and show that a line extending into the imaginary layer is not deformed, but follows the natural shape imposed by the existent layers. In spline theory, this is analogous to the natural cubic spline condition. (47)

The set of equations thus becomes:

$$\begin{bmatrix} 1 & 4 & 1 \\ 0 & 1 & 2 \end{bmatrix} \begin{Bmatrix} \alpha_0 \\ \alpha_1 \\ \alpha_2 \end{Bmatrix} = \frac{3}{t} \begin{bmatrix} 0 & 1 \\ -1 & 1 \end{bmatrix} \begin{Bmatrix} \hat{u}_1 \\ \hat{u}_2 \end{Bmatrix} \tag{63}$$

Which is tractable since there are 2 equations and 2 unknowns.

Switching to a more general matrix notation yields the system:

$$[B]\{\phi\} = 3/t\ [A]\{\hat{u}\} \tag{64}$$

Solution of the system for $\langle\hat{u}\rangle$ gives:

$$\{\hat{u}\} = t/3\,[A]^{-1}[B]\{\phi\} = t/3\,[C]\{\phi\} \tag{65}$$

where

$$[A]^{-1} = \begin{bmatrix} 1 & -1 \\ 1 & 0 \end{bmatrix} \quad ; \quad [C] = [A]^{-1}[B] \tag{66}$$

Written out, the solution is:

$$\begin{Bmatrix} \hat{u}_1 \\ \hat{u}_2 \end{Bmatrix} = t/3 \begin{bmatrix} 1 & 3 & -1 \\ 1 & 4 & 1 \end{bmatrix} \begin{Bmatrix} \phi_0 \\ \phi_1 \\ \phi_2 \end{Bmatrix} \tag{67}$$

These values for $\langle u\rangle$ are substituted into eqn (58) to yield the cubic spline approximation for the displacements in the layers in terms of the interlaminar rotations $\langle\phi\rangle$.

If we define $s(z)_j$ as the cubic approximation for $\hat{u}(z)$ in the jth layer, we see that for this two ply case the

interpolating splines are:

$$\Delta(z)_1 = H_{11}\phi_0 + H_{12}\phi_1 + H_{13}\phi_2 \tag{68}$$

where

$$H_{11} = \left\{ \frac{(z_1 - z)^2 (z - z_0)}{t^2} + \frac{(z - z_0)^2 [2(z_1 - z) + t]}{3t^2} C_{11} \right\}$$

$$H_{12} = \left\{ - \frac{(z - z_0)^2 (z_1 - z)}{t^2} + \frac{(z - z_0)^2 [2(z_1 - z) + t]}{3t^2} C_{12} \right\} \tag{69}$$

$$H_{13} = \left\{ 0 + \frac{(z - z_0)^2 [2(z_1 - z) + t]}{3t^2} C_{13} \right\}$$

and

$$\Delta(z)_2 = H_{21}\phi_0 + H_{22}\phi_1 + H_{23}\phi_2 \tag{70}$$

where

$$H_{21} = \left\{ \frac{(z_2 - z)^2 [2(z - z_1) + t]}{3t^2} C_{11} + \frac{(z - z_1)^2 [2(z_2 - z) + t]}{3t^2} C_{21} \right\}$$

$$H_{22} = \left\{ \frac{(z_2 - z)^2 (z - z_1)}{t^2} + \frac{(z_2 - z)^2 [2(z - z_1) + t]}{3t^2} C_{12} + \frac{(z - z_1)^2 [2(z_2 - z) + t}{3t^2} C_{22} \right\} \tag{71}$$

$$H_{23} = \left\{ - \frac{(z - z_1)^2 (z_2 - z)}{t^2} + \frac{(z_2 - z)^2 [2(z - z_1) + t}{3t^2} C_{13} + \frac{(z - z_1)^2 [2(z_2 - z) + t]}{3t^2} C_{23} \right\}$$

(The C_{ij}'s are the elements of the [C] matrix of eqn (67))

If one were to go through this exercise for a successively increasing number of plies, he would see a recursion relation emerge and would find that in general:

$$H_{ji} = \left\{ \delta_{ij} \frac{(z_j - z)^2 (z - z_{j-1})}{t^2} - \delta_{(i-1)j} \frac{(z - z_{j-1})^2 (z_j - z)}{t^2} + \right.$$

$$\left. C_{j-1,i} \frac{(z_j - z)^2 [2(z - z_{j-1}) + t]}{3t^2} + C_{ji} \frac{(z - z_{j-1})^2 [2(z_j - z) + t]}{3t^2} \right\} \qquad (72)$$

where δ_{ij} is Kronecker's delta and $C_{0i} = 0$.

Using the expression for H_{ji}, one may write the interpolating spline in the jth layer as:

$$s(z)_j = \sum_{i=1}^{M+1} H_{ji} q_{i-1} \qquad (73)$$

or (adopting a summation convention) as:

$$s(z)_j = H_{ji} q_{i-1} \quad (i = 1, 2, \ldots M+1) \qquad (74)$$

In this form, the H_{ji} can be thought of as a set of shape functions in the z direction. It should be noted that this derivation for H_{ji} is original work and represents a variation in cubic spline theory which to the best of the author's knowledge has not been previously explored.

If we turn our attention to the $\hat{v}$ component of displacement and make the same assumptions and arguments as we did for $\hat{u}$, we would obtain expressions for H_{ji} which are identical to those already obtained.

FINITE ELEMENT APPLICATION:

At this juncture attention is concentrated on the in-plane directions. Using the finite element shape functions N_k for the in plane distributions, we write (adopting the summation convention):

$$q_i = N_k q_{ki} \tag{75}$$

where q_{ki} is the partial of $\hat{u}$ with respect to z for the kth node at the ith interface. Substituting (75) into (74):

$$s(z)_j = H_{ji} N_k q_{ki-1} \begin{cases} i = 1, 2, \cdots M+1 \\ k = 1, 2, \cdots n \text{ number of nodes} \\ j = 1, M \end{cases} \tag{76}$$

Remembering that $s(z)_j$ is the cubic approximation for $\hat{u}(z)$ in the jth layer, we recall that for the jth layer:

$$u(z)_j = \tilde{u} + \hat{u}(z)_j \tag{77}$$

Upon substitution for $\hat{u}(z)_j$ we have:

$$u(z)_j = \tilde{u} + s(z)_j \tag{78}$$

The forgoing arguments are carried out on the $\hat{v}$ displacements, this time letting θ_{ki} be the partial of $\hat{v}$ with respect to to z at the kth node and ith interface so that one obtains a similar result for the $\hat{v}$ components as those for the $\hat{u}$ components.

Casting all of the preceding development in finite element terms is straight forward. We choose an n-noded isoparametric element and define our nodal degrees of freedom for the kth node as:

$$\{a_k\} = \begin{Bmatrix} \tilde{u}_k \\ \theta_{k0} \\ \vdots \\ \theta_{kn} \\ \tilde{v}_k \\ \theta_{k0} \\ \vdots \\ \theta_{kn} \\ w_k \end{Bmatrix} \tag{79}$$

This choice for the ordering of ⟨a⟩ allows for variation in the element type that is very efficient in terms of computer implementation.

The shape functions for the kth node are then:

$$[N_k] = \begin{bmatrix} N_k & H_{j1}N_k & \cdots & H_{jM}N_k & 0 & 0 & \cdots & 0 & 0 \\ 0 & 0 & \cdots & 0 & N_k & H_{j1}N_k & \cdots & H_{jM}N_k & 0 \\ 0 & 0 & \cdots & 0 & 0 & 0 & \cdots & 0 & N_k \end{bmatrix} \tag{80}$$

where the H_{ji}'s are given by eqn (72) and the N_k's are the in-plane shape functions.

For the purposes of illustration and for subsequent use, the isoparametric quadrilateral flat plate element is considered. The shape functions are given by (see Fig. 4)

$$N_K = (1+\xi_0)(1+\eta_0)/4 \tag{81}$$

where

$$\xi_0 = \xi_K \xi \quad ; \quad \eta_0 = \eta_K \eta \tag{82}$$

The displacement vector is thus seen to be:

$$\{u\} = \begin{Bmatrix} \tilde{u}+\hat{u} \\ \tilde{v}+\hat{v} \\ w \end{Bmatrix} = [N]\{a\} \tag{83}$$

At this point in the development, all of the pieces are available for derivation of the finite element equations. This derivation is readily carried out by application of Hamilton's Principle which states:

$$\delta \int_{\hat{t}_0}^{\hat{t}_1} (T-V)\, d\hat{t} + \int_{\hat{t}_0}^{\hat{t}_1} \delta W \, d\hat{t} = 0 \tag{84}$$

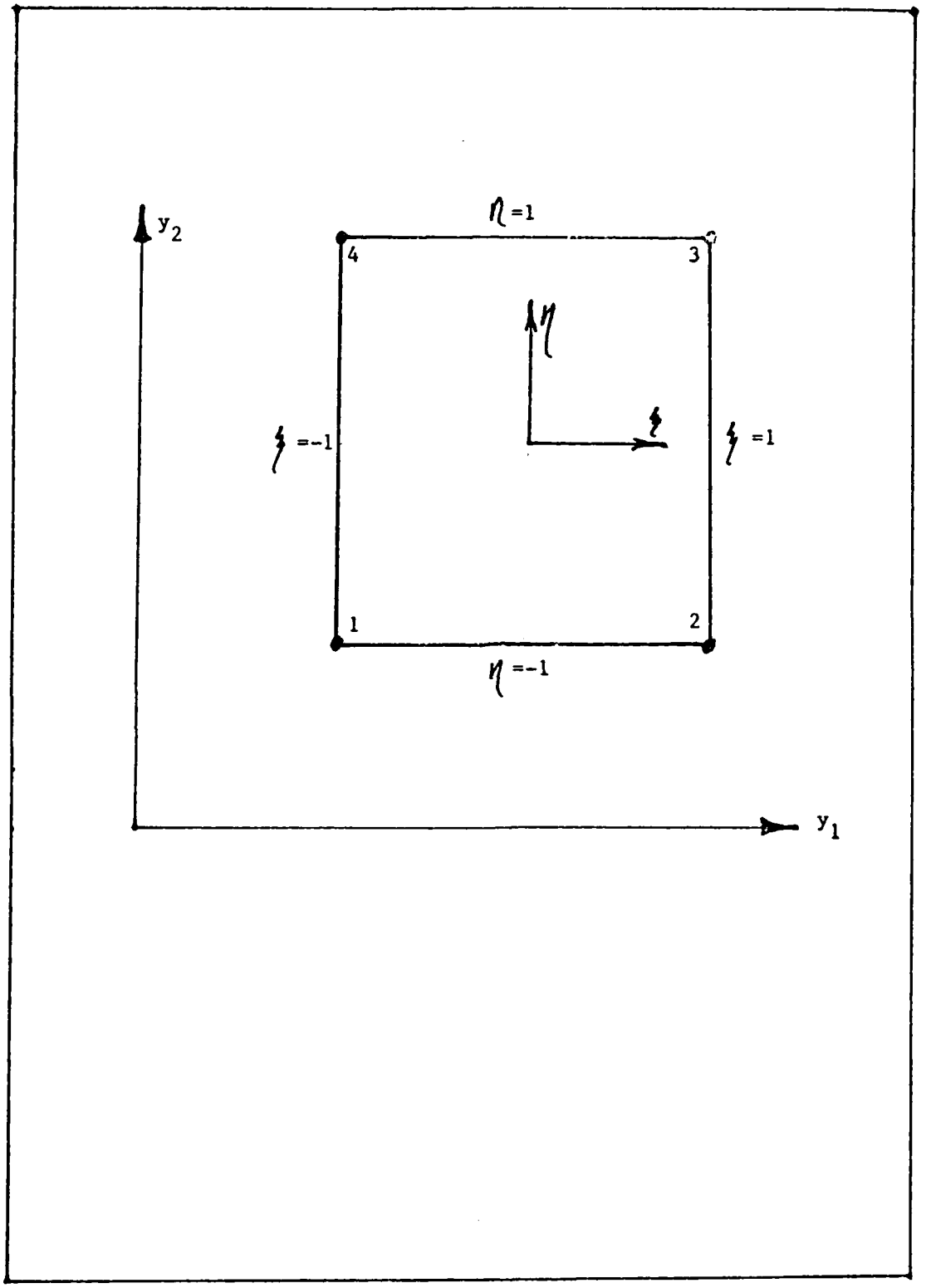

Fig. 4 Isoparametric Quadrilateral Element

where T is the kinetic energy, V is the strain energy, and W is the external work.

Looking at these terms in detail, it is seen that:

$$W = \int_{Vol} \{u\}^T \{b\}\, dVol + \int_{\Gamma} \{u\}^T \{f\}\, d\Gamma \tag{85}$$

where $\langle b \rangle$ is a vector of body forces and $\langle f \rangle$ is a vector of surface tractions.

$$V = \frac{1}{2} \int_{Vol} \{e\}^T \{S\}\, dVol \tag{86}$$

where $\langle S \rangle$ is the energy complement of the Lagrangian strain known as the second *Piola-Kirchhoff stress vector.* (56) The stress-strain relation is given by $\langle S \rangle = [D]\langle e \rangle$.

$$T = \frac{1}{2} \int_{Vol} \{\dot{u}\}^T [\rho] \{\dot{u}\}\, dVol \tag{87}$$

where the dot($\cdot$) denotes time differentiation, and $[\rho]$ is a matrix of mass density for the structure.

Substitution of these expressions into Hamilton's Principle yields:

$$\delta \int_{\hat{t}_0}^{\hat{t}_1} \frac{1}{2} \int_{Vol} \{\dot{u}\}^T [\rho] \{\dot{u}\} - \{e\}^T \{S\}\, dVol\, d\hat{t} + \int_{\hat{t}_0}^{\hat{t}_1} \delta \left(\int_{Vol} \{u\}^T \{b\}\, dVol + \int_{\Gamma} \{u\}^T \{f\}\, d\Gamma \right) d\hat{t} \tag{88}$$

where $\hat{t}$ is time.

Substitution for ⟨u⟩,⟨e⟩, and ⟨S⟩ in terms of [L], [N], and ⟨a⟩ yields:

$$\delta\int_{\hat{t}_0}^{\hat{t}_1}\int_{Vol}\{\dot{a}\}^T[N]^T[\rho][N]\{\dot{a}\} - \{a\}^T[N]^T[L]^T[D][L][N]\{a\}dVol\,d\hat{t}$$

$$+\int_{\hat{t}_0}^{\hat{t}_1}\delta\left(\int_{Vol}\{a\}^T[N]^T\{b\}dVol + \int_{\Gamma}\{a\}^T[N]^T\{f\}d\Gamma\right)d\hat{t} = 0 \qquad (89)$$

Upon taking the indicated variations and reordering, it is seen that:

$$\int_{Vol}[N]^T[\rho][N]dVol\{\ddot{a}\} + \int_{Vol}[N]^T[L]^T[D][L][N]dVol\{a\} =$$
$$\int_{Vol}[N]^T\{b\}dVol + \int_{\Gamma}[N]^T\{f\}d\Gamma \qquad (90)$$

or

$$[M]\{\ddot{a}\} + [K]\{a\} = \{B\} + \{F\} \qquad (91)$$

Equation (91) represents an equation of motion for a structure of interest. This equation is simplified by limiting our attention to static problems while neglecting body forces. Thus:

$$[K]\{a\} = \{F\} \qquad (92)$$

The definition of ⟨a⟩ has been well established in equation (79). The formation of [K] and ⟨F⟩in eqn (92) are presented to provide clarity and completeness.

The stiffness matrix [K] is given by:

$$[K] = \int_{Vol} [N]^T [L]^T [D] [L] [N] \, dVol \tag{93}$$

Account for the varying material properties through the thickness as well as the changes in [N] is taken by forming the sum over the number of layers as:

$$[K] = \sum_{j=1}^{M} \int_{Vol} [N]_j^T \cdot [L]^T [D]_j \cdot [L] [N]_j \cdot dVol \tag{94}$$

Since the operator matrix [L] is given by [L]=[L0]+[L1]+[L2], further factoring of [K] is accomplished as [K]=[K0]+[K1]+[K2] where:

$$[K0] = \sum_{j=1}^{M} \int_{Vol} [N]_j^T \cdot [L0]^T [D]_j \cdot [L0] [N]_j \cdot dVol \tag{95a}$$

$$[K1] = \sum_{j=1}^{M} \int_{Vol} [N]_j^T \cdot [L0]^T [D]_j \cdot [L1] [N]_j \cdot + [N]_j^T \cdot [L1]^T [D]_j \cdot [L0] [N]_j \cdot + [N]_j^T \cdot [L1]^T [D]_j \cdot [L1] [N]_j \cdot dVol \tag{95b}$$

$$[K2] = \sum_{j=1}^{M} \int_{Vol} [N]_j^T [L0]^T [D]_j [L2][N]_j + [N]_j^T [L2]^T [D]_j [L0][N]_j + \quad (95c)$$

$$[N]_j^T [L1]^T [D]_j [L2][N]_j +$$

$$[N]_j^T [L2]^T [D]_j [L1][N]_j +$$

$$[N]_j^T [L2]^T [D]_j [L2][N]_j \; dVol$$

This way of writing the stiffness matrix lends itself well to gaining an understanding of the meaning of the various terms. The [K0] term is seen to contain only linear operators [L0] which are displacement independent. Inclusion of only this term in the computation of [K] is accounting for the commonly used small displacement, small strain components in the matrix. Further inclusion of the [K1] terms accounts for the nonlinearities arising from large displacements and interaction between those displacements in the reference surface and the small strain terms. Finally, inclusion of the [K2] terms accounts for nonlinearities arising from interactions taking place between the in-plane reference surface deformations and rotations, the through-the-thickness deformations and rotations, and the small strain deformations.

In practice, inclusion of one or all of the terms [K0] through [K2] is a simple matter and is left to the discretion of the user. Some examples of their inclusion are

given in Chapter IV.

The determination of $[D]_j$ deserves some attention as the orientation of the fibers may vary from layer to layer. Consider a single orthotropic layer in the fiber oriented reference system as shown in Fig (5). If $\langle e\rangle_j = [G]_j \langle S\rangle_j$ then one may write:

$$[G]_j = \begin{bmatrix} 1/E_1 & -\frac{\nu_{12}}{E1} & -\frac{\nu_{12}}{E1} & 0 & 0 & 0 \\ & 1/E_2 & -\frac{\nu_{12}}{E_2} & 0 & 0 & 0 \\ & & 1/E_2 & 0 & 0 & 0 \\ & \text{SYM} & & 1/G_{23} & 0 & 0 \\ & & & & 1/G_{12} & 0 \\ & & & & & 1/G_{12} \end{bmatrix}_j \qquad (96)$$

and $[D_l]_j = [G]_j^{-1}$. To transfer from the fiber oriented system to the global system requires a tensor transformation:

$$[D_g]_j = [T]\,[D_l]_j\,[T]^T \qquad (97)$$

where

$$[T] = \begin{bmatrix} \cos^2\alpha & \sin^2\alpha & 0 & 0 & 0 & -2\sin\alpha\cos\alpha \\ \sin^2\alpha & \cos^2\alpha & 0 & 0 & 0 & 2\sin\alpha\cos\alpha \\ 0 & 0 & 1 & 0 & 0 & 0 \\ 0 & 0 & 0 & \cos\alpha & \sin\alpha & 0 \\ 0 & 0 & 0 & -\sin\alpha & \cos\alpha & 0 \\ \sin\alpha\cos\alpha & -\sin\alpha\cos\alpha & 0 & 0 & 0 & \cos^2\alpha-\sin^2\alpha \end{bmatrix} \qquad (98)$$

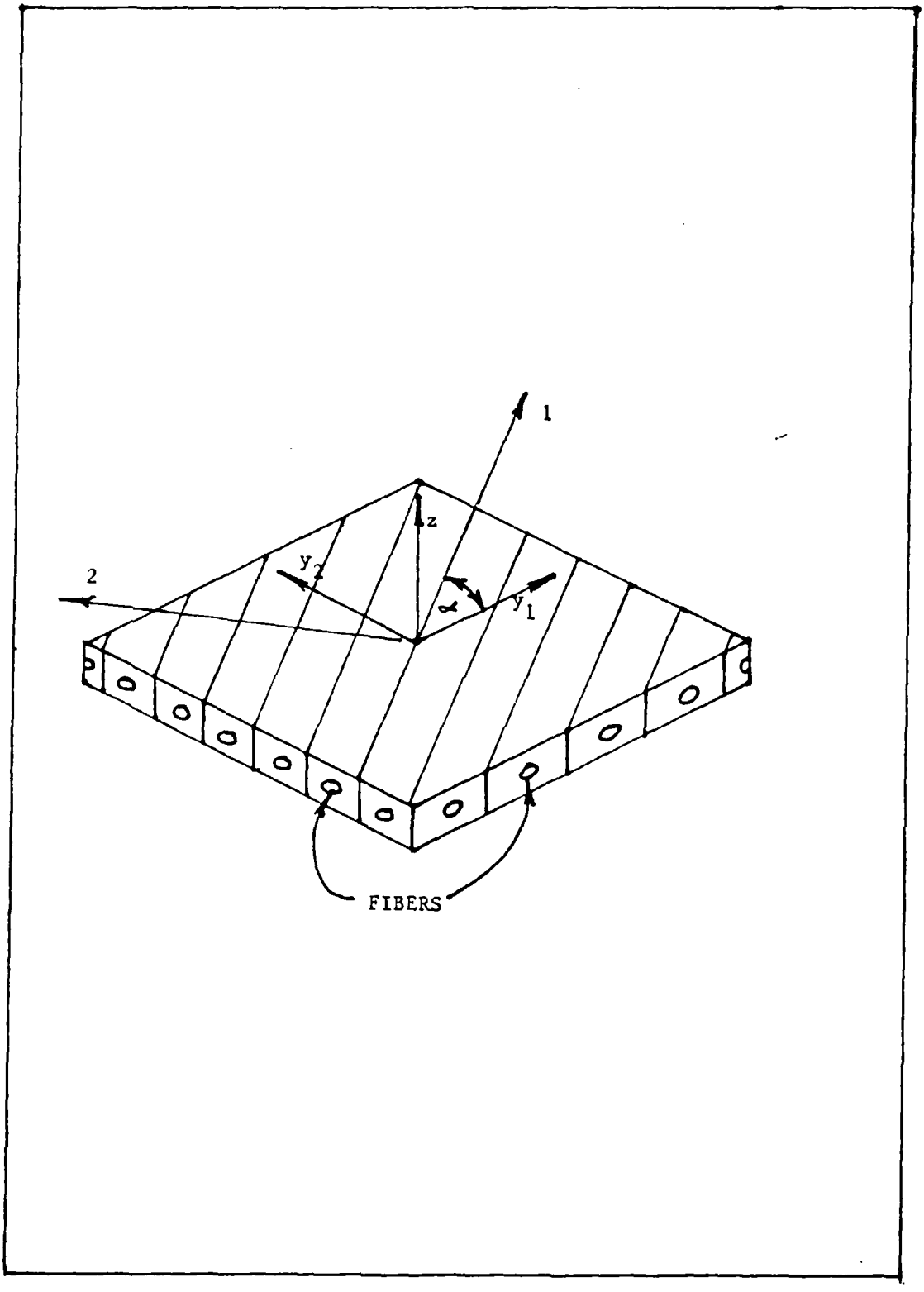

Fig. 3 Fiber Oriented Reference System

Following this transformation, $[D_g]_j$ is seen to be:

$$[D_g]_j = \begin{bmatrix} D11 & D12 & D13 & 0 & 0 & D16 \\ & D22 & D23 & 0 & 0 & D26 \\ & & D33 & 0 & 0 & D36 \\ & & & D44 & D45 & 0 \\ & SYM & & & D55 & 0 \\ & & & & & D66 \end{bmatrix}_j \tag{99}$$

$[D_l]_j$ is the constitutive matrix in the local fiber-oriented reference system, and $[D_g]_j$ is the matrix in the global system. Note that if α =0 or 90, then D16=D26=D36=D45=0.

To illustrate the formulation of $\langle F \rangle$ we return to the two layer example and note in detail how the various terms enter in. Considering only the kth node:

$$\{F\}_k = \sum_{j=1}^{M} \int_{\Gamma} \begin{bmatrix} N_k & 0 & 0 \\ H_{j1}N_k & 0 & 0 \\ H_{j2}N_k & 0 & 0 \\ H_{j3}N_k & 0 & 0 \\ 0 & N_k & 0 \\ 0 & H_{j1}N_k & 0 \\ 0 & H_{j2}N_k & 0 \\ 0 & H_{j3}N_k & 0 \\ 0 & 0 & N_k \end{bmatrix} \begin{Bmatrix} f_u \\ f_v \\ f_w \end{Bmatrix} \tag{100}$$

where f_u, f_v, f_w are the surface tractions in each of the u,v, and w directions. If one has only f_u, then the force vector

would appear as:

$$\{F\} = \begin{Bmatrix} F_u \\ F_{\ell_0} \\ F_{\ell_1} \\ F_{\ell_2} \end{Bmatrix} = \begin{Bmatrix} \int_{z_0}^{z_1}\int_{\rho_0}^{\rho_1} N_k f_u \, d\rho dz + \int_{z_1}^{z_2}\int_{\rho_0}^{\rho_1} N_k f_u \, d\rho dz \\ \int_{z_0}^{z_1}\int_{\rho_0}^{\rho_1} f_u H_{11} N_k \, d\rho dz + \int_{z_1}^{z_2}\int_{\rho_0}^{\rho_1} f_u H_{21} N_k d\rho dz \\ \int_{z_0}^{z_1}\int_{\rho_0}^{\rho_1} f_u H_{12} N_k d\rho dz + \int_{z_1}^{z_2}\int_{\rho_0}^{\rho_1} f_u H_{22} N_k d\rho dz \\ \int_{z_0}^{z_1}\int_{\rho_0}^{\rho_1} f_u H_{13} N_k d\rho dz + \int_{z_1}^{z_2}\int_{\rho_0}^{\rho_1} f_u H_{23} N_k d\rho dz \end{Bmatrix} \quad (101)$$

F_u, F_{ℓ_0}, F_{ℓ_1}, F_{ℓ_2} are then the generalized forces applied to the u, ℓ_0, ℓ_1, ℓ_2, degrees of freedom at the kth node. The limits of integration p are either or depending on which face the load is applied.

The solution of the strictly linear problem was a straight forward Crout variation on the Gauss elimination method. The method consists of a factorization of the stiffness matrix into the product of a lower triangular matrix and an upper triangular matrix. The use of this scheme with active column profile (skyline) storage of the stiffness matrix led to a very compact program and allowed for inclusion of a resolve capability (i.e., new load cases) without any significant additional programming effort. (56)

The solution of the nonlinear problem was accomplished by implementing the Newton-Raphson or modified Newton-Raphson method on the system of equations. The algorithm for these methods is essentially the same with the exception that the stiffness matrix is not recalculated at each iteration for the modified method. A detailed description of these methods is found in Zienkewicz (48). Appendix III also contains further discussion on the nonlinear solution technique as related to specific test problems.

Chapter III is devoted to an explanation in further detail as to how the computer program was written to account for the integrations, assemblies and solutions of the preceding expressions.

CHAPTER III

THE FINITE ELEMENT ANALYSIS PROGRAM

To validate the theory presented, a finite element analysis program was written to solve some flat plate problems which could be compared with previous works.

As was stated in the theoretical derivation given in Chapter II, every effort was made to keep the computer program element-independent. That is, the program was written to use any element in the family of 2-D isoparametric elements ranging from the simple 3-noded triangles to an 8-noded Serendipity quadrilateral and including transition elements as needed. The code thus written lends itself to great flexibility in element selection.

Shape function routines were written to allow the user to discretize problems quickly and reliably. The shape function subprograms evaluate not only the shape function, but also its derivatives with respect to the global coordinate frame (see Fig. 4). The basis for the subprograms is the 4-noded isoparametric quadrilateral where:

$$N_k = (1+\xi_k\xi)(1+\eta_k\eta)/4 \qquad (102)$$

and ξ_k, η_k are the ξ, η coordinates of the nodes. Making use of the isoparametric concept yields (adopting the summation convention):

$$x = N_k x_k$$
$$y = N_k y_k \tag{103}$$

and derivatives given as

$$\begin{Bmatrix} N_{k,\xi} \\ N_{k,\eta} \end{Bmatrix} = \begin{bmatrix} x_{,\xi} & y_{,\xi} \\ x_{,\eta} & y_{,\eta} \end{bmatrix} \begin{Bmatrix} N_{k,x} \\ N_{k,y} \end{Bmatrix} \tag{104}$$

or

$$\begin{Bmatrix} N_{k,x} \\ N_{k,y} \end{Bmatrix} = \frac{1}{J} \begin{bmatrix} y_{,\eta} & -y_{,\xi} \\ -x_{,\eta} & x_{,\xi} \end{bmatrix} \begin{Bmatrix} N_{k,\xi} \\ N_{k,\eta} \end{Bmatrix} \tag{105}$$

where J is the Jacobian determinant and ( ),x denotes the partial derivative. These relations define steps for the shape function routine where it is assumed that the nodal coordinates have been transformed to the local element coordinate system.

The extension of the 4-node routine to higher (or lower) order elements is accomplished simply by adjusting the shape

functions to account for the addition (or deletion) of nodes. In the case of the triangle for instance, the third and fourth nodal shape functions are added together. In the case of the 8-noded serendipity quadrilateral element, each of the corner nodal shape functions is adjusted for the presence of the midside nodes. The elements which one may wish to use as a transition from linear to quadratic are obtained simply by omitting the midside node for the linear edge.

The generation of the stiffness matrix [K] deserves special attention, since many zeros exist in [N], [L], and [D]. Concentrating attention on a single node i, we define $[B]_i=[L]_i[N]_i$ and consider the matrix triple product $[K]_{ij}=[B]_i^T[D][B]_j$. One can readily see from the dimensions of the matrices that formal matrix multiplication would require $24M^2+192M+330$ multiplications per layer where M is the number of layers. If, on the other hand, one were to form the product explicitly accounting for the zeros, he would find that the number of multiplications would be $4M^2+40M+71$ per layer. For instance, given M=3, we see that one would perform 1122 multiplications per layer formally as compared with 227 when the zeros of the matrices are taken into account. Since there is significant difference in these numbers, the triple product was formed explicitly and then programmed.

The choice for the nodal degree of freedom vector $\langle a \rangle$ as defined by eqn (80) of Chapter II was made because this form becomes very efficient when adding nodes as one's choice of elements changes. For instance, suppose one wishes to use a triangular element. Then

$$\{a\} = \begin{Bmatrix} a_1 \\ \cdots \\ a_2 \\ \cdots \\ a_3 \end{Bmatrix} \quad ; \quad [N] = [N_1 \vdots N_2 \vdots N_3] \tag{106}$$

If, on the other hand, one were to choose the 4-noded quadrilateral element, the $\langle a \rangle$ and [N] matrices would simply be augmented by the addition of a_4 and N_4.

Another advantage of this choice for $\langle a \rangle$ has been alluded to previously in the way that [K] is formed. Looking at the triangular element, one can see that the system of equations would appear as:

$$\begin{bmatrix} [K_{11}] & [K_{12}] & [K_{13}] \\ & [K_{22}] & [K_{23}] \\ \text{SYM} & & [K_{33}] \end{bmatrix} \begin{Bmatrix} \{a_1\} \\ \{a_2\} \\ \{a_3\} \end{Bmatrix} = \begin{Bmatrix} \{F_1\} \\ \{F_2\} \\ \{F_3\} \end{Bmatrix} \tag{107}$$

where

$$[K]_{ij} = \int_{Vol} [B]_i^T [D] [B]_j \, dVol \tag{108}$$

The program was written to take advantage of this submatrix structure. Thus the whole [K] matrix is formed by successive calculation of $[K]_{ij}$ through subscript incrementation and proper stacking of each submatrix. Furthermore, since [K] is always symmetric, only the upper triangular portion need be calculated. The lower half was formed by reflection.

In order to facilitate the flexibility of varying elements, it was necessary to incorporate a numerical integration scheme for performing the necessary integrations. The Gauss-Legendre quadrature formulae were utilized for this purpose since "they give the highest accuracy for effort expended." (48)

This choice necessitated that the limits of integration in each of the three coordinate directions be on the interval from -1 to +1. The use of the 2-D isoparametric formulation readily accounted for the in-plane directions. The through-the-thickness coordinate was transformed as follows:

$$z = \sum_{j=0}^{k} t_j - \frac{t_k}{2}(1 - \zeta_k) \tag{109}$$

where k indicates the layer, t_k is the thickness of the kth layer, and ζ_k is the transformed variable. In the case where the layers are of the same thickness, the transformation becomes:

$$z = \epsilon\left(1 + \frac{\zeta_k - 1}{2}\right) \tag{110}$$

and thus

$$dz = \frac{\epsilon}{2}\, d\zeta_k \tag{111}$$

The use of this new variable yields the following integral for the evaluation of $[K]_{ij}$:

$$[K]_{ij} = \sum_{k=1}^{M} \int_{-1}^{1}\int\int [B_k]_i^T\, [D_g]_k\, [B_k]_j\, |J|\, \frac{\epsilon}{2}\, d\xi\, d\eta\, d\zeta_k \tag{112}$$

Cast in terms of the Gauss-Legendre quadrature relations one obtains:

$$[K]_{ij} = \sum_{k}^{M}\sum_{r}^{n}\sum_{s}^{n}\sum_{t}^{p} Q_r Q_s Q_t \left[B_k(\xi_r, \eta_s, \zeta_t)\right]_i^T \cdot [D_g]_k \left[B_k(\xi_r, \eta_s, \zeta_t)\right]_j \cdot |J|\, \frac{\epsilon}{2} \tag{113}$$

where Q_r, Q_s, Q_t are the weights associated with the sampling points $\xi_r \cdot \eta_s \cdot \zeta_t$. The order of integration is n in the ξ and η directions and p in the z direction. The program was written to use the same integration order for both in-plane directions. Orders of integration for those directions may

be chosen from the range 1 through 3. The through the thickness direction integrations may be chosen as either second or third order.(see Fig. 6) This limitation was imposed based on the polynomial forms encountered in the development of $[K]_{ij}$. A detailed description of the Gauss-Legendre quadrature formulae development and error analysis may be found in refs. (49) and (50). See Appendix III for a more detailed description of the element and a discussion of computer times and considerations for specific test problems.

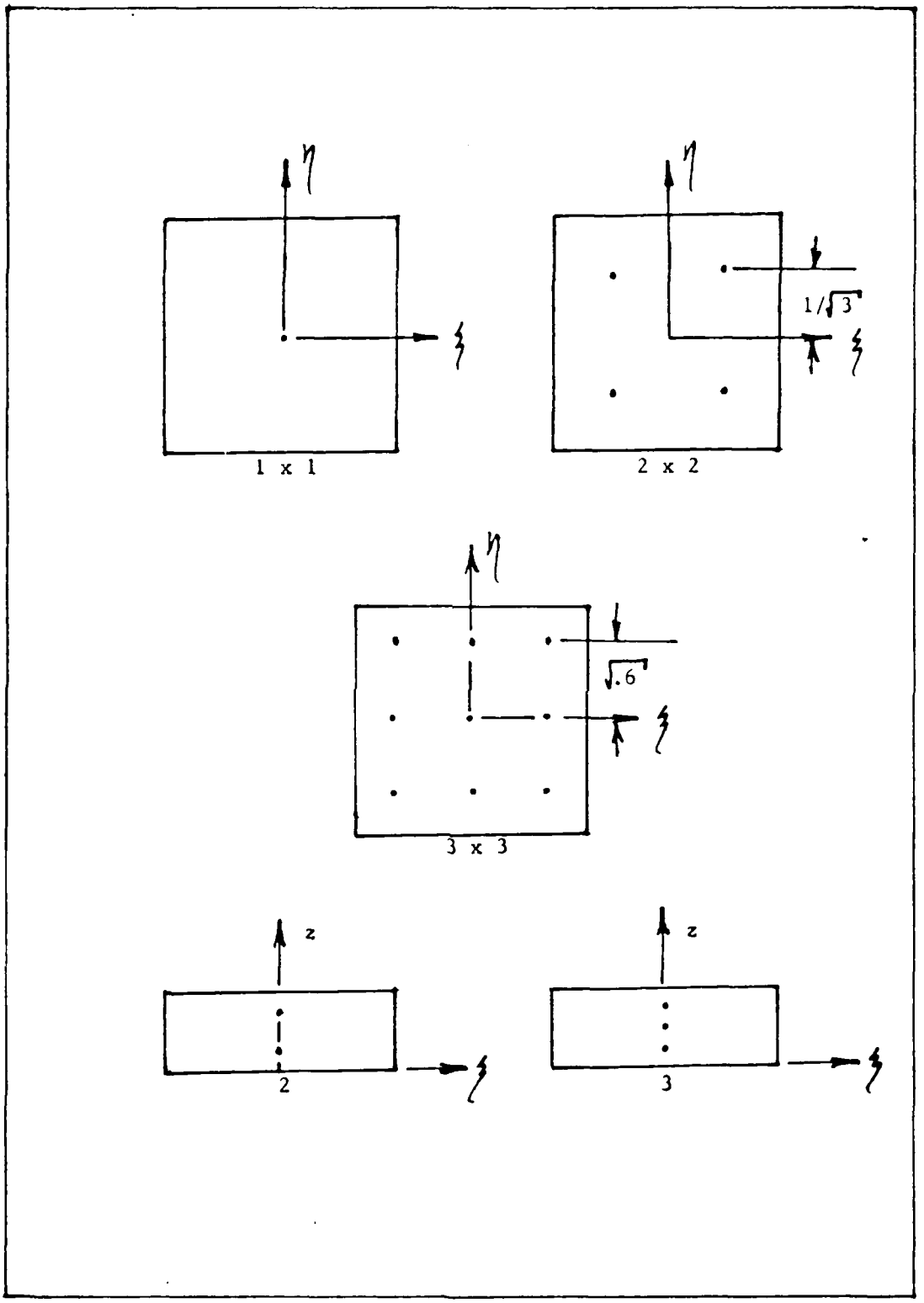

Fig. 6 Element Integration Points

CHAPTER IV

APPLICABILITY AND RANGE

In this chapter, the applicability and range of the theory are presented. The first application examined is that of a plate strip (see Fig. 7). A plate strip is infinitely long in one direction (in this case, the y-direction). The simply supported strip is loaded laterally (as shown in Fig. 7) so as to cause cylindrical bending to occur. This cylindrical bending implies that the displacements (w) in the z-direction are symmetric about the center line of the strip and are independent of y and displacements (v) in the y-direction are zero.

The first case studied was that of the isotropic plate strip loaded uniformly. This problem posed some difficulty for Witt's (30) parabolic theory using the constant strain triangle to represent the reference surface displacements. The decision to solve this problem was motivated by Witt's difficulty. With the present cubic theory and a family of finite elements to choose from, a study could be carried out to investigate how Witt's difficulties could be overcome.

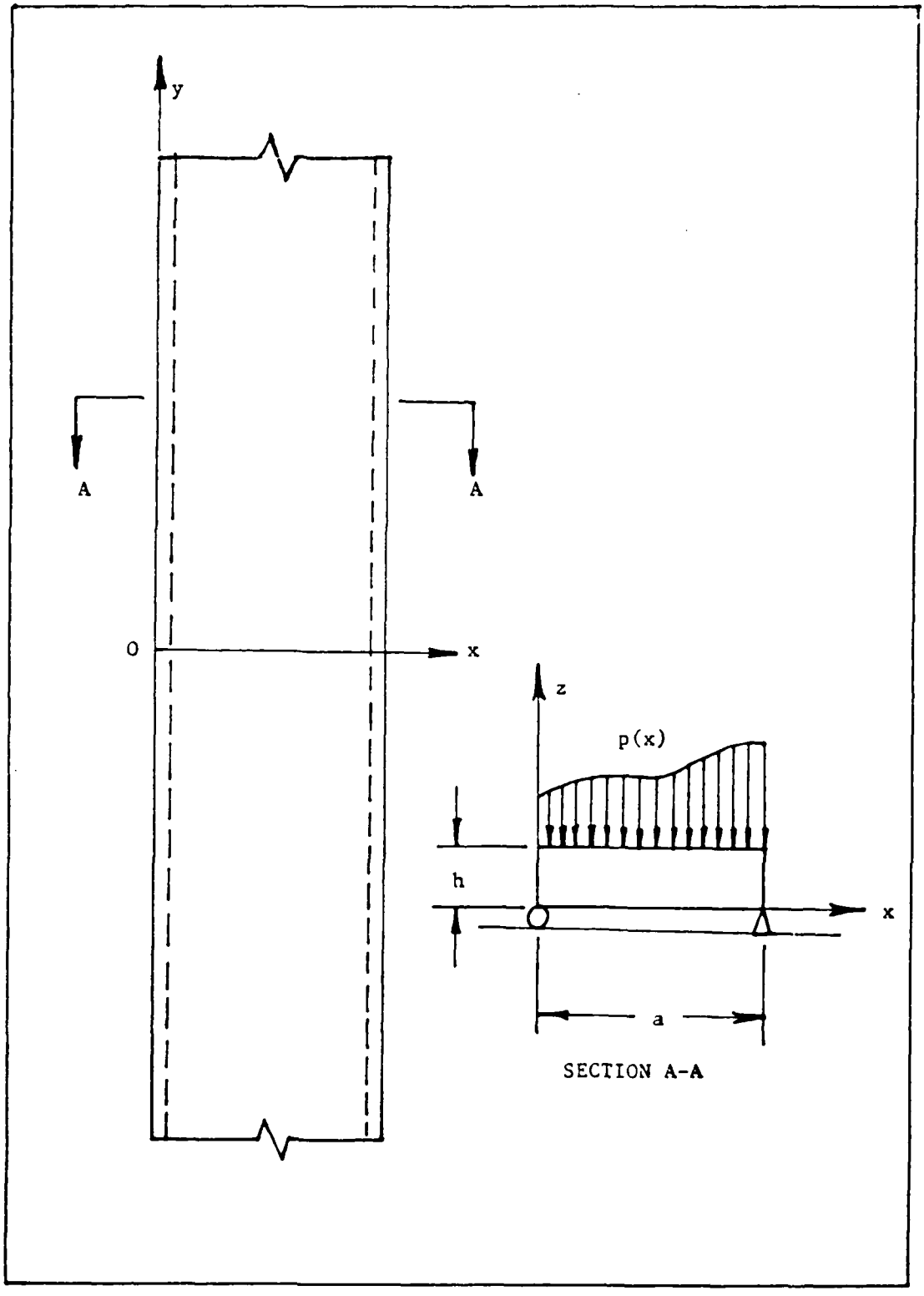

Fig. 7 Plate Strip Problem

The plan of action was to see how the cubic theory compared with the parabolic theory. This was accomplished by solving the thin isotropic plate strip problem using the constant strain triangle. Improvements on the results were expected when the 4-noded and 8-noded quadrilaterals were employed, since these elements would permit more bending. The logic of going to a higher order interpolation for the in-plane quantities was suggested in Witt's (30) work. He noted that the transverse shear strains were functions of the derivatives of the in-plane displacements with respect to the z coordinate and the derivatives of the transverse displacement with respect to the x and y coordinates. Since u and v varied quadratically with respect to z, their derivatives were linear. Since w varied linearly with respect to x and y, that derivative was always a constant. Therefore, he argued that no matter how small he made his element, the transverse strains would never go to zero, and thus there would always be this shear penalty as the plate got thinner.

The material properties for the plate strip were:

$$E = 3.0 \times 10^{7} \text{ psi}$$

$$\nu = 0.25$$

$$h = 0.2 \text{ inches}$$

$$a = 10 \text{ inches}$$

The analytical solution for this problem was determined from Fourier analysis using Navier's method. The maximum (w) was readily found to be: (55)

$$w_{max} = \frac{4P_0 a^4}{\pi^5 D} \sum_m \frac{1}{m^5} \sin \frac{m\pi}{2} \quad (m = 1, 3, 5 \cdots) \qquad (114)$$

where $D = Eh^3/[12(1-\nu^2)]$.

A two-layered finite element convergence study was performed to observe the way the elements responded to the given load. Fig. 8 shows the various finite element arrangements used. Note that the symmetry of the problem was exploited to limit the size of the problem. Note, also that in each case considered, the aspect ratio of the elements was kept equal to unity. This was done by keeping the dimension (b) in the y-direction equal to the length of each element in the x-direction. Such a technique was possible because of the "strip" nature of the problem.

The boundary conditions imposed in each case were: (see Fig. 8)

1. at x=0:

$v = 0$

$u = 0$

$v_{,z} = 0$

$w = 0$

2. at x=a/2:

$u = 0$

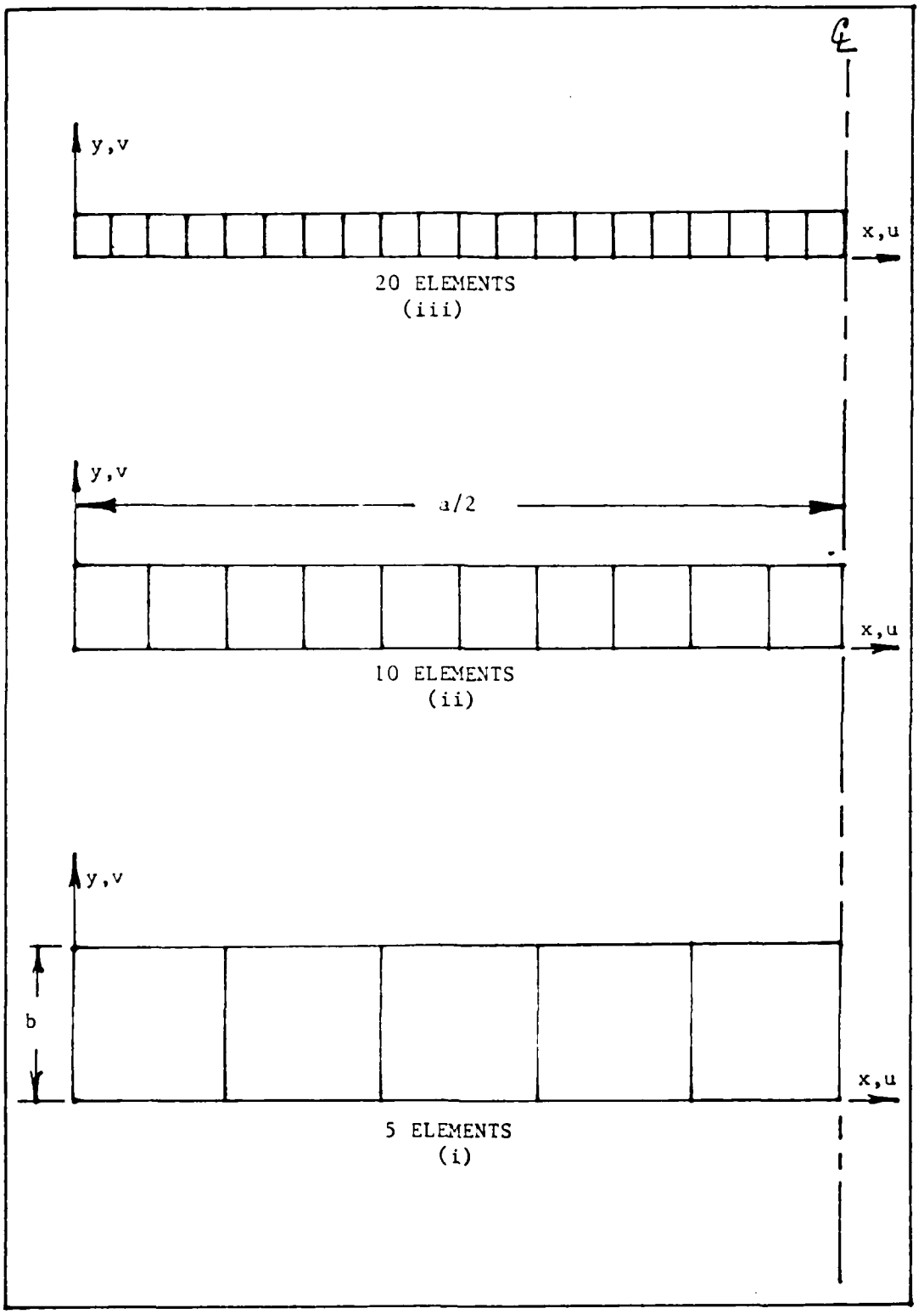

Fig. 8 Finite Element Models of Plate Strip Problem

$$v = 0$$

$$u_{,z} = 0$$

$$v_{,z} = 0$$

3. at $y=0,b$:

$$v = 0$$

$$v_{,z} = 0$$

The 3-noded (constant strain), 4-noded (bi-linear), 8-noded (bi-quadratic) elements were studied in this fashion. In each case, two sampling points were used to perform the integrations in the z-direction of each layer (see Fig. 6). Since there were two layers, this meant integrations through the thickness were performed with 4 sampling points. The sampling in the (ξ) and (η) directions were varied to observe the reactions of the elements to different integration schemes. For the constant strain and bilinear elements 1 x 1 and 2 x 2 schemes were employed, while for the quadratic element, 2 x 2 and 3 x 3 schemes were used. Figs. 9-11 present the results of this convergence study.

In Fig. 9, one sees the results for the constant strain triangle. Note that the present theory, when used in conjunction with the 2x2 integration scheme, virtually duplicates the results obtained by Witt. The only

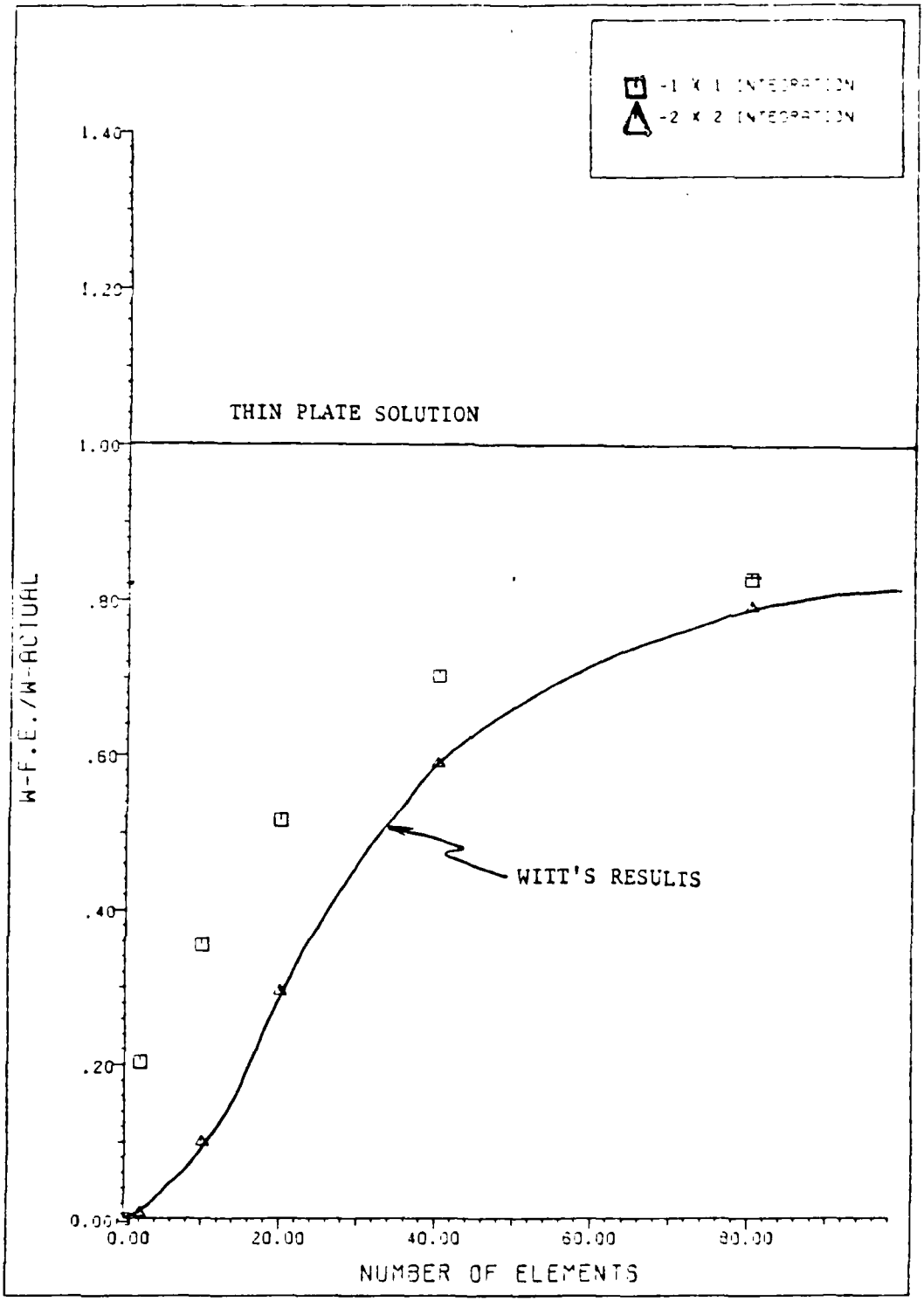

Fig. 9 Convergence of 3-node Elements--Isotropic Plate

difference is that in Witt's work, two pseudolayers were used to model each of the two lamina, where the present method uses no pseudolayers. In other words, the present theory using two lamina appears equivalent to Witt's method using 4 lamina. Note that the 1x1 point integration scheme converges more quickly early on. This is to be expected as the 1x1 scheme represents a "reduced" (48) integration for the constant strain triangle. The 2x2 scheme, on the other hand represents an "exact" integration method. Both integration schemes suffer from the same drawbacks as did Witt's 3-noded element. That is, the finite element solution converges very slowly towards the analytical results. The best solution for this case was 82% of the analytical solution obtained with 80 elements using the 1x1 integration scheme. Although both of the schemes would continue to converge to the exact solution, the rate of convergence becomes slower and slower and, therefore, the study was terminated.

Fig. 10 shows the comparisons obtained for the bilinear element. Note, again, that the 1 x 1 integration scheme appears to converge to the thin plate solution very quickly early on when compared to the 2 x 2 scheme. Again, as with the triangle, this is to be expected as the 1x1 scheme is a reduced integration method.(48) There was a marked improvement in the convergence of this element over

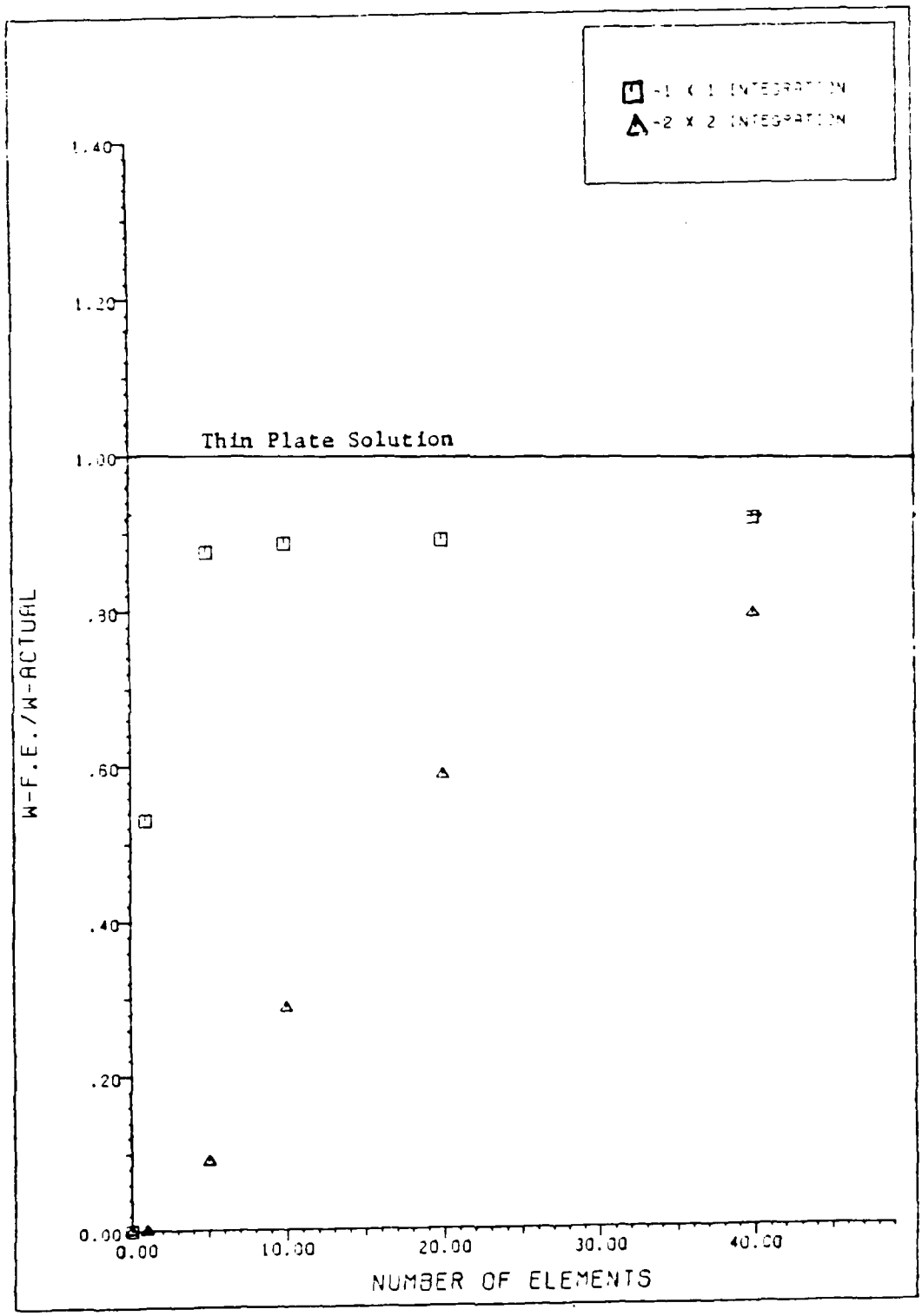

Fig. 10 Convergence of 4-node Elements--Isotropic Plate

the constant strain element and Witt's triangular element. The best solution acquired was 92% of the analytical results, obtained using 40 elements with 1 x 1 integration. A direct comparison with the triangular element can be made because the same number of nodal points (and thus degrees of freedom) were used in both cases. Again, however, the convergence was very slow, and a prohibitive number of elements would be required to obtain 100% of the analytical solution.

The results obtained with the 2x2 integration scheme on the 4-noded element are virtually identical to those obtained with the 2x2 integration on the triangular element. This leads to the conclusion that any improvement hoped for by employing the quadrilateral element would only be realized when used in conjunction with the 1x1 integration scheme.

The results for the 8-noded biquadratic element are displayed in Fig. 11. The best results in this case were obtained by using 2 x 2 integration. Again, about 92% was the best this element could do with the isotropic problem. The 3 x 3 integration scheme fell far short of approaching either the 2 x 2 scheme or the analytical solution. This method appeared to level out at about 74% of the analytical solution--18% below the 2 x 2 method. The 3 x 3 scheme represents a full integration method which has been shown by other authors (for instance Cook (36)) to cause this

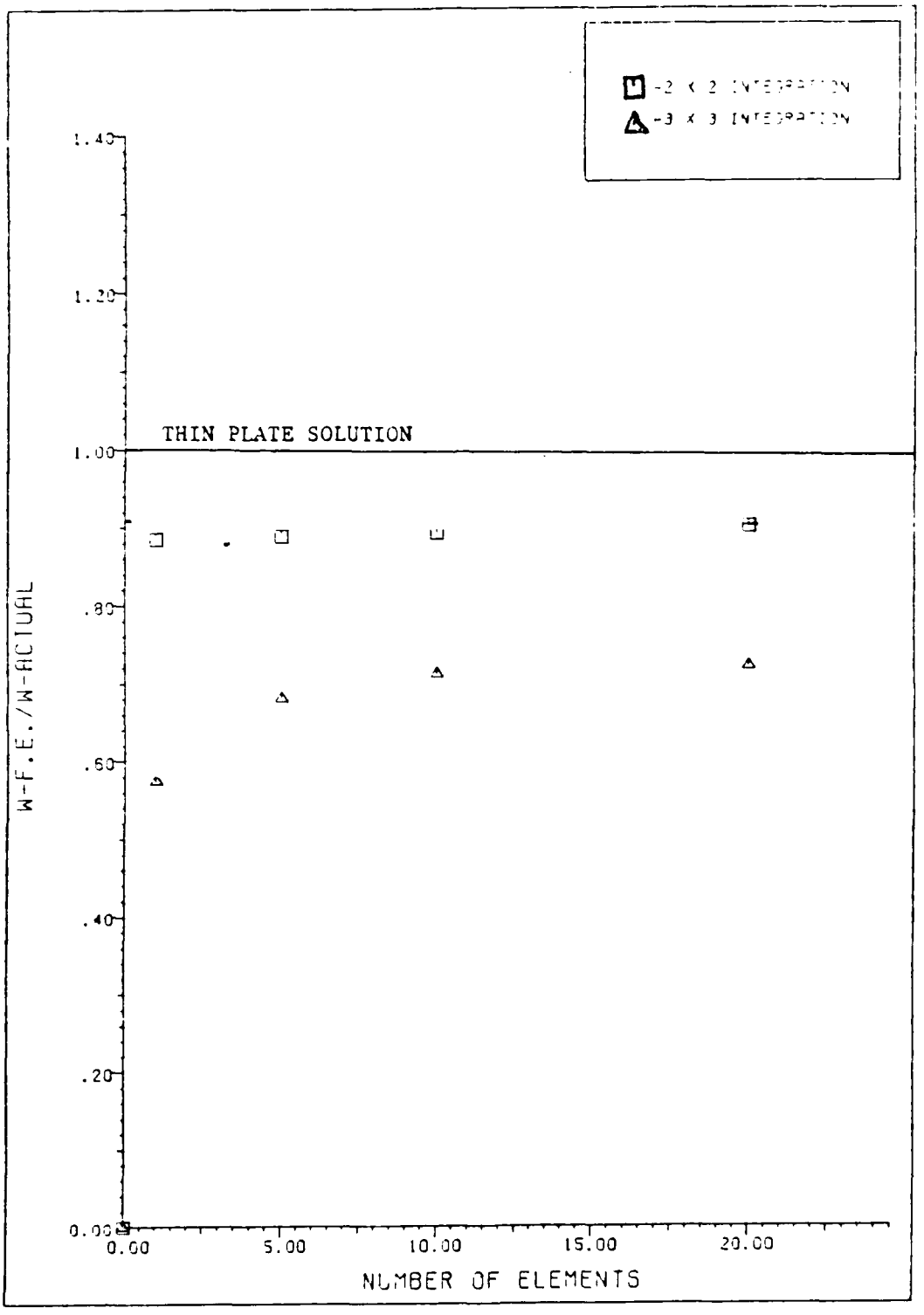

Fig. 11 Convergence of 8-node Elements--Isotropic Plate

difficulty as the plate thickness is reduced.

Since the 2x2 integration scheme is a reduced method of integration for the 8-noded quadratic element, the results observed in Fig. 11 are not surprising. When the reduced integration scheme of the 8-noded element is compared with the reduced scheme for the 4-noded element, one sees that they are nearly identical. This leads to the conclusion that improvements in performance in solving the isotropic problem are a result of the reduced integration and not necessarily a result of the higher order interpolation function for the reference surface displacements.

It should be stressed, however, that in each case where Witt used pseudolayers the present method used none. This means comparable results were obtained in each case using full integration while using fewer degrees of freedom than Witt. In the cases where reduced integration was used, results better than Witt's were obtained. Also, since only one fourth as many integration points were used for the reduced scheme, those solutions were obtained with about one fourth the computer time of the full integration scheme.

In every case, an attempt was made to obtain a better solution by increasing the number of layers. That is,

pseudolayers were tried. The use of these pseudolayers is comparable to increasing the number of elements in the z direction. In every case, increasing the number of layers made neglibile improvement.

A review of the literature (51,52) shows that this failure of the "thick-plate" element to converge to the "thin-plate" solution is common. These "thick plate" theories are essentially of the Mindlin type where the normal to a reference surface before deformation remains straight but not necessarily normal after deformation. These assumptions lead to stiffness matrices which characterize bending independent of the transverse shear effects. The difficulty encountered by these elements as the plate becomes thin is that the shear stiffness matrix remains too stiff. Normally, this is looked upon as a "penalty" and a number of techniques are formulated which attempt to reduce the penalty. The methods of penalty reduction involve reduced or selective integration or formulation of a penalty function which is essentially a multiplier on the shear stiffness matrix which approaches zero as the plate thickness is reduced. The failure of the thick plate element to converge to the thin plate solution has been attributed to the "locking" phenomena.

The present formulation is not of the Mindlin type

since reference surface normals are allowed to deform after loading. Furthermore, the derivation of the stiffness matrix is carried out from an elasticity point of view. The stiffness matrix is not characterized by a bending part and a shear part.

The thin-plate solution is a result of Kirchhoff's hypotheses which neglect both the direct strain ϵ_z and the shear strains γ_{xz}, γ_{yz}. In addition, the normal stress is assumed small compared to σ_x and σ_y so that it is neglected in the stress-strain relations. These assumptions lead to a theory which is based on only the transverse displacement w. In the present work, the direct transverse strain is neglected, but the shear strains are not. The problem is not reduced as is the classical thin plate problem. The effects of the transverse shear terms are always present.

An attempt was made to find a method for reducing the effects brought about by the shear strains. The method arrived at was to lower the magnitudes of the shear modulli G_{13}, and G_{23}. This reduction resulted in a softening of the element and a convergence to the thin-plate solution. Fig. 12 shows the effects of varying the reduction factor. The vertical axis shows the choices for factors to use to multiply G_{13} and G_{23}. The horizontal axis shows the resul-

tant maximum w displacement for the isotropic strip problem. Note that the thin isotropic plate solution (w=1) is obtained when a multiplication factor of 1/100 was used.

Looking back at the "locking" problem and methods which have been used to eliminate the locking, one sees that in each case there was an attempt to soften the element in some way so as to eliminate the effects of transverse shear. In effect, what was being done was to artificially reduce the effects of G13 and G23 on the solution of the problem. The present work takes a less artificial and more direct approach to the problem. Since the element was designed for a thick structure, the three dimensional effects had to be considered. Direct transverse stress and transverse shear strains were always considered. The only way to reduce their effects was through the constitutive relation [D].

Since this case was that of a thin isotropic plate (S=a/h=50), it lent itself well to observing the way a normal line segment would deform under the load. A thin plate line element normal to the reference surface should come close to duplicating the assumptions of Kirchoff's hypothesis. That is, the normal should remain straight and perpendicular to the reference surface. Fig. 13 is a plot of u vs. z, which shows that Kirchhoff's hypothesis is

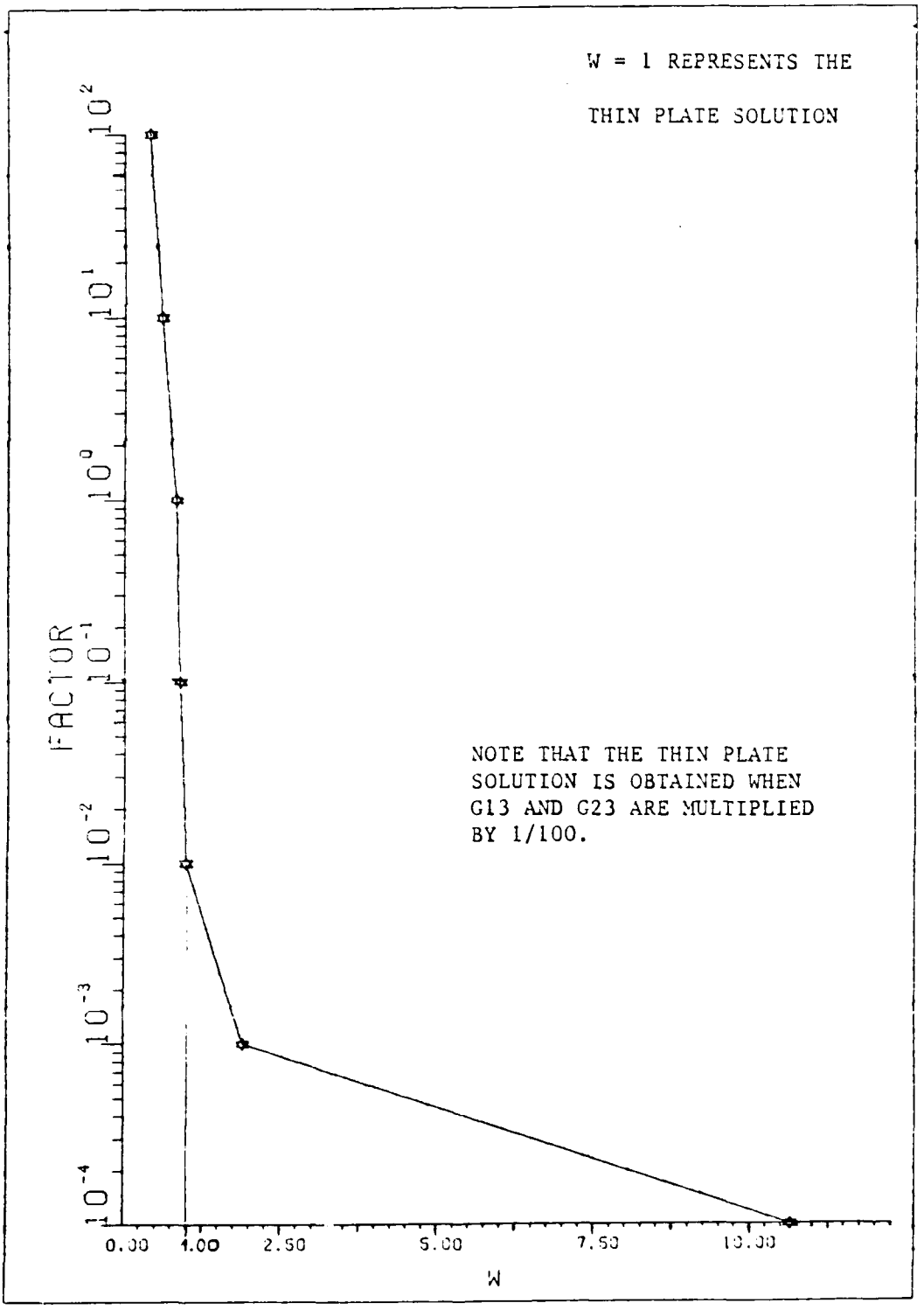

Fig 12 Multiplication Factor for G13 and G23--Isotropic

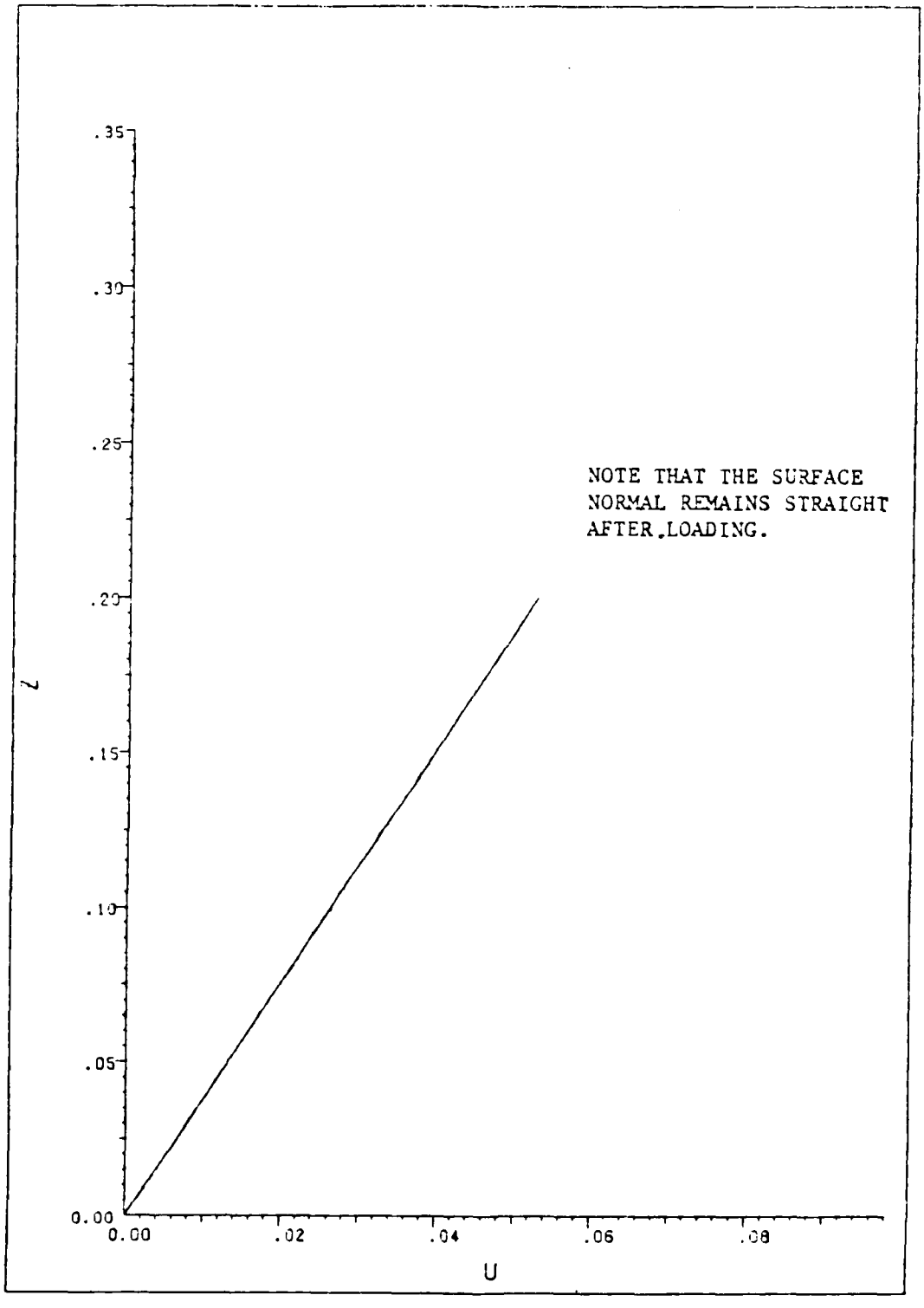

Fig. 13 Check of Kirchhoff's Hypothesis--Isotropic Plate

being met by the cubic assumption for u in the z-direction. The rotations $\langle \phi_i \rangle$ are such that the normals do indeed remain straight and normal after loading.

The second case studied was identical to the first, except that orthotropic materials were used for the two layers. The plies were oriented at 0 deg. and loaded uniformly at 163.84 psi. The material properties used were:

$$E_1 = 2.5 \times 10^7 \text{ psi}$$

$$E_2 = 1.0 \times 10^6 \text{ psi}$$

$$(\nu_{12}) = 0.25$$

$$G_{12} = 5.0 \times 10^6 \text{ psi}$$

$$G_{13} = 5.0 \times 10^6 \text{ psi}$$

$$G_{23} = 2.0 \times 10^6 \text{ psi}$$

$$h = 0.2 \text{ inches}$$

$$a = 10.0 \text{ inches}$$

The analytical solution for this problem was determined as before. The only difference being that $D=Q_{11}h^3/12$ where $Q_{11} = E_1^2/[E_1 - \nu_{12}^2 E_2]$.

Figs. 14-16 show the convergence study carried out for the elements of interest. In nearly each case, convergence to the exact solution was obtained. Note, also, that in each case, the reduced integration scheme converged more

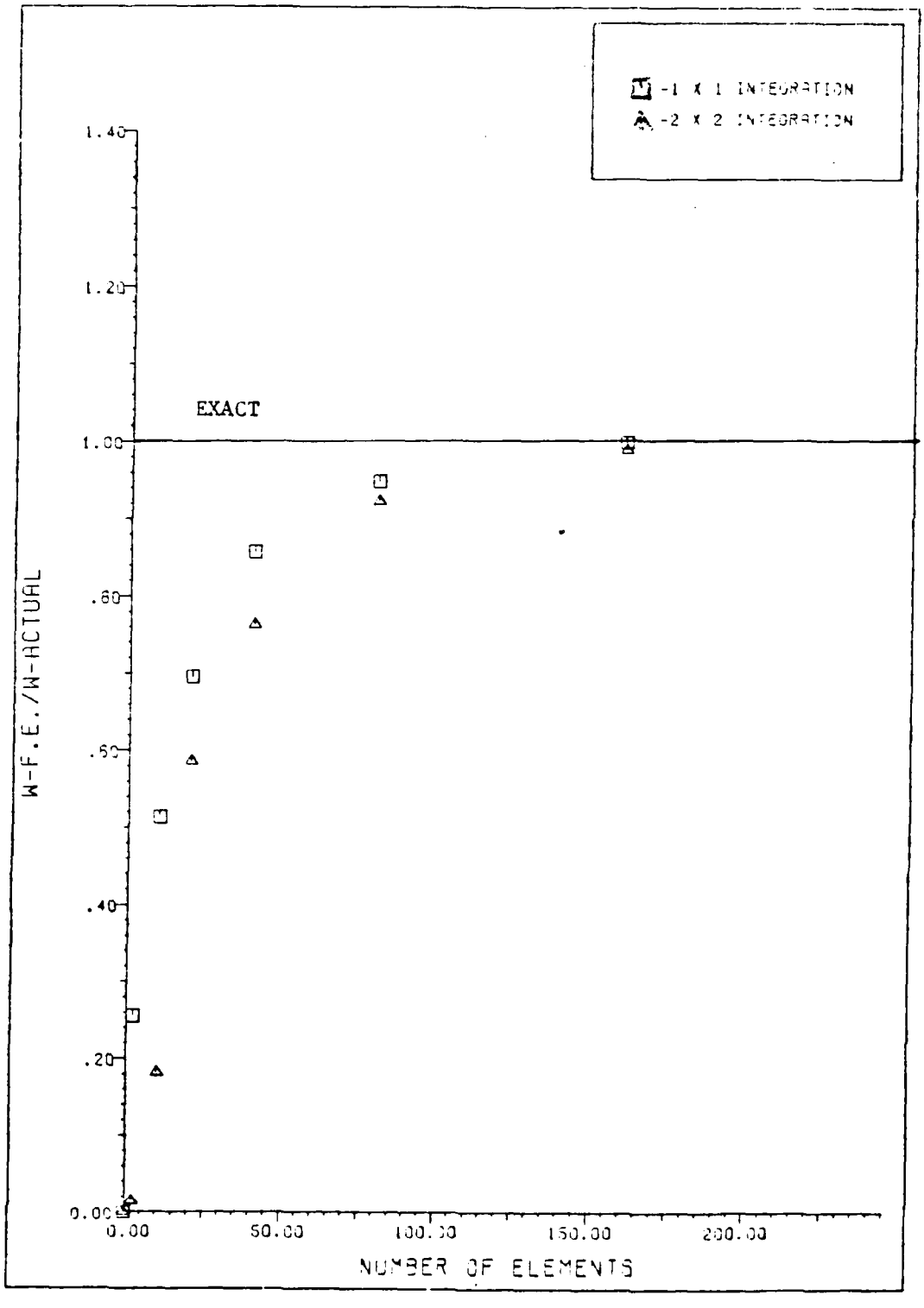

Fig. 14 Convergence of 3-node Elements--Orthotropic Plate

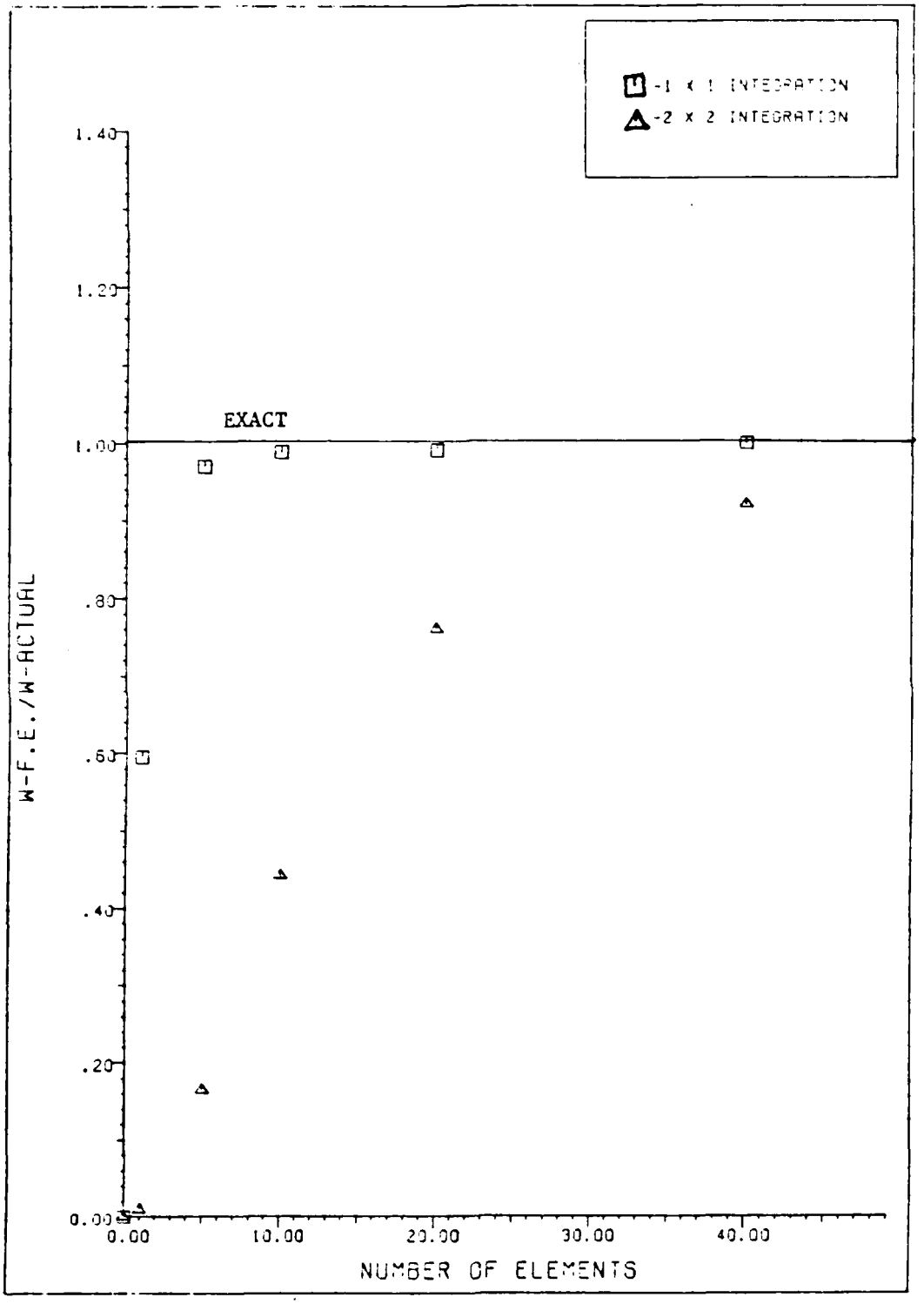

Fig. 15 Convergence of 4-node Elements--Orthotropic Plate

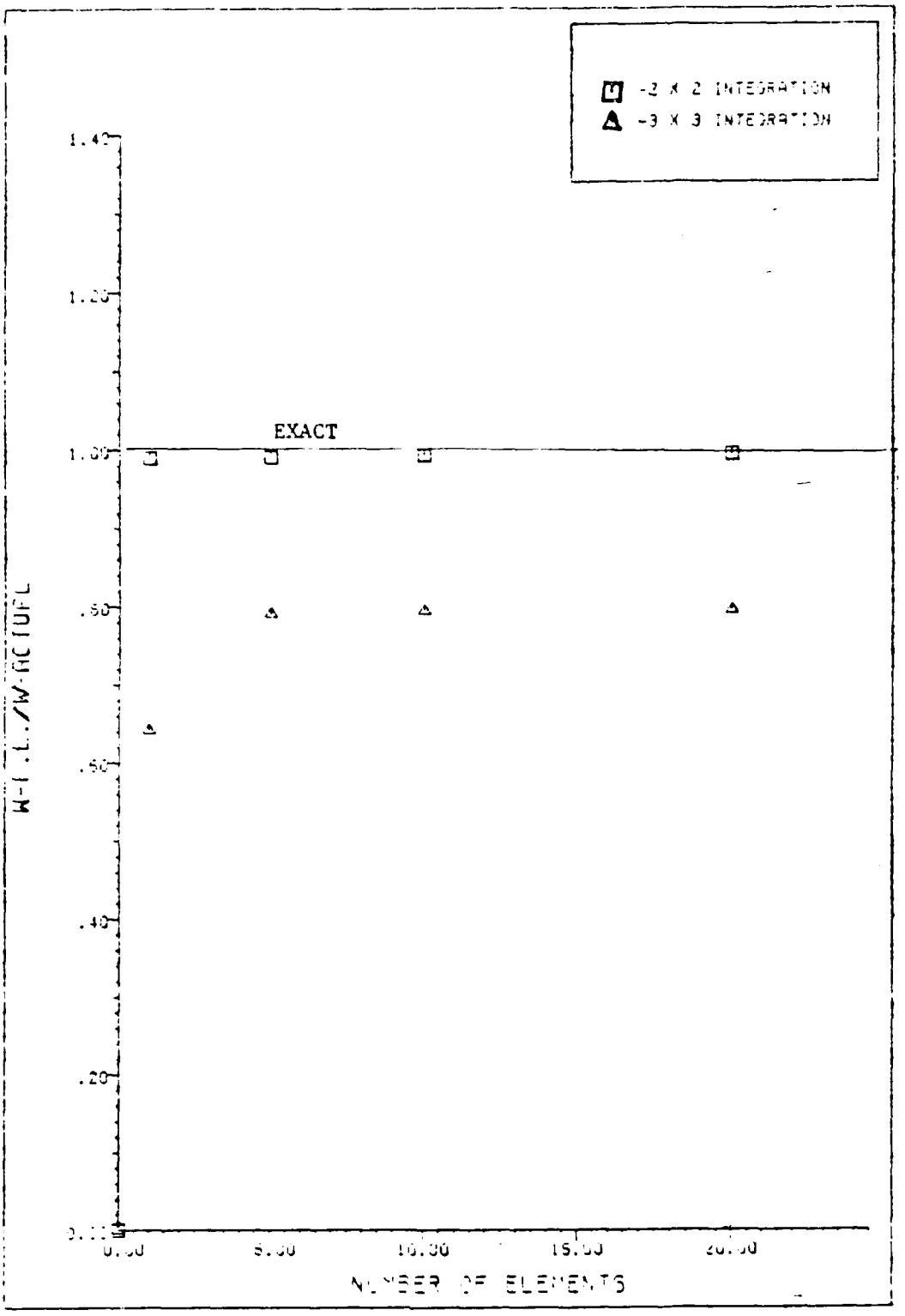

Fig. 16 Convergence of 8-node Elements--Orthotropic Plate

rapidly than the full integration scheme. In the cases of the 3-noded and 4-noded elements using full integration, the convergence to the thin plate solution was obtained only when the dimensions of the elements were reduced to about one third of the thickness of the element. This is totally unacceptable from a practical standpoint and led to the conclusion that for this thin plate problem reduced integration of the 3-noded or 4-noded element was imperative.

The only case which did not converge was that of the quadratic element using 3 x 3 integration. As with the isotropic problem, the element again appeared to converge to a solution which was nearly 20% below the solution obtained by the 2 x 2 scheme and the exact solution. The 3x3 integration scheme appears to make the 8-noded element too stiff. This problem seems to be common with the 8-noded element and is referred to specifically in reference (56).

The choice of element is always left to the discretion of the user. It appears, however, that the 8-noded element with 2X2 integration is the most desirable based on this convergence study. Even a single element produced results which were 99% of the exact solution.

As with the isotropic case, u vs z was plotted at x=0

in order to observe the deformation of the normal. Fig. 17 shows that the normal remained undeformed and normal to the reference surface. This was in accord with the expectations of the author since the plate was thin (S=50) and the plies were both oriented at 0 degrees.

The third case studied was again cylindrical bending of a strip plate. This time, however, different ply lay-ups were studied in order to observe the element's performance for symmetric as well as asymmetric problems. Comparisons were made with analytical results obtained by Pagano (7). More specifically, three ply lay-ups were examined--(0,0), (0,90), and (0,90,0). The material properties used in the previous case were also employed here. For this case, however, the loading was changed from uniform to sinusoidal. That is,

$$p(x)=p_0 \sin(\pi x/a) \qquad (115)$$

$$p_0=162.755 \text{ psi}$$

The reason for choosing sinusoidal load was to check the solution against Pagano's (7) solution. Additionally, this provided a check on the ability of the program to handle a more complex loading situation.

The finite element arrangement shown in Fig. 8(i) was

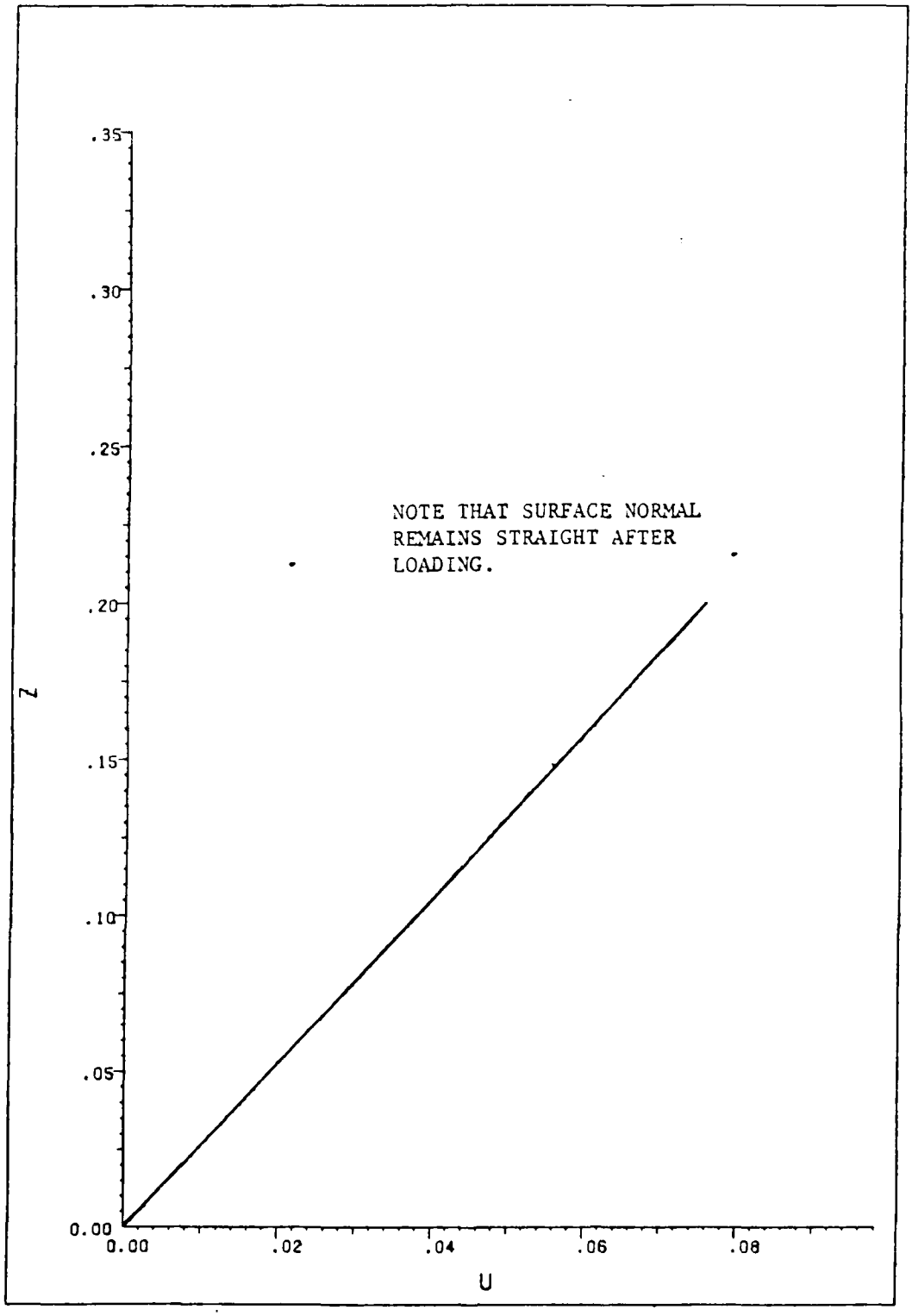

Fig. 17 Check of Kirchhoff's Hypothesis--Orthotropic Plate

used for this case. That is, five 8-noded elements were used, and 2X2 integration was employed. The boundary conditions were the same as in previous cases.

The element's response to the problem of plates of various thicknesses was of interest. In order that the reader may better visualize the plates and gain a perspective of "thickness", refer to Fig. 18. This represents values for S=a/h from 50 to 4. S=10 is considered (for orthotropic plates) to be a thick plate, because the effects of shear stress result in displacements which are much greater than predicted by the classical laminated plate theory.

Figs. 19--21 are plots of $\bar{w}$ vs. S for the various ply orientations, where $\bar{w}=[100E_2h^3/(p_0a^4)]w_{max}$. These figures compare the finite element results with those obtained from Pagano's elasticity solution, a finite element solution by Owen (32) and the classical laminated plate theory (CLPT). In each instance, the finite element method duplicated the elasticity results showing that the element has application over a wide range of thicknesses for orthotropic plate problems. The figures also serve to amplify the statement made in Chapter I that the transverse shear deformations must be considered when analyzing thick composite plates.

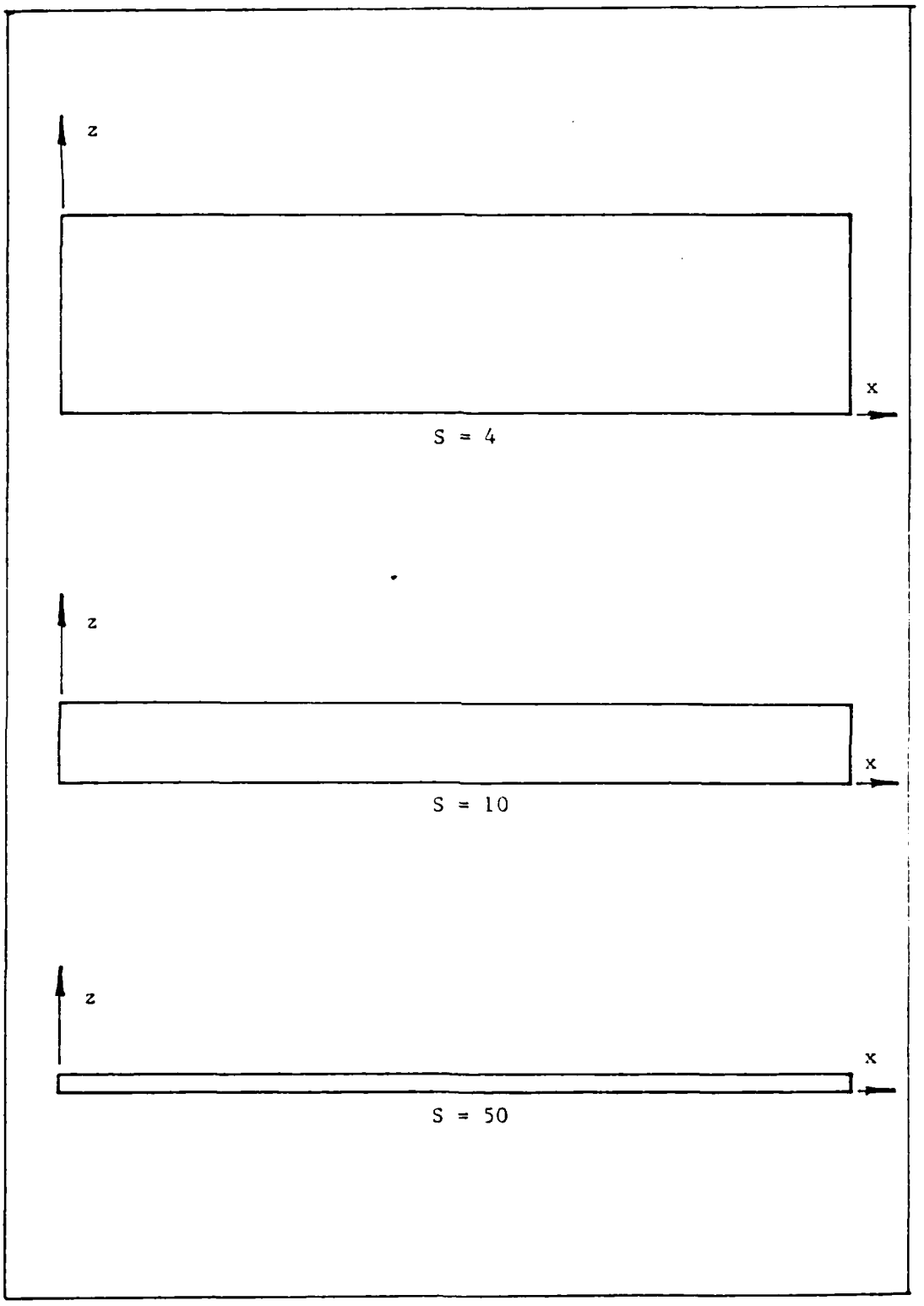

Fig. 18 Visualization of the Thickness Parameter S

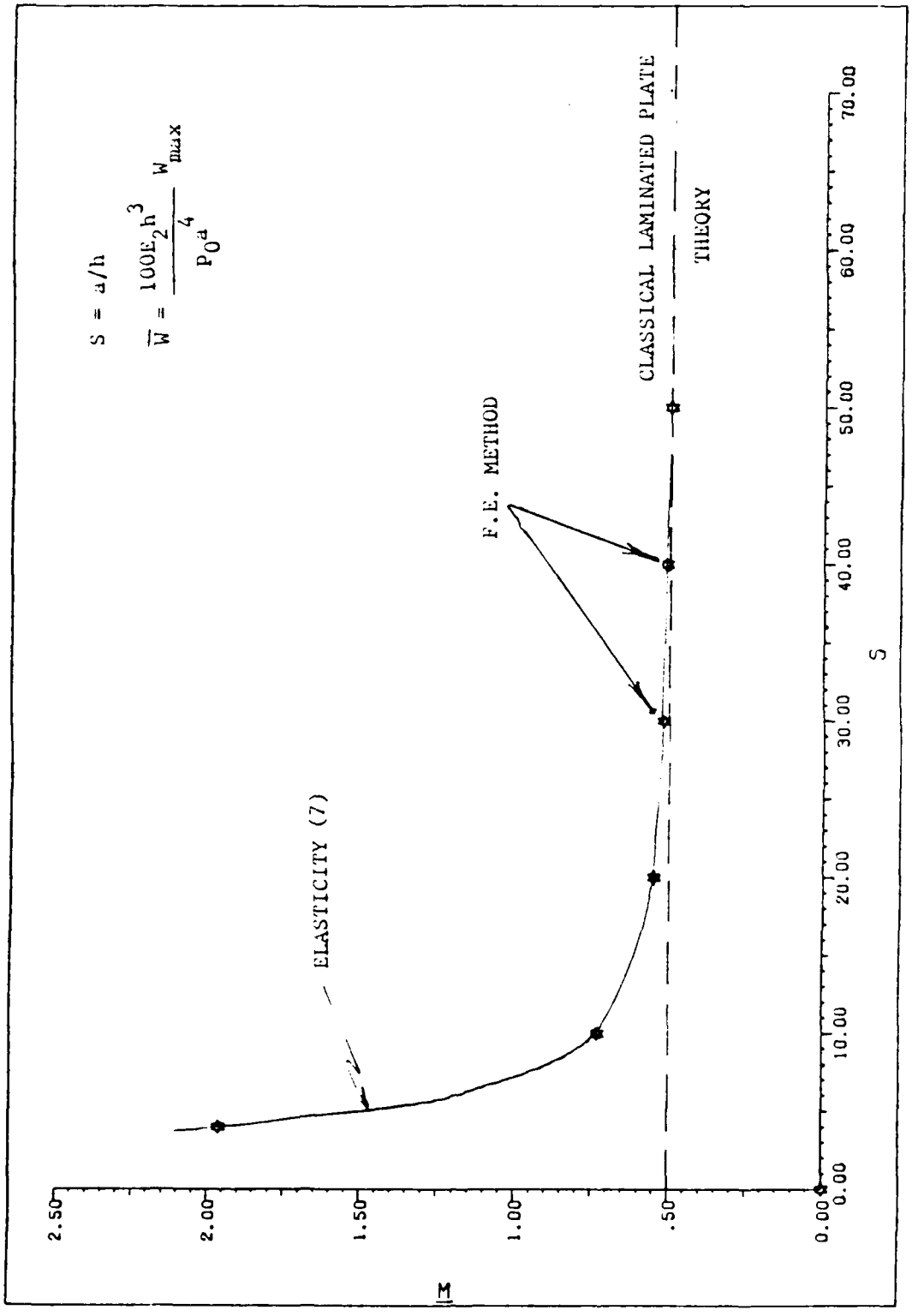

Fig. 19 S vs $\overline{W}$--Fiber Orientation (0,0)

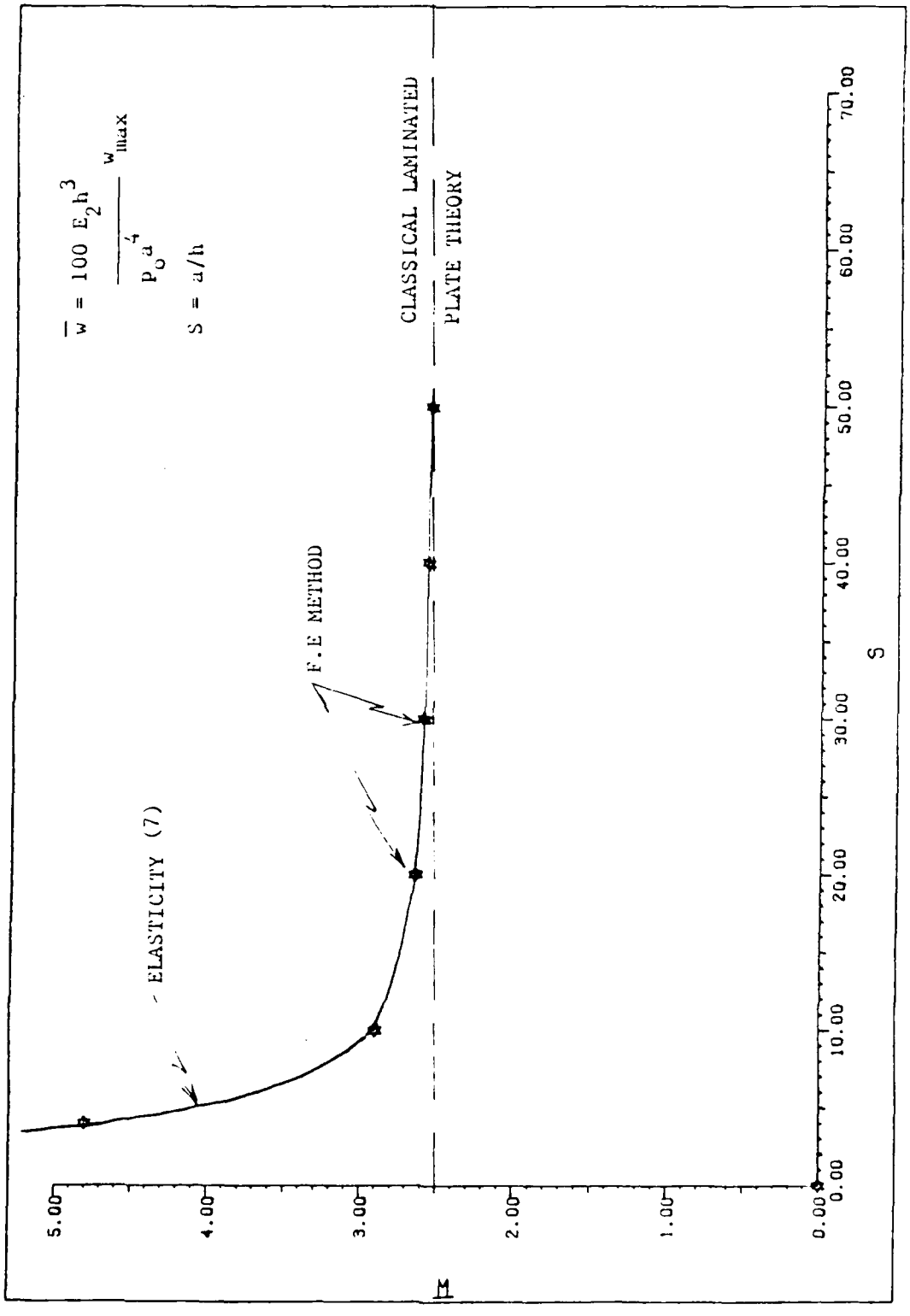

Fig. 20 S vs $\bar{w}$--Fiber Orientation (0,90)

AD-A152 115 THE NONLINEAR ANALYSIS OF THICK COMPOSITE PLATES USING A CUBIC SPLINE FUNCTION(U) AIR FORCE INST OF TECH WRIGHT-PATTERSON AFB OH SCHOOL OF ENGI.. 2/2

UNCLASSIFIED R L HINRICHSEN SEP 84 AFIT/DS/AE/84-2 F/G 12/1 NL

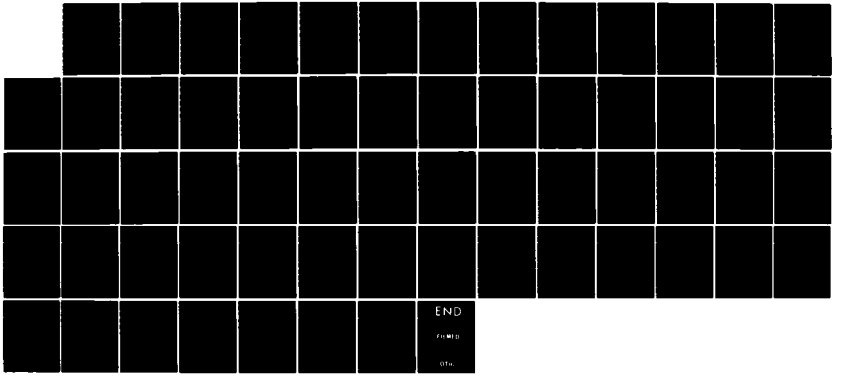

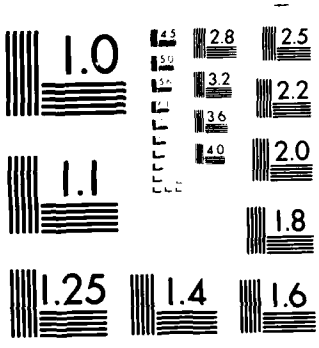

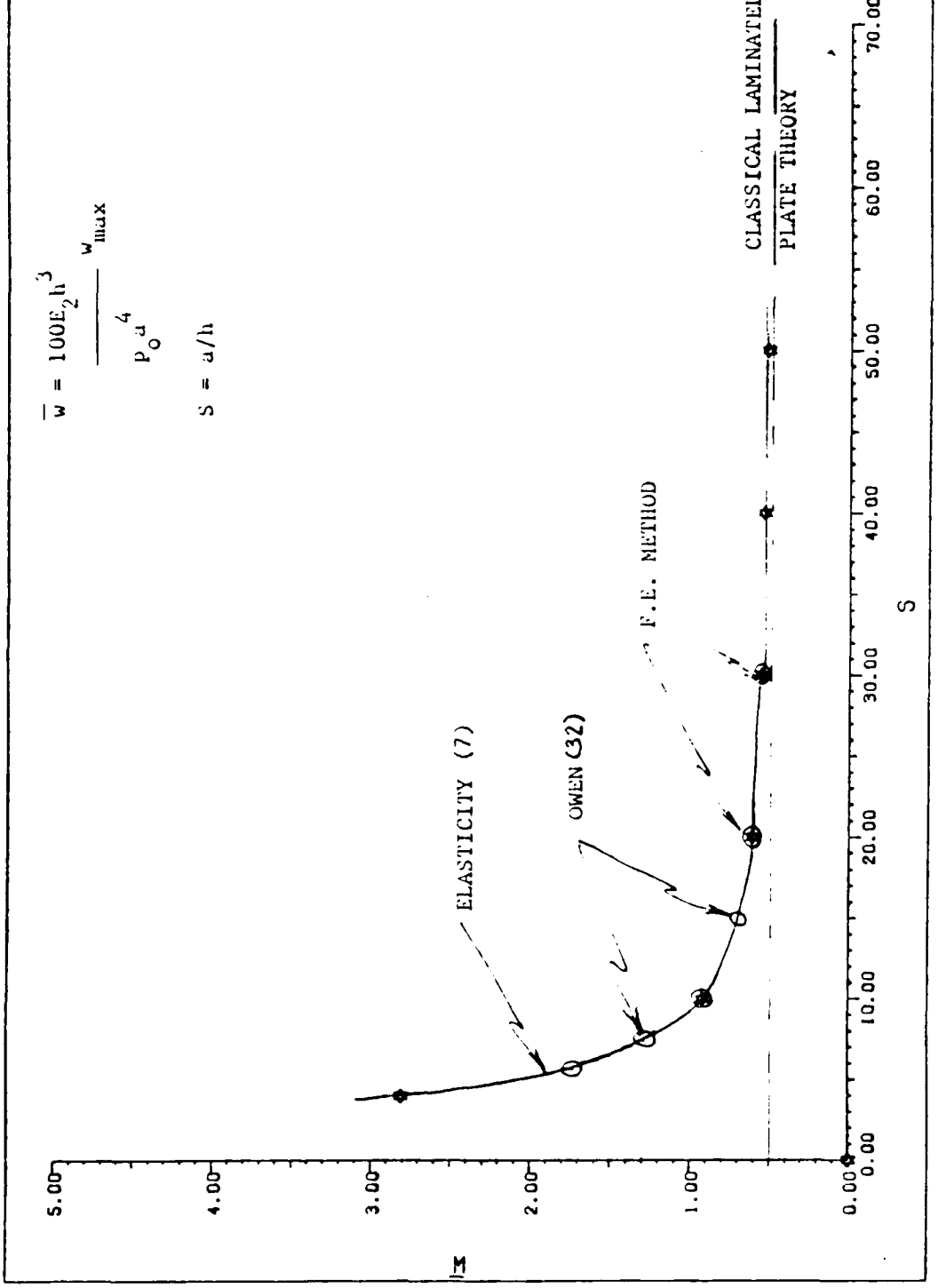

Fig. 21 S vs $\bar{w}$--Fiber Orientation (0,90,0)

To gain a perspective of why the transverse shear deformation becomes more and more important as plate thickness is increased, it is instructive to observe Figs. 22--24 which present plots of $\bar{u}$ vs. $\bar{z}$ at x=0, where $\bar{u}=E_2 u/hp_0$ and $\bar{z}=z/h$.

Fig. 22 displays a very thick (S=4) asymmetrically oriented (0,90) plate. Note that the F.E. method follows very closely the results obtained by Pagano through the elasticity approach. Figs. 23 and 24 show u vs. z for the symmetric ply lay-up (0,90,0). In each case, the finite element method follows the elasticity solution closely. The influence on thickness is readily observed by comparison of these two curves. In the first (S=10), the normal deformation effect due to shear is seen to be quite close to the CLPT solution. As the thickness increased to S=4, the normal deformation became much more apparent and one readily sees how this deformation becomes more important as the thickness is increased.

Figs. 23 and 24 also show the cubic nature of the approximation for u(z). Note particularly the inflection point in the middle ply at $\bar{z}=0.5$. The "smooth" nature of the approximation is also readily observed in these figures. The interlaminar boundary discontinuity of Pagano's solution is not duplicated because of the cubic approxima-

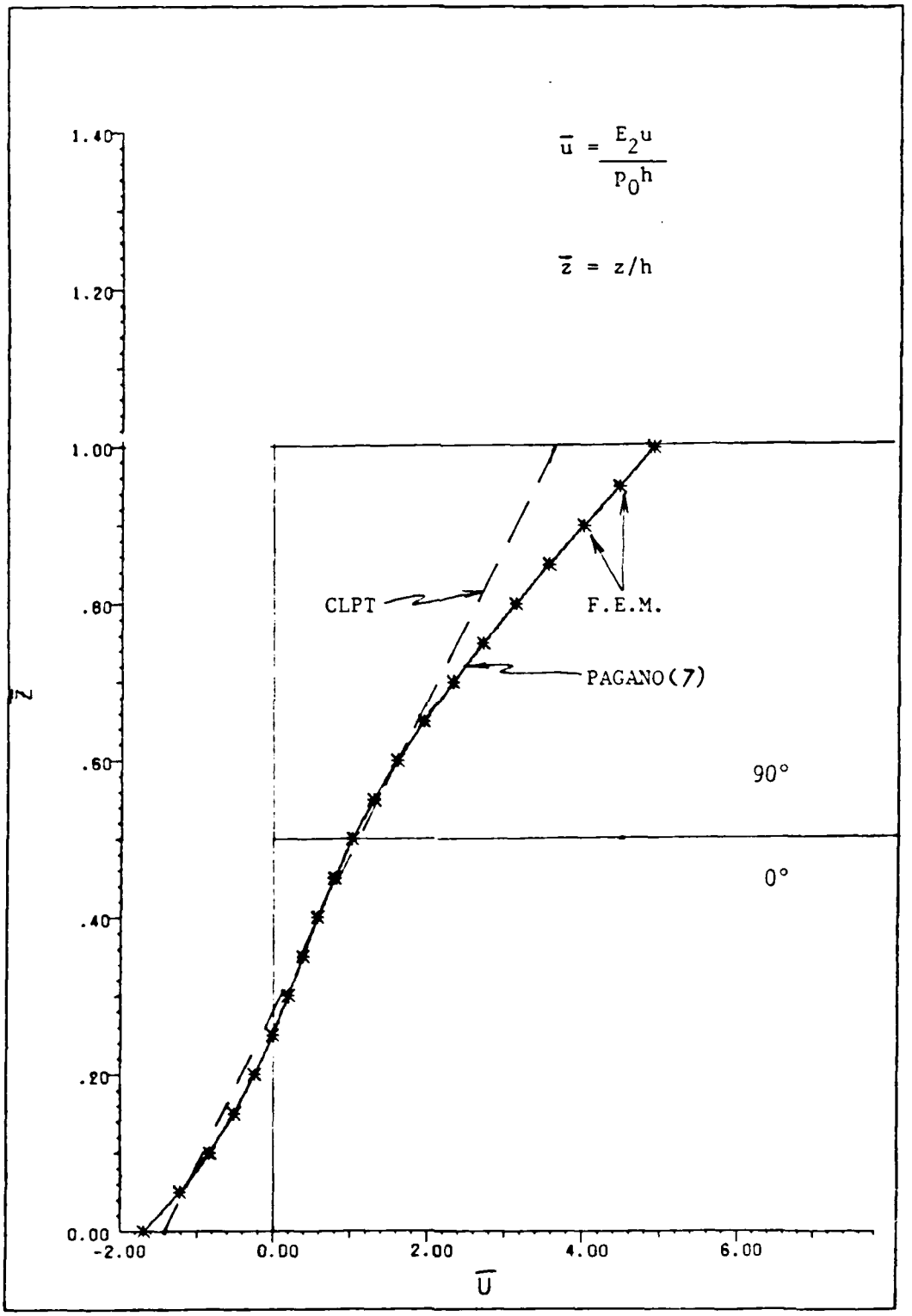

Fig. 22 $\bar{u}$ vs $\bar{z}$--Fiber Orientation (0,90)--(S=4)

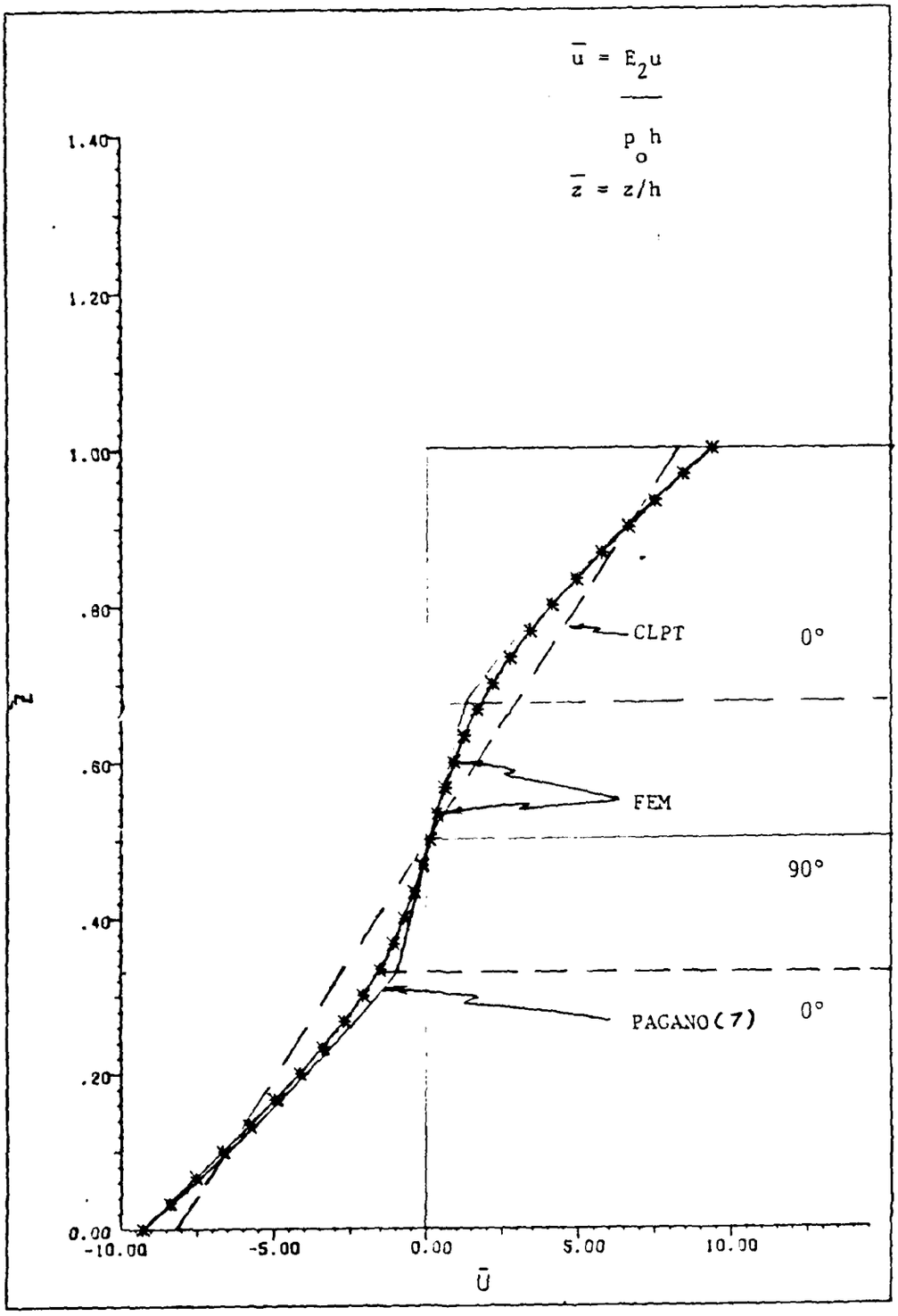

Fig. 23 $\bar{u}$ vs $\bar{z}$--Fiber Orientation (0,90,0)--(S=10)

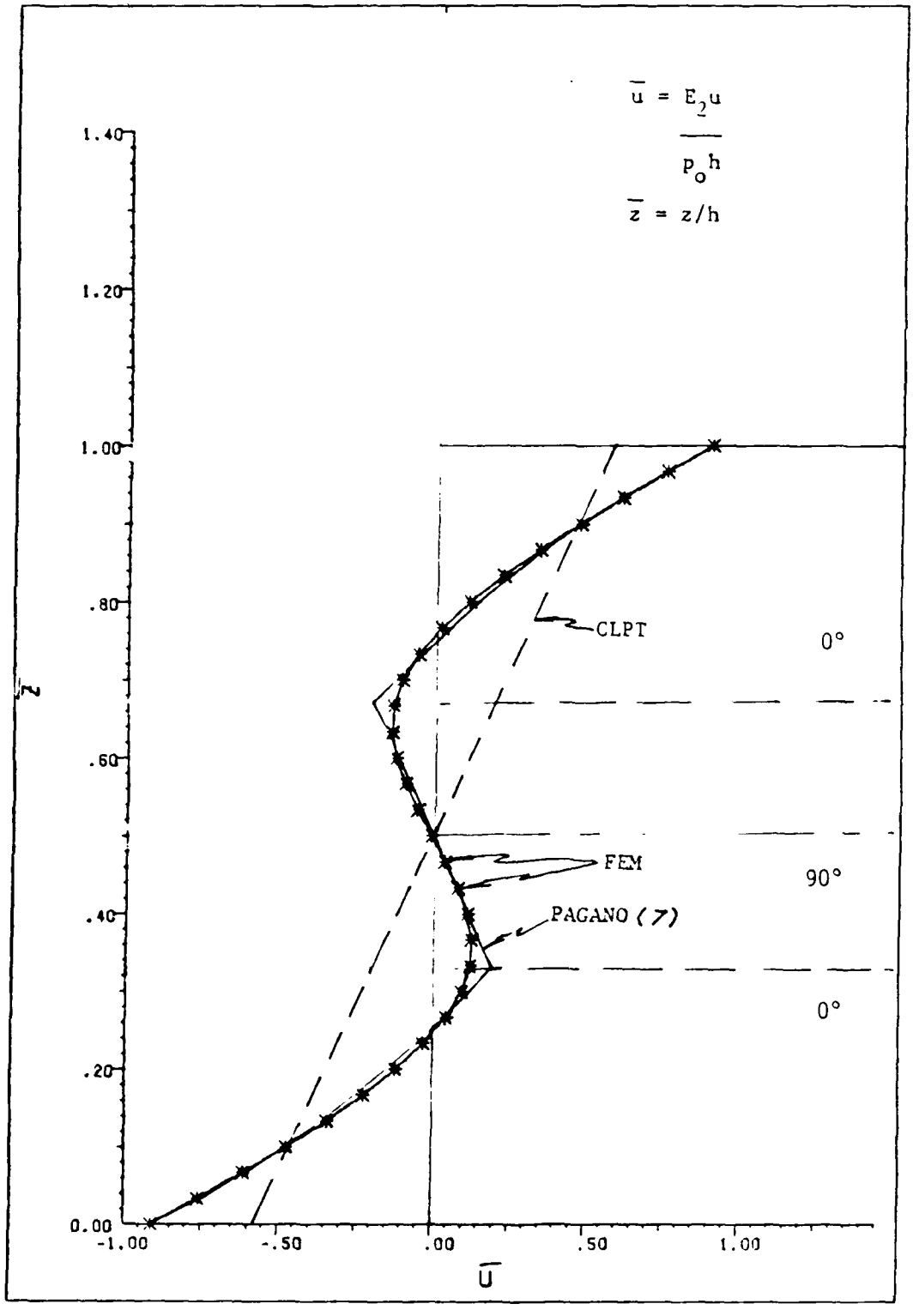

Fig. 24 $\bar{u}$ vs $\bar{z}$--Fiber Orientation (0,90,0)--(S=4)

tion. This smoothing has an impact on the evaluation of $\hat{u}_{,z}$ and thus on (τ_{xz}) near the boundary (as shown in Figs. 26--28).

Figs. 25--28 show plots of $(\bar{\tau}_{xz})$ vs. $\bar{z}$ at x=0 where $(\bar{\tau}_{xz})=(\tau_{xz})/p_0$. In the case of a thick (S=4) two-ply plate with fibers oriented at (0,0), one sees (Fig. 25) that the F.E. values follow quite closely those predicted by the elasticity solution. When the fiber orientation is changed to (0,90), there is a small degradation in the results for the shear near the interlaminar boundary (see Fig. 26). For the 3-ply (0,90,0) cases, Figs. 27--28 show that the F.E. method follows the exact solution well, except at the boundaries. In Pagano's solution, (σ_x), (τ_{xz}), u, and w were kept continuous across the interlaminar boundaries. In this F.E. solution, the continuity is imposed on u and $u_{,z}$ with w constant through the thickness. These differences in boundary conditions at the interfaces account for the differences between the two solutions. In other words, by imposing an assumption for the continuity of the first derivative of u with respect to z at the interlaminar boundries, the theory is seen to violate equilibrium at those discrete points through the thickness where abrupt changes in material properties occur. In terms of the stress resultants which are obtained by integration of the stresses through the thickness, equilibrium is satisfied.

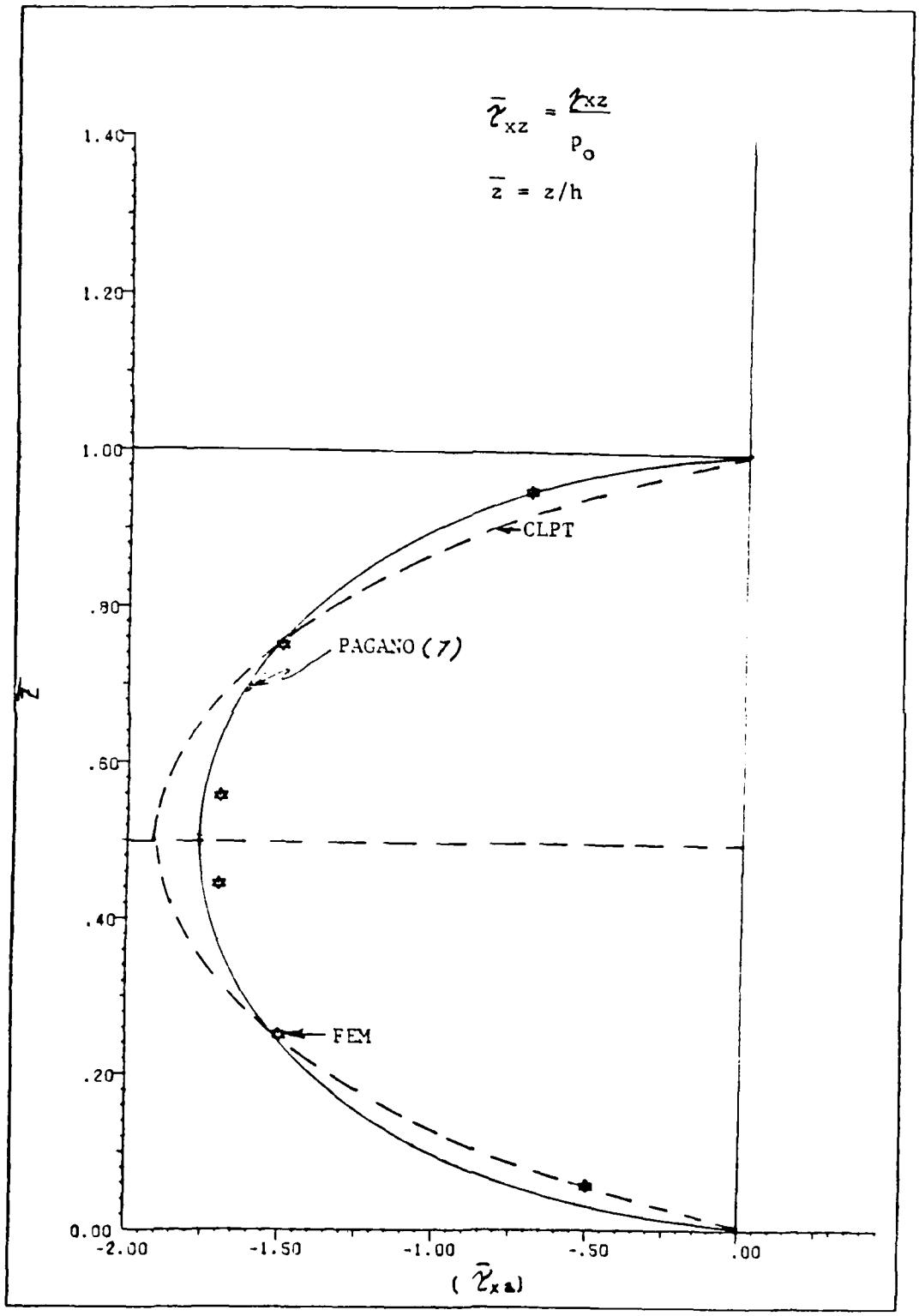

Fig. 23 $\bar{\tau}_{xz}$ vs $\bar{z}$--Fiber Orientation (0,0)--(S=4)

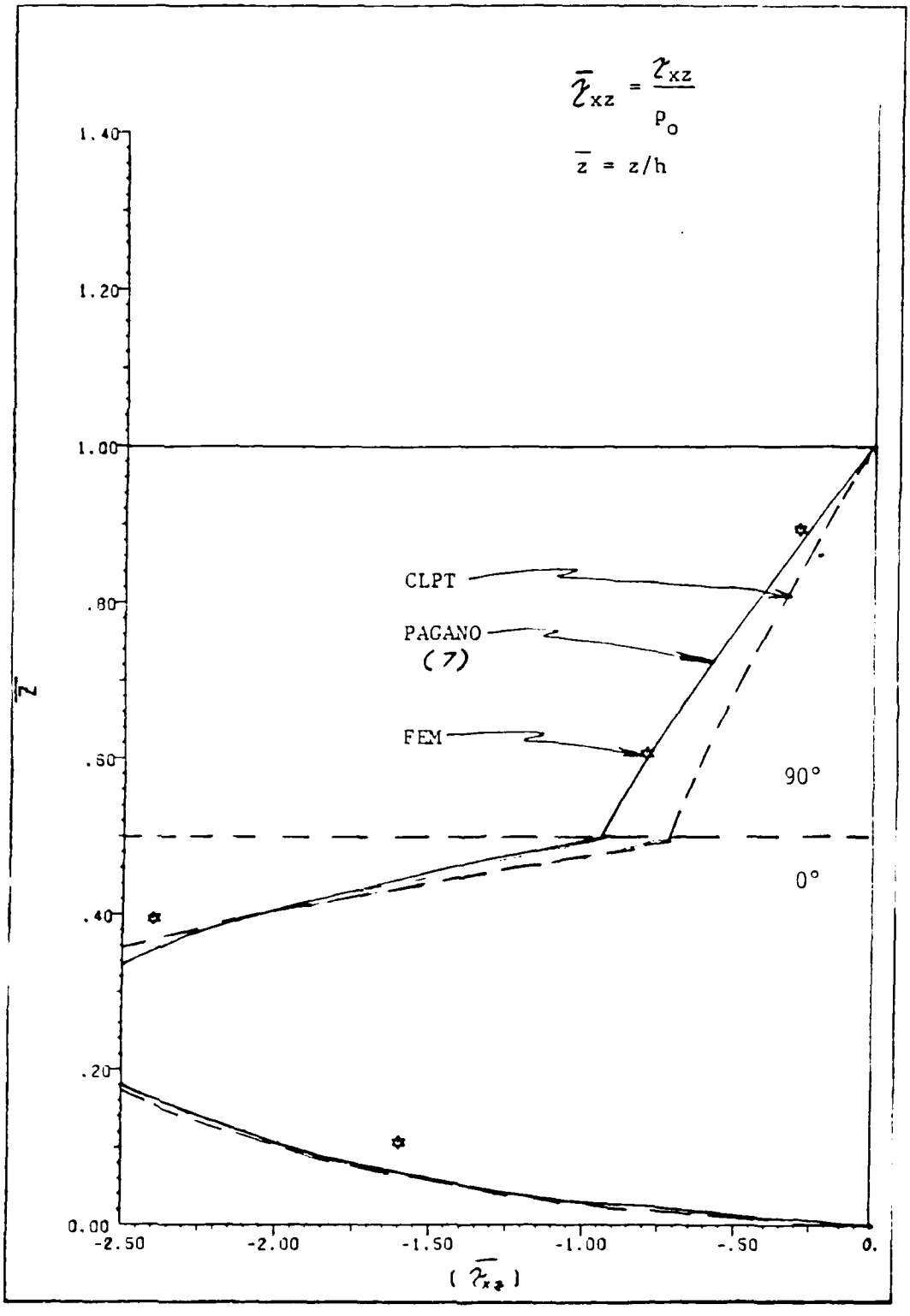

Fig. 26 $\bar{\tau}_{xz}$ vs $\bar{z}$--Fiber Orientation (0,90)--(S=4)

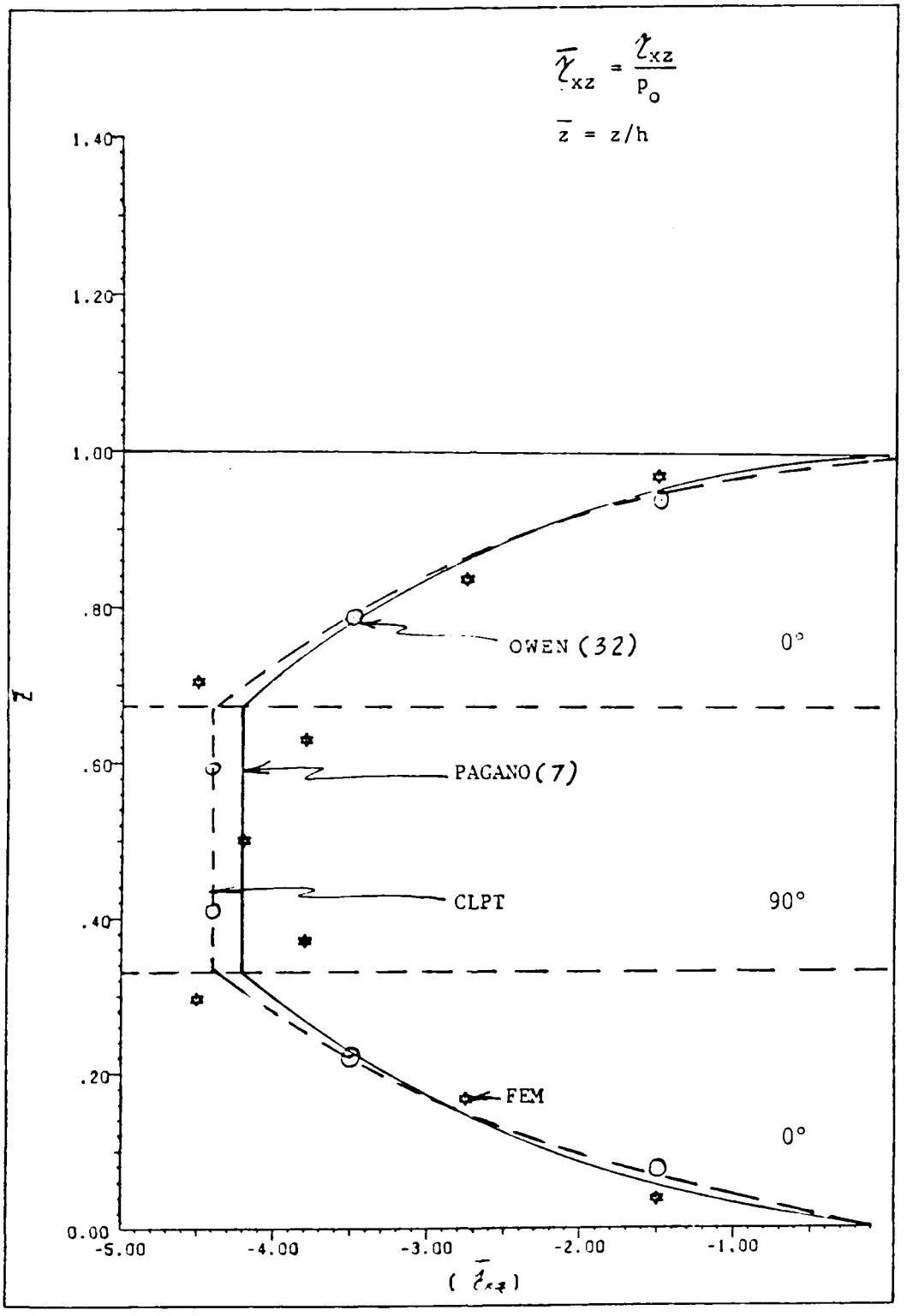

Fig. 27 $\bar{\tau}_{xz}$ vs $\bar{z}$--Fiber Orientation (0,90,0)--(S=10)

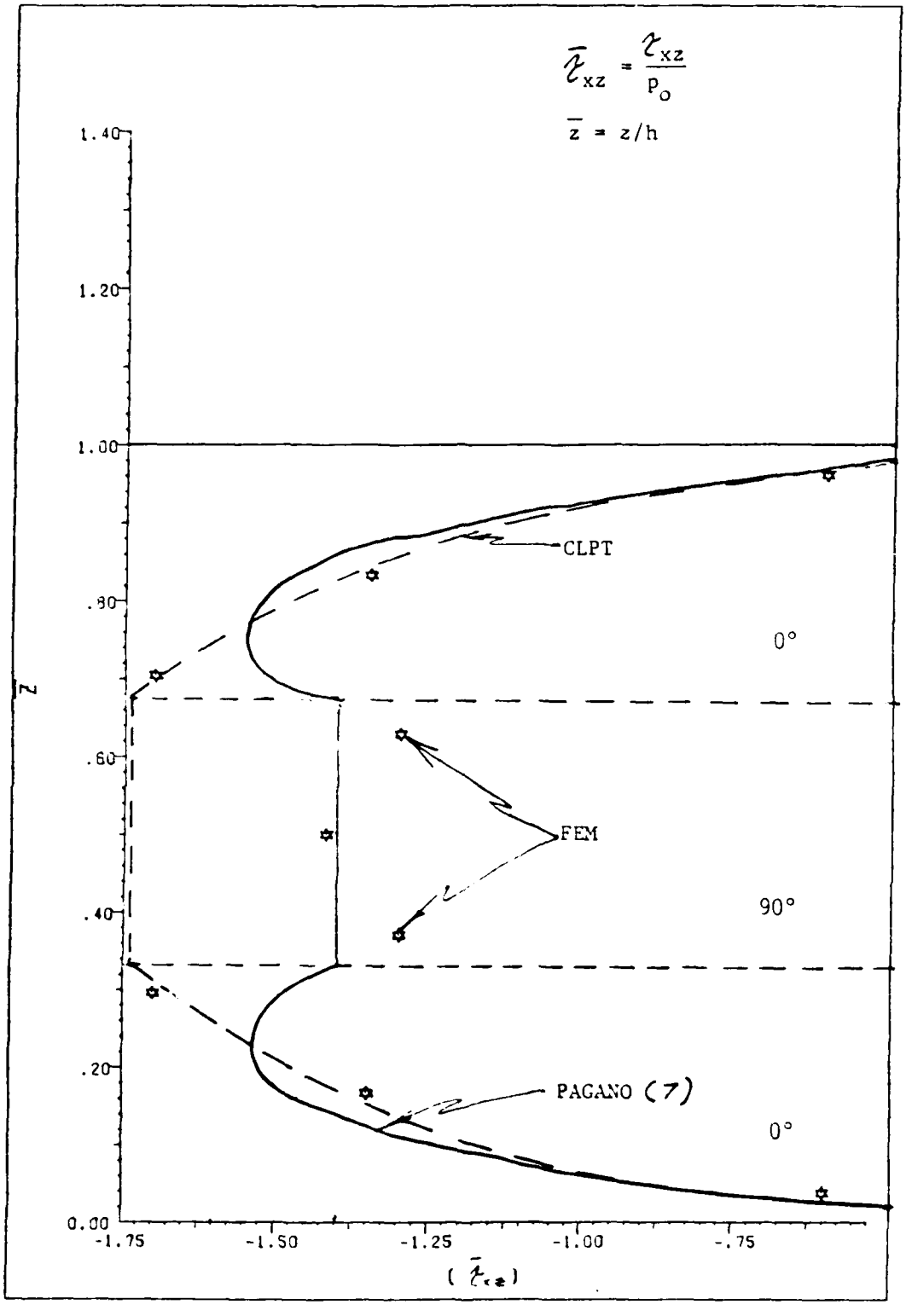

Fig. 28 $\bar{\tau}_{xz}$ vs $\bar{z}$--Fiber Orientation (0,90,0)--(S=4)

It should be noted that these stress results were obtained at the Gauss integration points of the 1st element and extrapolated linearly to the x=0 boundary. This extrapolation also may contribute to some of the differences observed at the interlaminar boundaries.

Figs. 29--33 show plots of $(\bar{\sigma}_x)$ vs. $\bar{z}$ at x=a/2 where $(\bar{\sigma}_x)=(\sigma_x)/p_0$. In each case, the elasticity solution is followed nearly identically.

The fourth case to be presented is that of the square orthotropic plate shown in Fig. 34. The plate was modelled using 25 8-noded elements for the quarter plate. Reduced (2x2) integration was employed. The material properties were again the same as in the previous orthotropic cases. Loading in this problem was a transverse sinusoidal load of the form:

$$p=p_0 \sin(\pi x/a)\sin(\pi y/a) \qquad (116)$$

The boundary conditions for this plate were simple supports all around. Along the edges, the transverse displacement, w, was fixed, and the normals to the reference surface at the edges were not allowed to rotate perpendicular to the boundary.The u and v displacements were free. The plate was a symmetric (0,90,90,0) lay up.

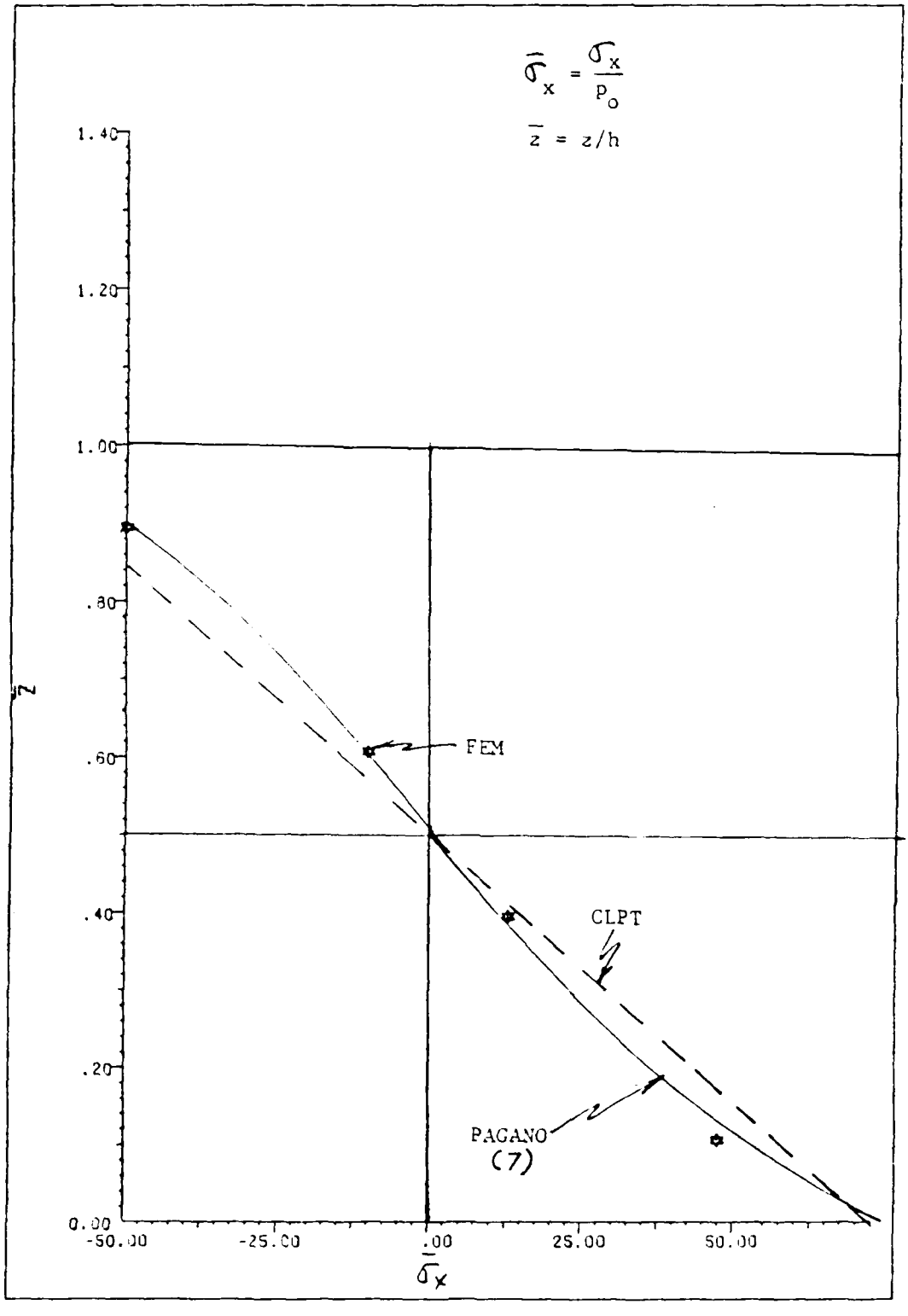

Fig. 29 $\bar{\sigma}_x$ vs $\bar{z}$--Fiber Orientation (0,0)--(S=10)

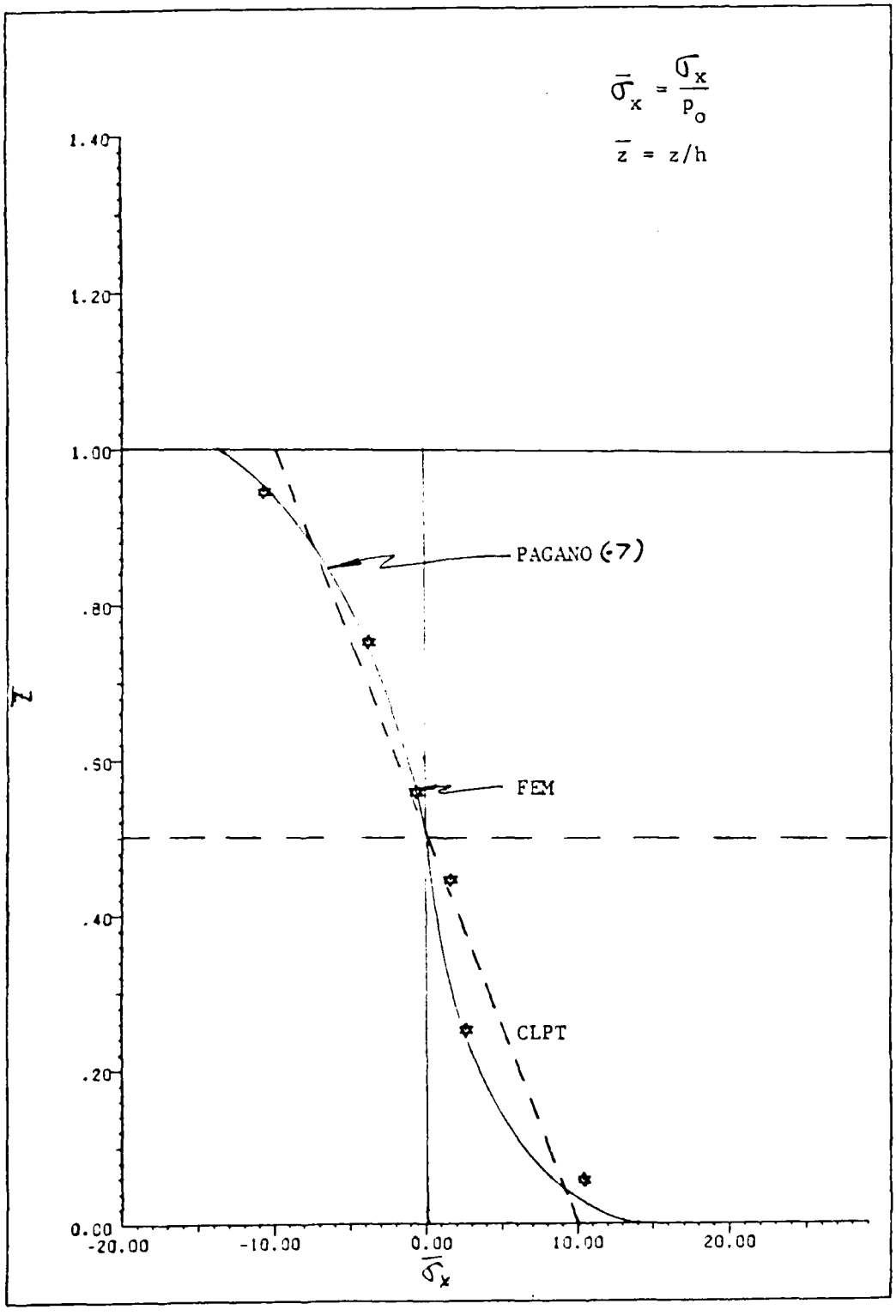

Fig. 30 $\bar{\sigma}_x$ vs $\bar{z}$--Fiber Orientation (0,0)--(S=4)

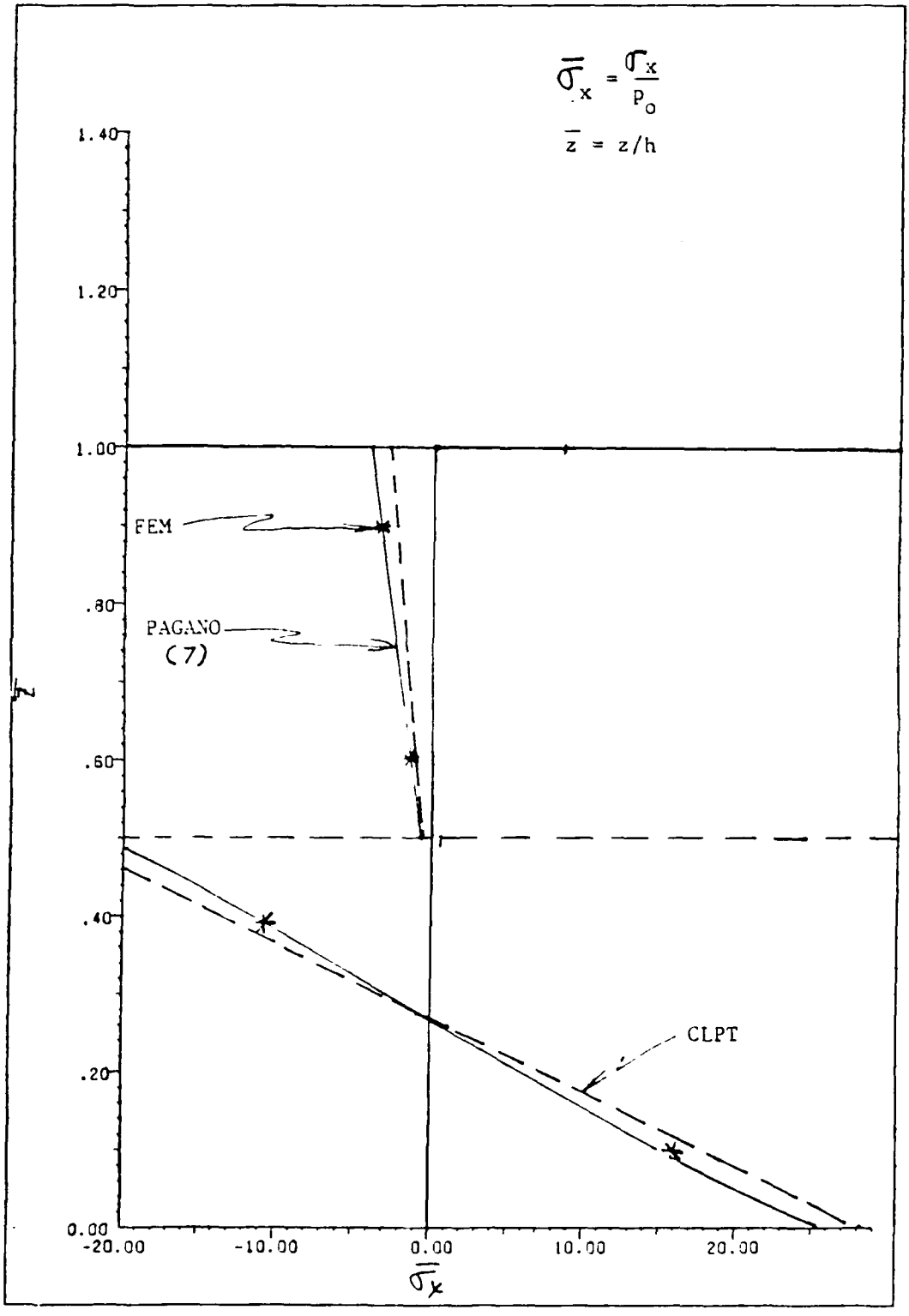

Fig. 31 $\bar{\sigma}_x$ vs $\bar{z}$--Fiber Orientation (0,90)--(S=4)

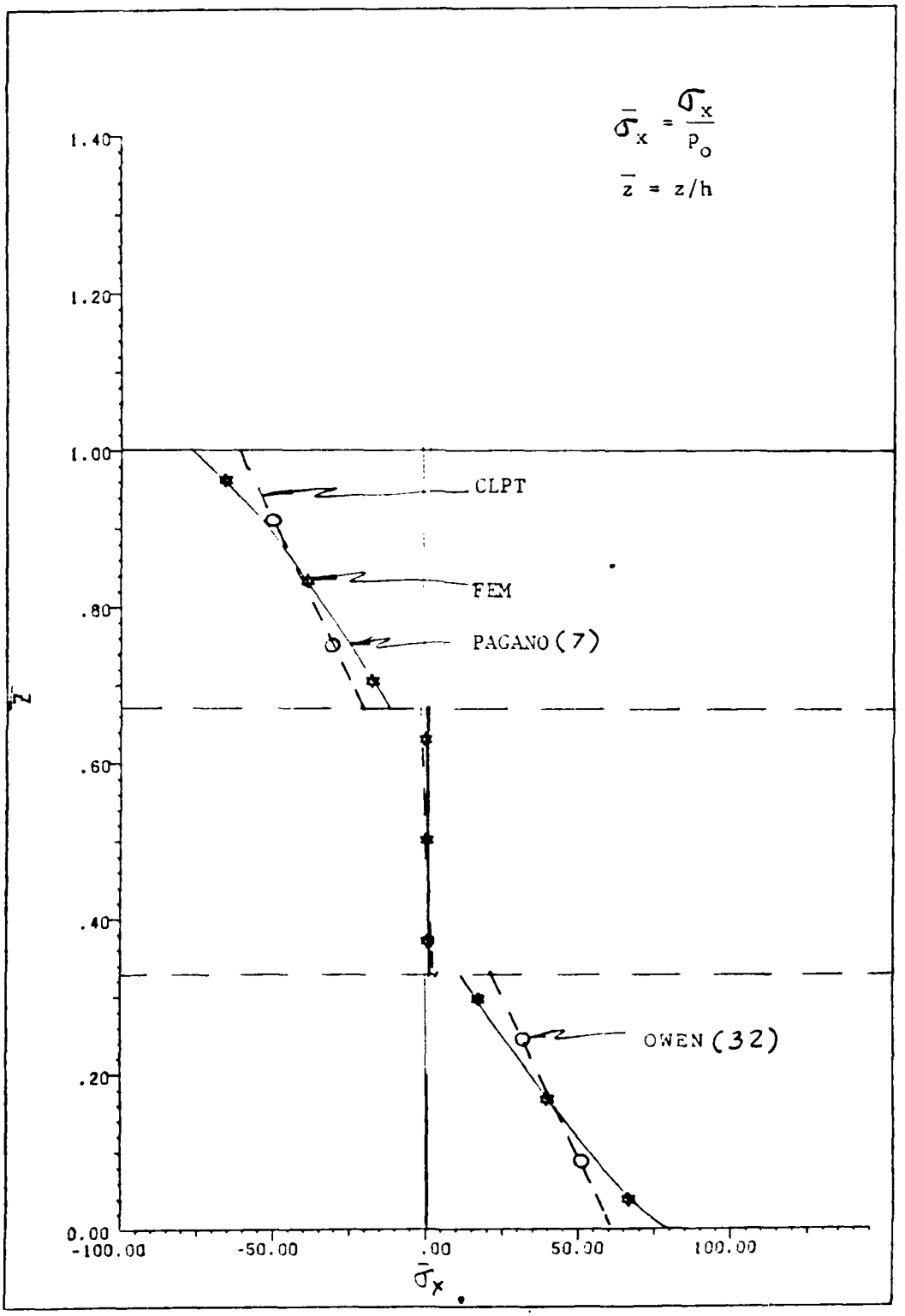

Fig. 32 $\bar{\sigma}_x$ vs $\bar{z}$--Fiber Orientation (0,90,0)--(S=10)

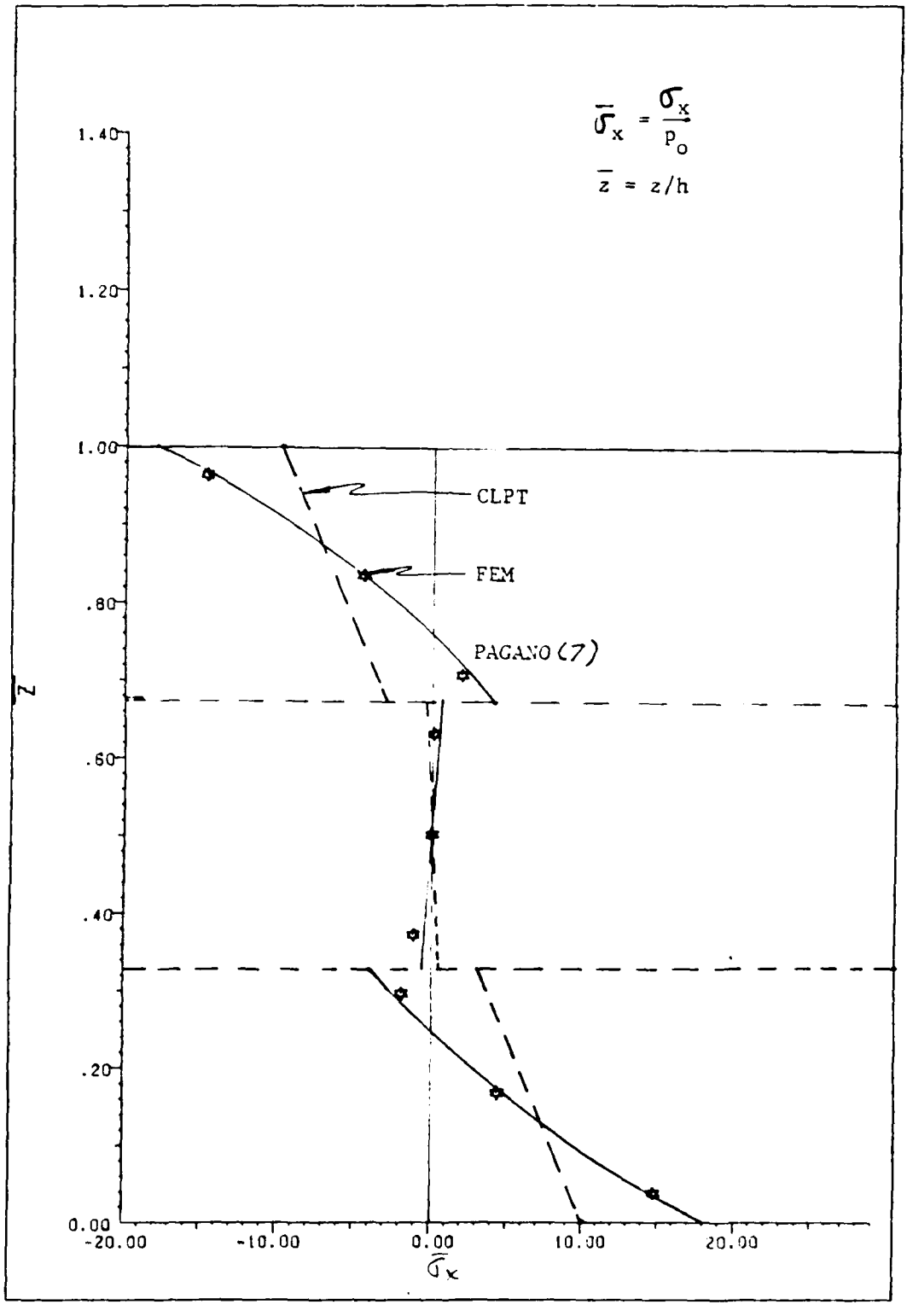

Fig. 33 $\bar{\sigma}_x$ vs $\bar{z}$--Fiber Orientation (0,90,0)--(S=4)

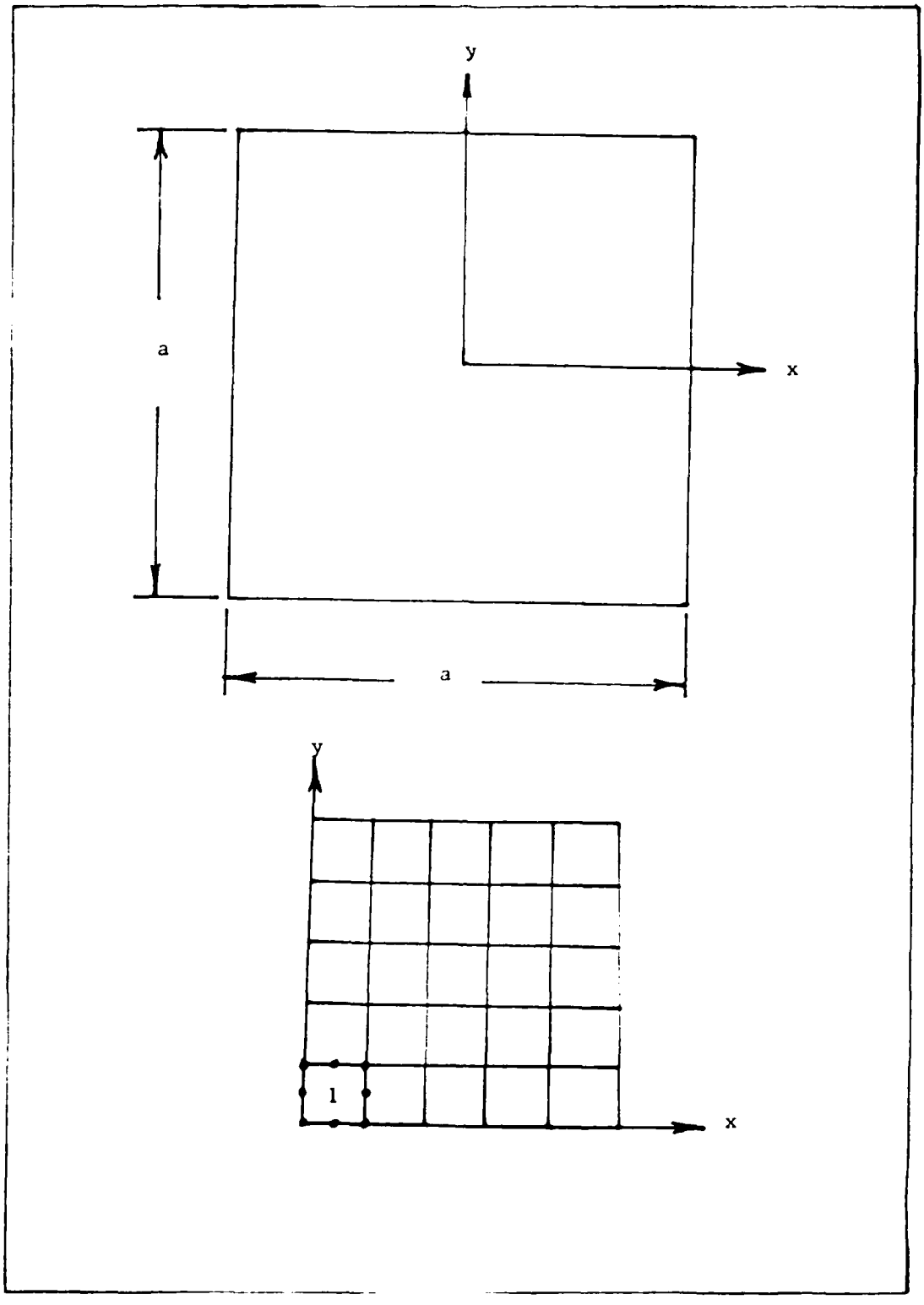

Fig. 34 Squate Orthotropic Plate Fininte Element Model

Fig. 35 shows a comparison of $\bar{w}$ vs S for this plate. The finite element solution compares nearly identically with the elasticity solution and gives results which are better than another F.E. solution by Pryor and Barker (25). Thus, the element appears to respond well to changes in geometric restraints and configurations.

To test the nonlinear theory, the symmetric (0,0) lay-up and the asymetric lay-up (0,90) cases of the plate strip problem were examined. Since the present theory allows the inclusion of two sets of nonlinear terms (K1 and K2), a check was made to determine the influence each of these terms had on the solution. As with the linear case, 5 8-noded elements (with 2x2 integration) were used to model the plate strip.

Fig. 36 shows plots of $\bar{w}$ vs $\bar{Q}$ for both the (0,0) and the (0,90) cases. The length to thickness ratio for these cases was chosen to be S=10, which means that this is a thick plate strip. As expected, the (0,90) strip is more flexible than the (0,0) strip. The solid line depicts the solution which was obtained by including only the [K0] or linear terms. The lines represented by the squares show the results of including the [K1] terms which contain nonlinearity with respect to the reference surface. The inclusion of the [K2] terms, which contain nonlinearities

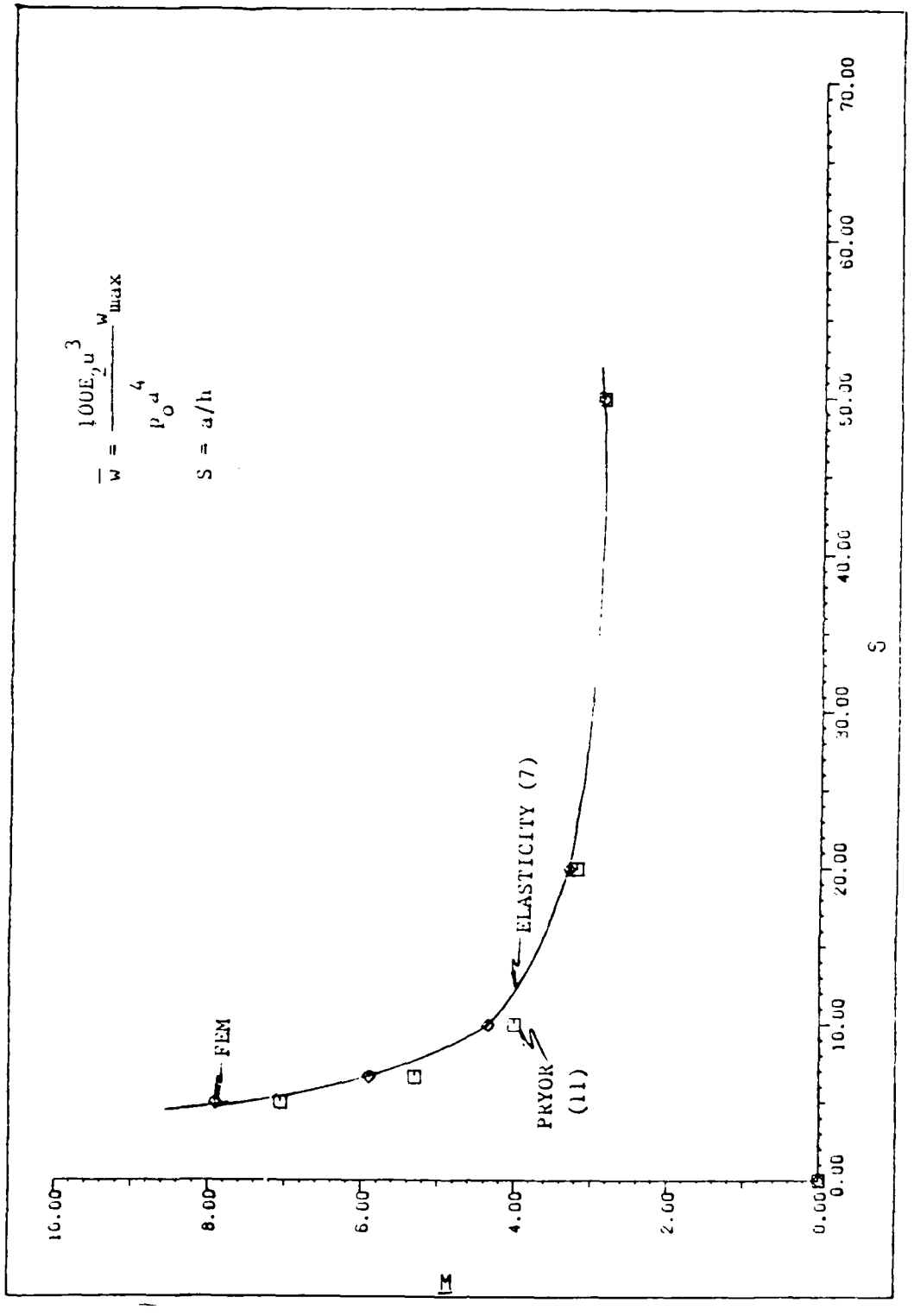

Fig. 35 $\bar{w}$ vs S--Square Plate (0,90,90,0)

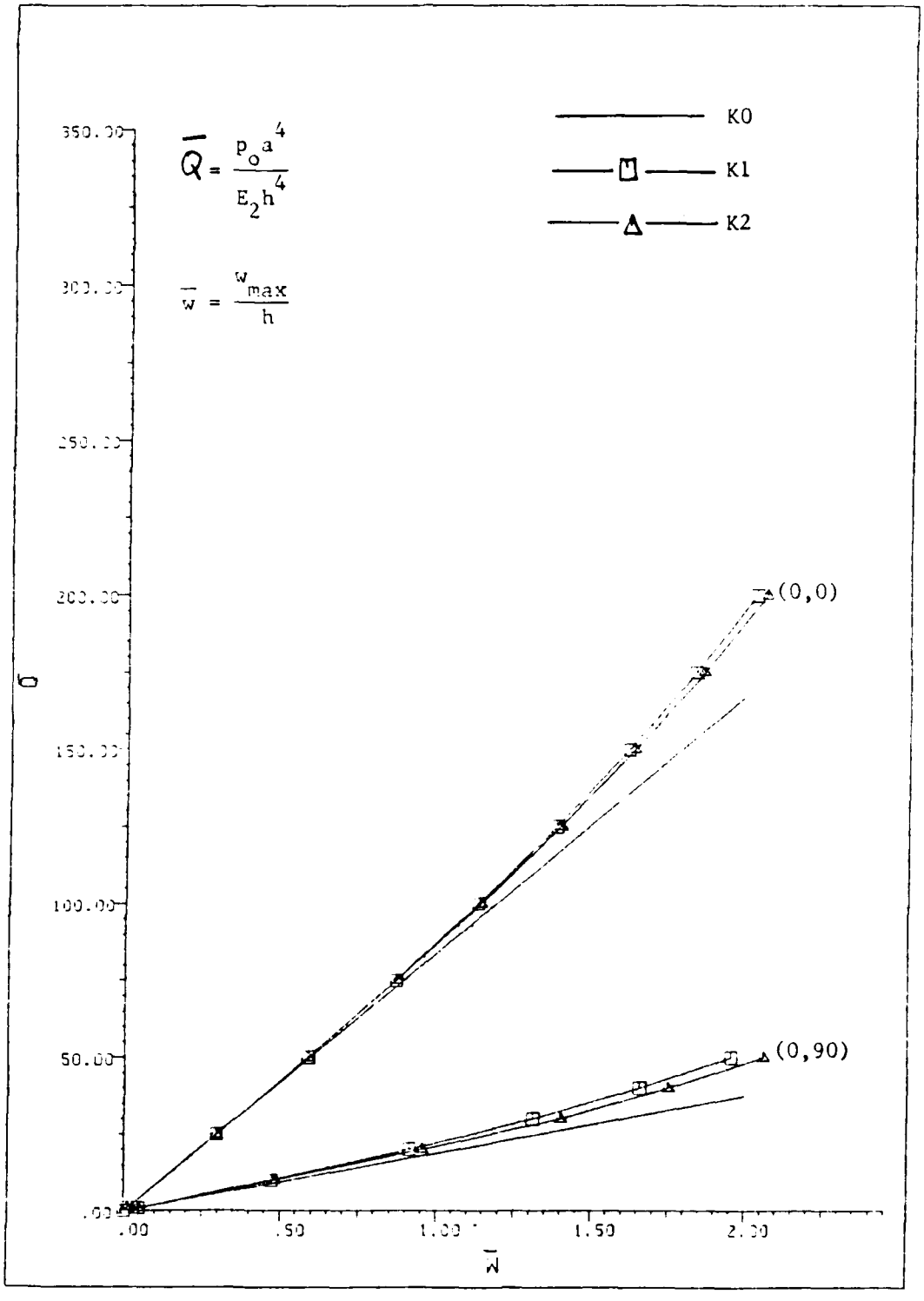

Fig 16 $\bar{w}$ vs $\bar{Q}$--Nonlinear Plate Strip Problems

with respect to the thickness, is depicted by the triangle symbols on the lines. Note that when the [K1] terms are included, there is a stiffening of the plate strip. That is, there is less displacement for a given load. Note also that when the [K2] terms are included, the solution is stiffer than the linear solution but more flexible than the solution obtained using the [K1] terms.

In Figs. 19 and 20 it was shown that when [K0] terms were used in the analysis, the solutions obtained were identical with the classical laminated plate theory. Further, it was shown that as the plate became thicker, the presence of the shear terms in the thickness direction produced transverse displacements (w) which were greater than the classical laminated plate theory. Since the [K0] terms contain linear expressions for u,v, and w (the reference surface displacements) and linear expressions for the rotations (ϕ_1) which account for the effects of the shear terms, [K0] was able to effectively represent the elasticity solution. This leads to the conclusion that when shear terms are taken into account, there is an accompanying increase in the transverse displacements. The inclusion of [K1] in the analysis takes into account nonlinear displacements in the reference surface but the terms for the effects of transverse shear are linear as they were in [K0]. Because of the presence of these nonlinear terms for the

reference surface displacements, the solution becomes stiffer in comparison with the solution obtained using only [K0]. When [K2] is included and the fully nonlinear formulation is used, the "softening" phenomena occurs. The softening is a direct result of the important nonlinear rotation terms which are contained in [K2].

Figs. 37 and 38 show the effects of including [K1] and [K2] on the $\bar{\sigma}_x$ and $\bar{\tau}_{xz}$ stresses. That is, the stresses increase when the [K2] terms are included.

The sixth case presented is again a square orthotropic plate (see Fig. 34). The material properties were retained from previous cases. The load for this case was distributed uniformly in the transverse direction as:

$$p=p_0$$

The boundaries of the plate were all clamped (clamped means that all degrees of freedom at the boundaries were fixed) and the ply lay-up was (0,0). The plate was modelled by using 16 4-noded elements (1x1 integration) for one quadrant instead of the 8-noded element with 2x2 integration simply to conserve computer time. This problem was chosen as a check of how the non-linear terms of the theory would respond to a change in geometry. The check was made by proportionally increasing the load p_0 and observing the transverse deflection (w) at the center of the plate where it was a maximum. Fig. 39 shows a graph of the results obtained. This plot gives a comparison between the present

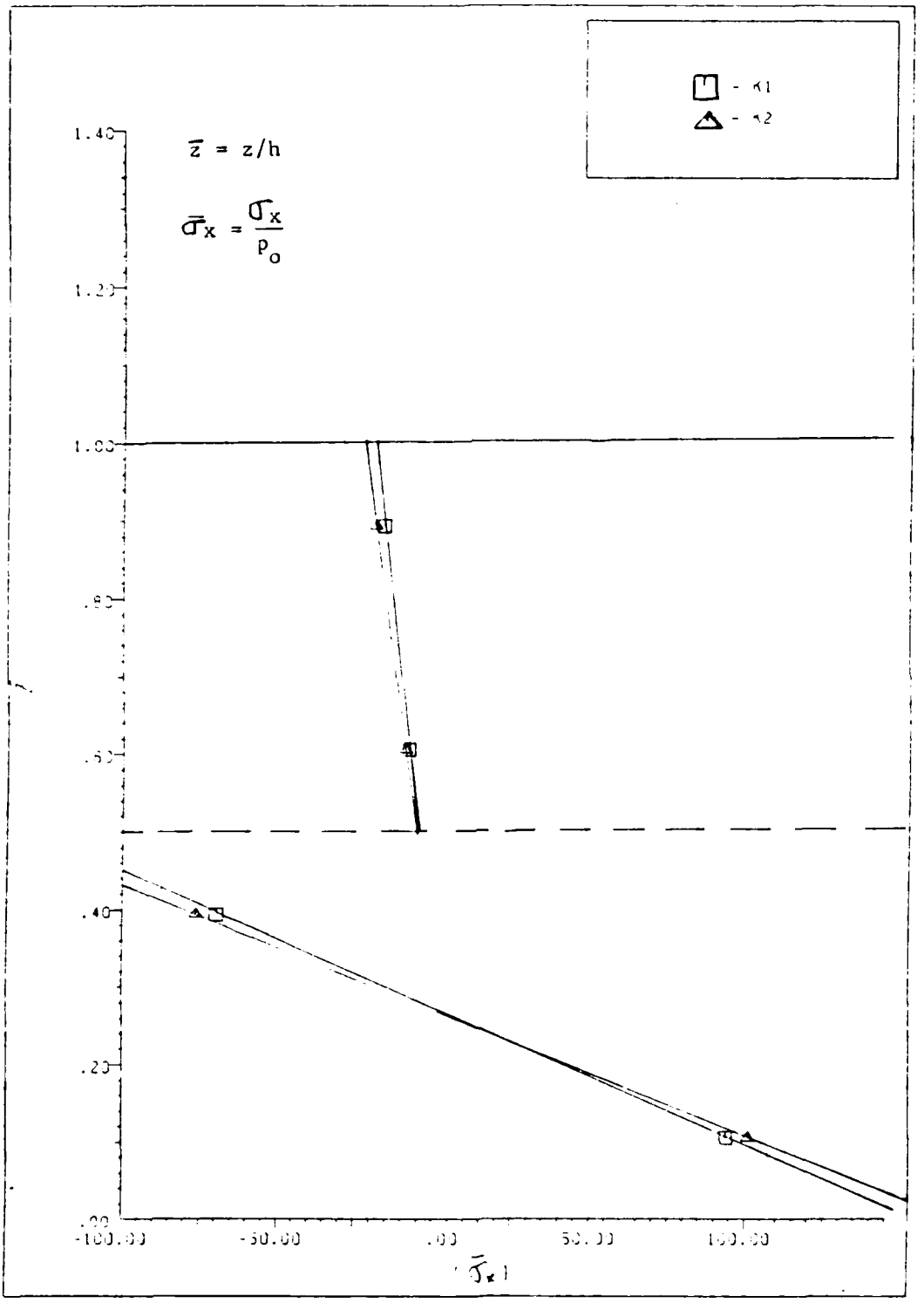

Fig. 37 $\bar{\sigma}_x$ vs $\bar{z}$--Nonlinear Plate Strip (0,90)

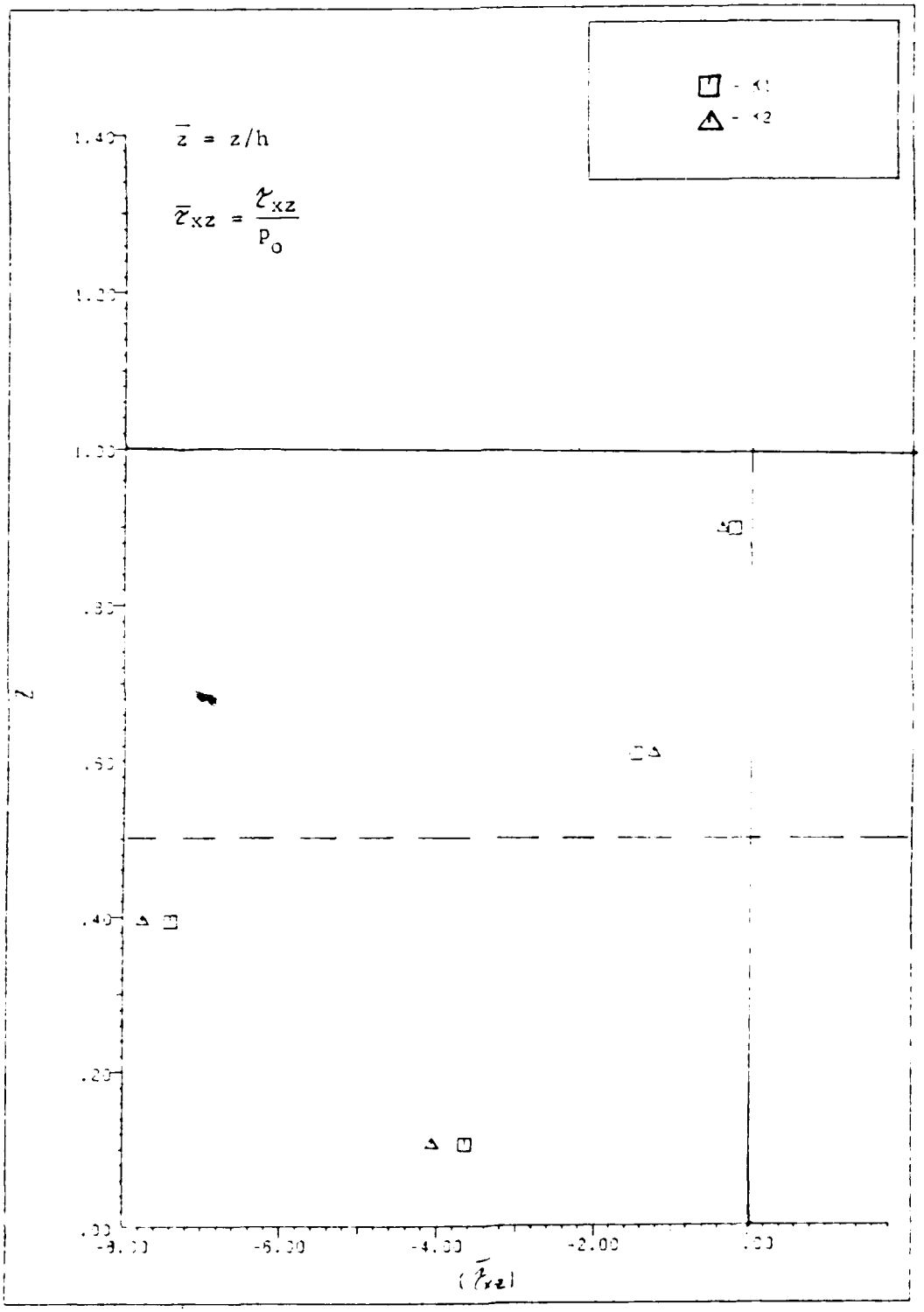

Fig. 38 $\bar{\tau}_{xz}$ vs $\bar{z}$--Nonlinear Plate Strip (0,90)

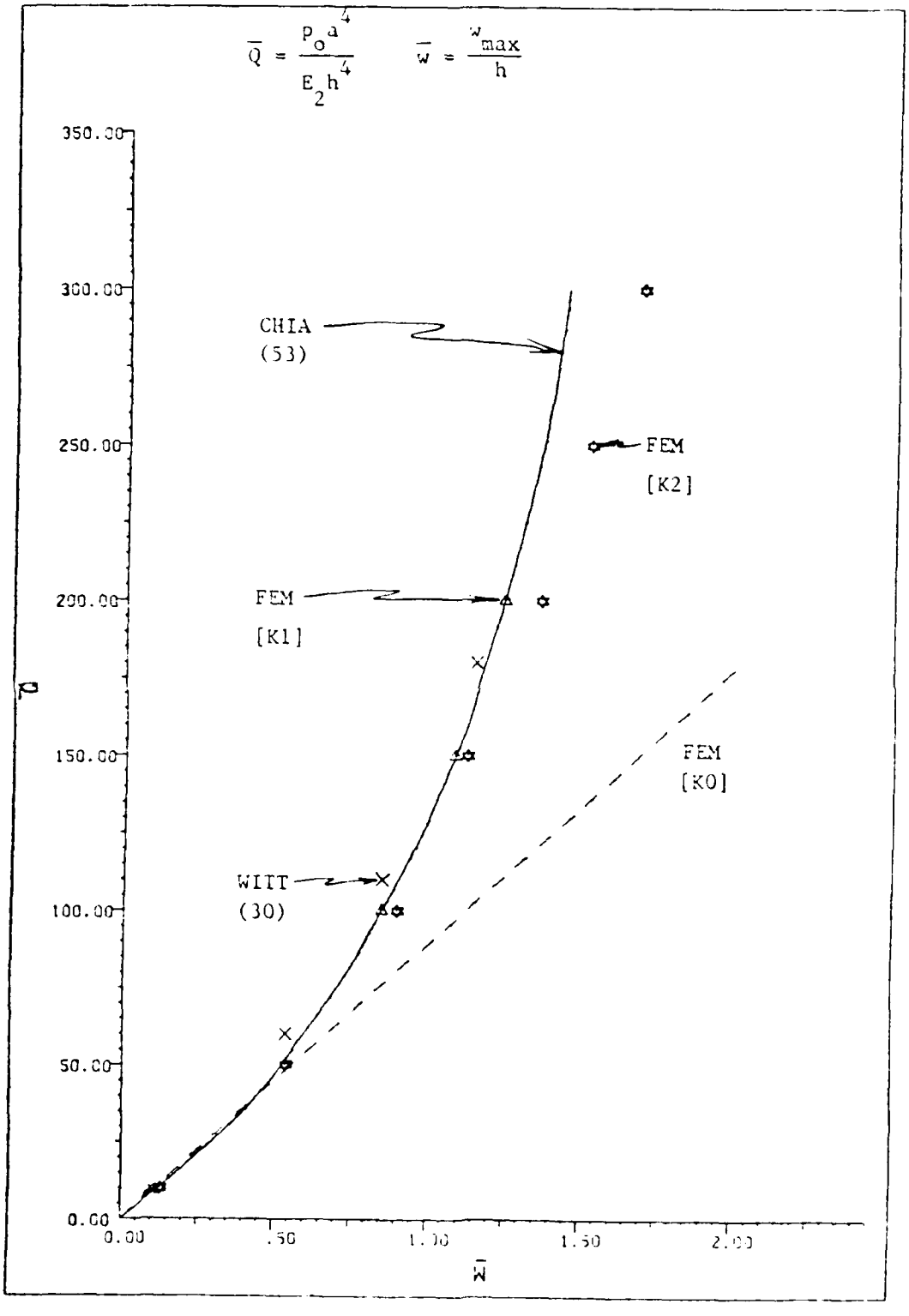

Fig. 39 $\bar{Q}$ vs $\bar{w}$--Nonlinear Square Orthotropic Plate

work, the work of Witt (30), and an approximate analytical solution obtained by Chia (30). Note in particular that the inclusion of the [K1] terms gives results which are somewhat better than those obtained by Witt who included [K1] and nearly identical to Chia's (who used a perturbation method on the Von Karman plate equations).The inclusion of the higher order terms of [K2] yields an expected softening of the element as the loads were increased. The same arguments as were put forth for the plate strip problems apply here.

Figs. 40 and 41 show how the shear stresses ($\bar{\varepsilon}_{yz}$) and ($\bar{\varepsilon}_{xz}$) vary with increasing loads and inclusion of [K1] and [K2] in the analysis. Note that the shear stresses decrease (proportionately) as the load level is increased. This is because more of the stress is picked up in bending through the direct stress $\bar{\sigma}_x$. When [K2] is included, note that the shear stresses are greater than for the [K1] terms. This is in accord with the observations made when solving the plate strip problem previously.

This work represents the first time that the inclusion of these [K2] terms has been performed and therefore no direct comparison to previous work can be made.

For a detailed account of computer time and technique

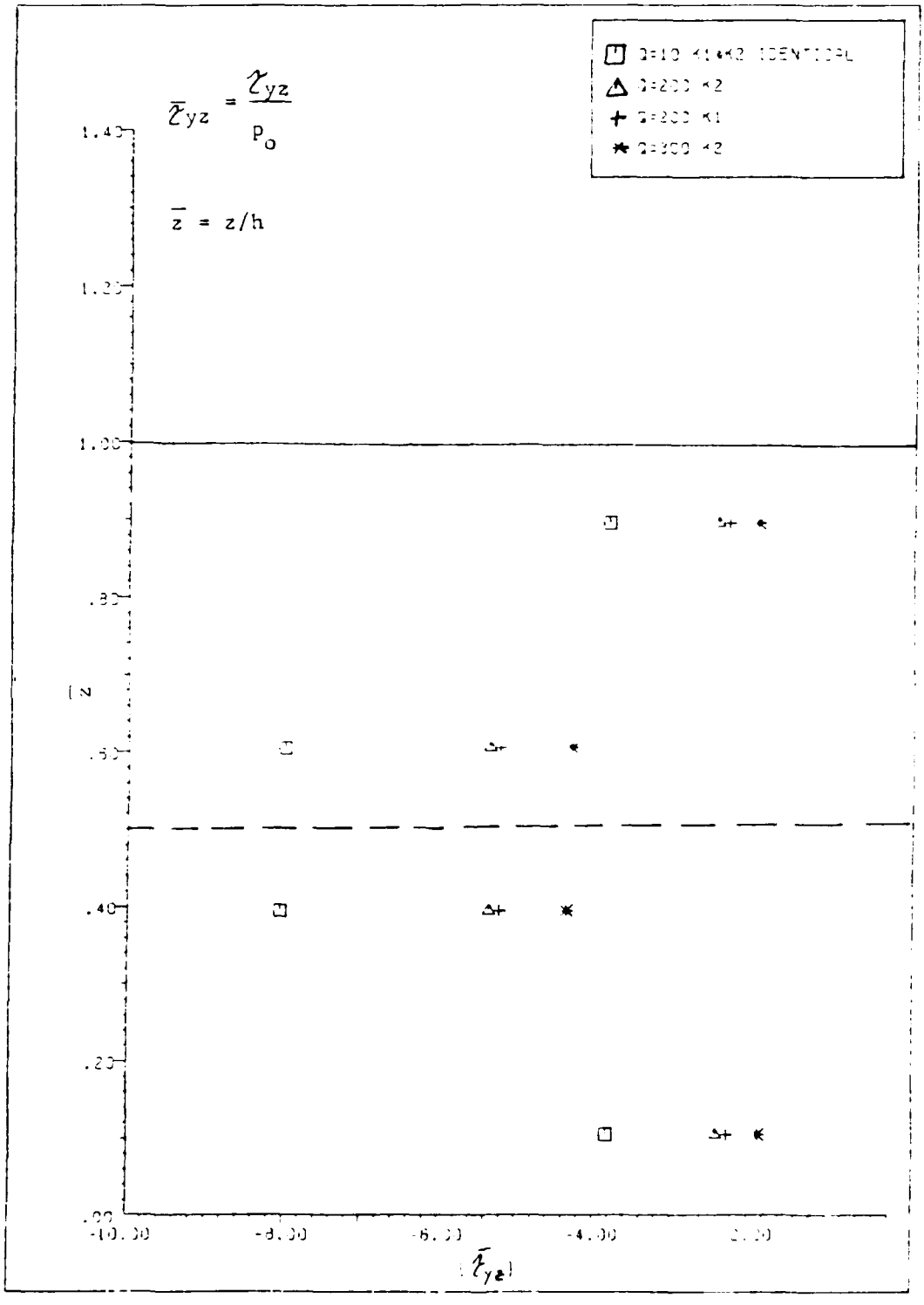

Fig. 40 $\bar{\tau}_{yz}$ vs $\bar{z}$--Nonlinear Square Orthotropic Plate

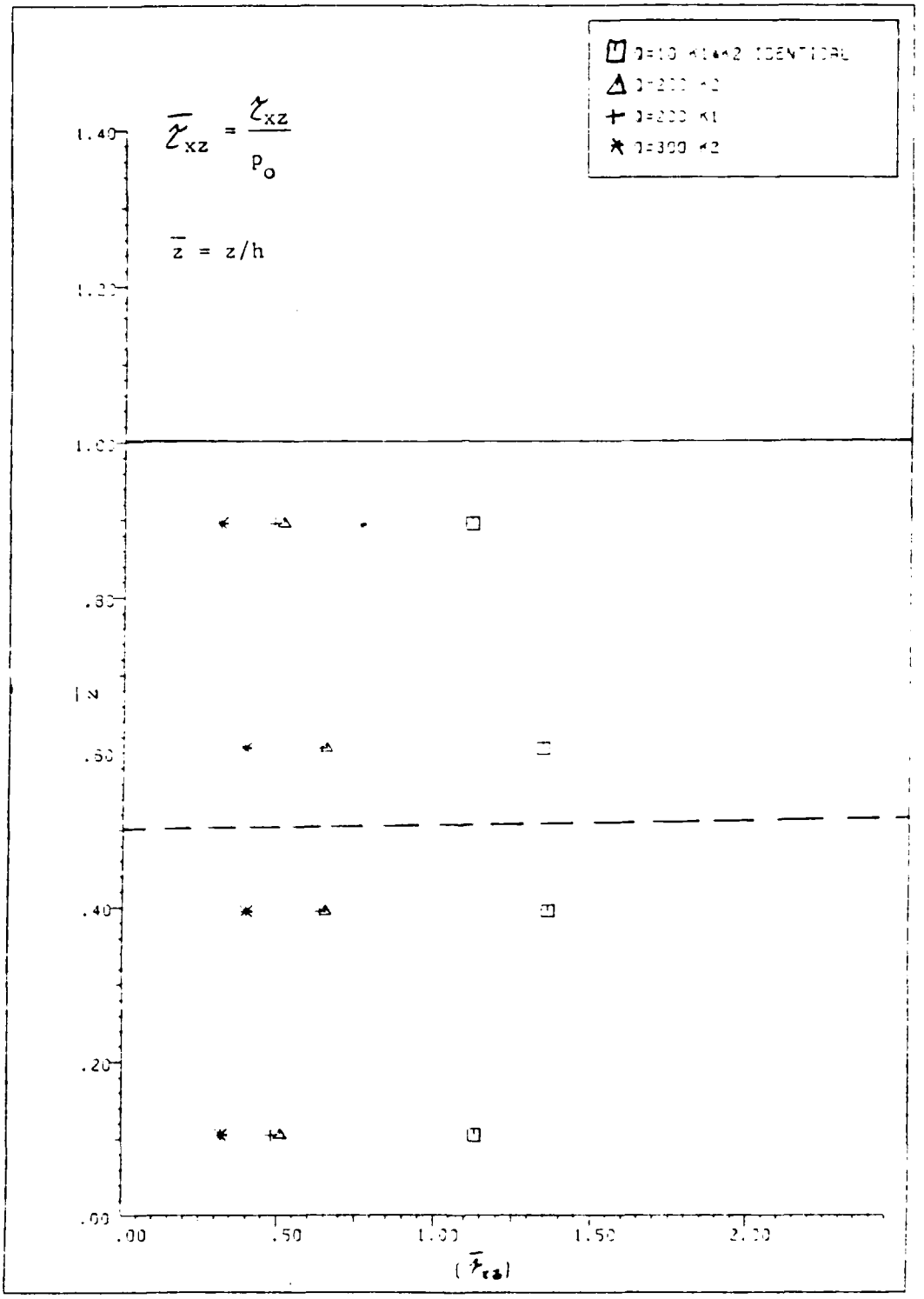

Fig. 41 $\bar{\tau}_{xz}$ vs $\bar{z}$--Nonlinear Square Orthotropic Plate

used in solving these nonlinear problems refer to Appendix III.

CHAPTER V

CONCLUSIONS

A number of conclusions have been made in the last chapter in conjunction with the discussions of the results.

One of the significant contributions of this work lies in the unique use of cubic spline theory which has been well known for many years in the field of interpolation and in the solution of differential equations. The most recent work with cubic splines in these fields has always concentrated on the displacements $\langle u \rangle$ being known and solving for the rotations $\langle \theta_i \rangle$ in terms of the known displacements. Here $\langle u \rangle$ is referred to, because of the context of the present use of spline theory. In reality, no one to the best of the author's knowledge has heretofore considered the cubic spline to model through-the-thickness displacements. In all previous uses of the cubic spline in conjunction with plate solutions, the spline was used to model in-plane displacements. In this work, the cubic spline equations are solved in the reverse sense. That is, the $\langle u \rangle$ is treated as the unknown and are solved for in terms of the $\langle \theta_i \rangle$. This process resulted in the development of a cubic shape function which did not introduce any new degrees of freedom over the previously derived para-

bolic representation. The use of the spline in this "reverse" role is a promising new technique in numerical approximation theory where the rotations $\langle \theta_i \rangle$ become the degrees of freedom and $\langle u \rangle$ is then represented in terms of them through the derived shape function.

A consequence of the use of an odd-degree'd spline (cubic in this case) is that the equations necessary to represent the interpolation functions are very compact and easily represented. A look at Palazotto's work (57), wherein he used (essentially) a parabolic spline, shows the complexity of the expressions which results. In terms of computer implementation, this is important not only in terms of computational effort, but also in terms of programmer effort. The cubic spline, although a higher order approximation, leads to a simplification of the equations and lends itself to less programmer effort. The reduction in programmer involvement results in fewer errors.

The results clearly show that the use of the cubic spline theory to represent through-the-thickness displacements in thick composite plates is a viable and effective application. Comparisons with previous works show that there is the ability to obtain equally accurate results with fewer degrees of freedom. Consider for instance work

of Epstein (42) (where a number of pseudolayers was necessary to obtain the results presented). This same technique was used by Witt in his work. With the cubic spline, each layer can be represented as a layer, and not a number of pseudolayers.

A comparison with the use of 3-D elements to represent each layer again clearly shows the reduction in the number of degrees of freedom and thus computational storage and time. In both the present work and Palazotto's (57) work there are 2(M+1)+3 degrees of freedom per node (where M is the number of layers). In Epsteins (42) formulation there are 3(M+1) degrees of freedom per node. With a variety of 3D brick elements to choose from there is a range from 3(M+1) to 5(M+1) degrees of freedom per node (or even more) depending on the choice of brick element used. When pseudolayers are used, there are essentially 2M layers used to represent M layers. In numerical terms, if one were to consider a 6-layered problem, one would find that Epstein's element with pseudolayers would require 39 DOF per node, Witt's element would require 29 DOF per node, the trilinear brick element with no pseudolayers would require 21 DOF per node, and the present element would require 17 DOF per node.

The difficulties in converging to the thin isotropic

plate solution were not overcome by using a higher order element for the in-plane interpolations. Reduced integrations of the bi-linear quadrilateral and the bi-quadratic quadrilateral improved the results from 82% to 92% of the thin plate solution. The thin isotropic plate solution was obtained when the effects of the transverse shear terms were reduced by reducing the transverse shear modulli by a factor of 100.

The inclusion of the [K2] terms in the nonlinear formulation is an advance in the state of the art in through-the thickness representations. It is seen to become more important as load levels are increased (assuming yield stress is not exceeded). Since [K2] contains nonlinear transverse rotational terms, it also would become more important whenever transverse shear terms affect the problem. The thicker the structure, the more important the inclusion of these terms becomes.

The inclusion of the [K2] terms leads to somewhat larger transverse stresses than those obtained with [K1]. This is due to the increase in the transverse displacements which accompanies the inclusion of the [K2] terms.

In summary, the cubic assumption for the variations of the displacements $\hat{u}$ and $\hat{v}$ through the thickness proved to

be an effective approach. In terms of degrees of freedom, there was actually a decrease over the parabolic assumption simply because accurate results could be obtained without resorting to pseudolayers. Secondly, difficulties of locking when applying this thick plate element to a thin plate were overcome by reducing the values for G_{13} and G_{23}. Thirdly, the continuously differentiable nature of the cubic assumption for $\hat{u}$ and $\hat{v}$ through the thickness resulted in discontinuities in the shear stresses at the interlaminar boundaries. This is seen as a limiting factor on the applicability of the element. It should be noted, however, that if the stresses were integrated through the thickness and resultant forces were considered then equillibrium is satisfied within the element. Fourthly, the inclusion of the nonlinear terms of [K2] which represent nonlinear effects arising through the thickness leads to greater displacements at a given load level than the inclusion of just the reference surface nonlinear terms of [K1]. In all, it is felt that the elements developed (namely the 4-noded with 1x1 integration and the 8-noded with 2x2 integration) are viable and accurate when compared to both the analytical solutions and other finite element solutions.

BIBLIOGRAPHY

1. Judge, John F.,"Composite Material, the Coming Revolution", Airline Management and Marketing, 85-91, (Sept 1969).

2. Reissner, E. and Stavsky, Y.,"Bending and Stretching of Certain Types of Heterogeneous Aeolotropic Elastic Plates", Journal of Applied Mechanics, 28, 402-408,(1961).

3. Whitney, J.M., and Leissa, A.W., "Analysis of Heterogeneous Anisotropic Plates", Journal of Applied Mechanics, 36, 262-266, (1969).

4. Ambartsumyan, S.A., Theory of Anisotropic Shells, NASA TTF-118, Washington, DC, National Aeronautics and Space Administration, (May 1964).

5. Calcote, L.R., The Analysis of Laminated Composite Structures. New York: Van Nostrand Reinhold Co., 1969.

6. Jones, R.M., Mechanics of Composite Materials. Washington DC: Scripto Book Co., 1975.

7. Pagano, N.J., "Exact Solutions for Composite Laminates in Cylindrical Bending", Journal of Composite Materials, 3, 398-411, (July, 1969).

8. Pagano, N.J., "Influence of Shear Coupling in Cylindrical Bending of Anisotropic Plates", Journal of Composite Materials, 4, 330-343, (1970).

9. Pagano, N.J. and Hatfield, S.J., "Elastic Behavior of Multilayered Bidirectional Composites", AIAA Journal, 10, 931-933, (1972).

10. Srinivas, S. and Rao, A.K., "Bending, Vibration, and Buckling of Simply Supported Thick Orthotropic Rectangular Plates and Laminates", International Journal Solids and Structures, 6, 1463-1481, (1970).

11. Pryor, C.W. Jr., and Barker, R.M., "A Finite Element Analysis Including Transverse Shear Effects for Applications to Laminated Plates", AIAA Journal, 9, 912-917, (1971).

12. Ambartsumyan, S.A., Theory of Anisotropic Plates. Stanford, Conn: Technomic Publishing Co., 1970.

13. Hsu, T-M, and Wang, JT-S, "A Theory of Laminated Cylindrical Shells Consisting of Layers of Orthotropic Laminae", AIAA Journal, 8, 2141-2146, (1970).

14. Yang, P.C., Norris, C.H., and Stavsky, Y., "Elastic Wave Propogation in Heterogeneous Plates", International Journal of Solids and Structures, 2, 665-684, (1966).

15. Whitney, J.M., "The Effect of Transverse Shear Deformation on the Bending of Laminated Plates", Journal of Composite Materials, 3, 534-547, (1969).

16. Whitney, J.M. and Pagano, N.J., "Shear Deformation in Heterogeneous Anisotropic Plates", Journal of Applied Mechanics, 37, 1031-1036, (1970).

17. Whitney, J.M., "Stress Analysis of Thick Laminated Composite and Sandwich Plates", Journal of Composite Materials, 6, 426-44, (1972).

18. Whitney, J.M. and Sun, C.T., "A Refined Theory of Laminated Anisotropic Cylindrical Shells", Transactions ASME Journal of Applied Mechanics, 41, 471,(1974).

19. Hildebrand, F.B., Reissner, E., and Thomas, G.B., "Notes on the Foundation of the Theory of Small Displacements of Orthotropic Shells", NACA-TN-1833, March 1949.

20. Krauss, H., Thin Elastic Shells, New York: Wiley, 1967.

21. Lo, K.J., Christensen, R.M., and Wu, E.M., "A Higher Order Theory of Plate Deformation, Part 1: Homogeneous Plates", Journal of Applied Mechanics, 44, 663-668, (1977).

22. Lo, K.J., Christensen, R.M., and Wu, E.M., "A Higher Order Theory of Plate Deformation, Part 2: Laminated Plates", Journal of Applied Mechanics, 44, 669-676, (1977).

23. Grot, R.A., "A Continuum Model for Curvilinear Laminated Composites", International Journal of Solids and Structures, 8, 439-462, (1972).

24. Srinivas, S., "A Refined Analysis of Composite Laminates", Journal of Sound and Vibration, 30, 495-507, (1973).

25. Epstein, M. and Glockner, P.G., "Nonlinear Analysis of Multilayered Shells", International Journal of Solids and Structures, 13, 1081-1089, (1977).

26. Mawenya, A.S. and Davies, J.D., "Finite Element Bending Analysis of Multilayered Plates", International Journal for Numerical Methods in Engineering, 8, 215-225,(1974).

27. Ahmad, S., Irons, B.M., and Zienkiewicz, O.C., "Analysis of Thick and Thin Shell Structures by Curved Finite Elements", International Journal for Numerical Methods in Engineering, 2, 419-451, (1970).

28. Panda, S.C., and Natarajan, R., "Finite Element Analysis of Laminated Composite Plates", International Journal for Numerical Methods in Engineering, 14, 69-79, (1979).

29. Panda, S.C., and Natarajan, R., "Analysis of Laminated Composite Shell Structures by Finite Element Method", Computers and Structures, 14, 225-230, (1981).

30. Witt, W., "Formulation of a Nonlinear Compatible Finite Element for the Analysis of Laminated Composites", Phd Dissertation, Air Force Institute of Technology, Wright-Patterson AFB, Ohio, (1983).

31. Pack, S.C. and Mandel, J.A., "2-D Multiplane Finite Element Technique for Solving a Class of 3-D Problems", International Journal for Numerical Methods in Engineering, 19, 113-124, (1983).

32. Owen, D.R.J. and Figueiras, J.A., "Anisotropic Elasto-Plastic Finite Element Analysis of Thick and Thin Plates and Shells", International Journal for Numerical Methods in Engineering, 19, 541-566, (1983).

33. Chang, T.Y. and Sawamiphakdi, K., "Large Deformation Analysis of Laminated Shells by the Finite Element Method", Computers and Structures, 13, 331-340, (1981).

34. Mau, S.T., Tang, P., and Pian, T.H.H., "Finite Element Solutions for Laminated Thick Plates", Journal of Composite Materials, 6, 304-311, (1972).

35. Spilker, R.L., Chou, S.C., and Orringer, O., "Alternate Hybrid Stress Elements for Analysis of Multilayer Composite Plates", Journal of Composite Materials, 11, 51-70, (1977).

36. Spilker, R.L., "A Hybrid Stress Finite Element Formulation for Thick Multilayer Laminates", Computers and Structures, 11, 507-514, (1980).

37. Spilker, R.L. and Munir, N.I., "Comparison of Hybrid Stress Element Through Thickness Distributions Corresponding to a High Order Plate Theory", Computers and Structures, 11, 579-586, (1980).

38. Noor, A.K. and Mathers, M.D., "Finite Element Analysis of Anisotropic Plates", International Journal for Numerical Methods in Engineering, 11, 289-307, (1977).

39. Noor, A.K. and Hartley, S.J., "Nonlinear Shell Analysis Via Mixed Isoparametric Elements", Computers and Structures, 7, 615-626, (1977).

40. Noor, A.K., Anderson, C.M., and Peters, J.M., "Reduced Basis Technique for Collapse Analysis of Shells", AIAA Journal, 19, 393-397, (1981).

41. Reddy, J.N. and Creamer, N.G., "A Refined Higher-Order Theory of Plates", Proceedings The Southeastern Conference on Theoretical and Applied Mechanics, May 10-11, 1984.

42. Epstein, M. and Glockner, P.G., "Deep and Multilayered Beams, Journal of Engineering Mechanics Division, ASCE, EM6, 107, 1029-1037, (1981).

43. Epstein, M. and Huttelmaier, H-P., "A Finite Element Formulation for Multilayered and Thick Plates", Computers and Structures, 16,5,643-650, (1983).

44. Lee, J.D., "Three Dimensional Finite Element Analysis of Damage Accumulation in Composite Laminate", Computers and Structures, 15,3,335-350, (1982).

45. Kuppusamy, T., and Reddy, J.N., "A Three Dimensional Nonlinear Analysis of Cross-Ply Rectangular Composite Plates", Computers and Structures, 18,2,263-272, (1984).

46. Saada, A.S., Elasticity Theory and Applications, New York: Pergamon Press Inc., 1974.

47. Ahlberg, J.H., Nilson, E.N., and Walsh, J.L., The Theory of Splines and Their Applications, New York: Academic Press, 1967.

48. Zienkiewicz, O.C., The Finite Element Method Third Edition, London, England: McGraw-Hill (UK), 1977.

49. Carnahan, B., Luther, H.A., Wilkes, J.O., Applied Numerical Methods, New York: Wiley and Sons Inc.,1969.

50. Hildebrand, F.B., Introduction to Numerical Analysis, New York: McGraw-Hill, 1956.

51. Pugh, E.D.L., Hinton, E., and Zienkiewicz, O.C., "A Study of Quadrilateral Plate Bending Elements With Reduced Integration", International Journal for Numerical Methods in Engineering, 12, 1059-1079, (1978).

52. Hughes, T.J.R., Cohen, M., and Haroun, M. "Reduced and Selective Integration Techniques in the F.E. Analysis of Plates", Nuclear Engineering Design, 46, 203-222, (1978).

53. Chia, C-Y, "Large Deflection of Rectangular Orthotropic Plates", Journal of the Engineering Mechanics Division ASCE, 98, EM5, (1972).

54. Bathe, K-J, Finite Element Procedures in Engineering Analysis, Englewood Cliffs, N.J.: Prentice-Hall, 1982.

55. Szilard, R., Theory and Analysis of Plates--Classical and Numerical Methods, Englewood Cliffs, N.J.: Prentice Hall, 1974.

56. Cook, R.D., Concepts and Applications of Finite Element Analysis, New York, N.Y.: John Wiley and Sons, 1974.

57. Palazotto, A.N. and Witt, W.P., "Formulation of a Nonlinear Compatible Finite Element for the Analysis of Laminated Composites", accepted for publication by Journal of Computers and Structures.

APPENDIX I

Based on the development of the nonlinear strains in Chapter II, the following expressions show the results of making substitutions for the h_i's and the $\vec{e}_{i,j}$'s and then simplifying to obtain the expressions for the Lagrangian strains appearing in the boxes.

$$\gamma_{11} = h_1 \bar{e}_1 \cdot (u_{1,1}\bar{e}_1 + u_1 \bar{e}_{1,1} + u_{2,1}\bar{e}_2 + u_2 \bar{e}_{2,1} + u_{3,1}\bar{e}_3 + u_3 \bar{e}_{3,1}) +$$
$$\tfrac{1}{2}\{(u_{1,1}\bar{e}_1 + u_1 \bar{e}_{1,1} + u_{2,1}\bar{e}_2 + u_2 \bar{e}_{2,1} + u_{3,1}\bar{e}_3 + u_3 \bar{e}_{3,1}) \cdot \qquad \text{(I.1)}$$
$$(u_{1,1}\bar{e}_1 + u_1 \bar{e}_{1,1} + u_{2,1}\bar{e}_2 + u_2 \bar{e}_{2,1} + u_{3,1}\bar{e}_3 + u_3 \bar{e}_{3,1})\}$$

$$\gamma_{11} = a_1(1 + y_3/R_1)\bar{e}_1 \cdot \{(u_{1,1} + u_2 \tfrac{a_{1,2}}{a_2} + u_3 \tfrac{a_1}{R_1})\bar{e}_1 +$$
$$(u_{2,1} - u_1 \tfrac{a_{1,2}}{a_2})\bar{e}_2 +$$
$$(u_{3,1} - u_1 \tfrac{a_1}{R_1})\bar{e}_3\} +$$
$$\tfrac{1}{2}\{[(u_{1,1} + u_2 \tfrac{a_{1,2}}{a_2} + u_3 \tfrac{a_1}{R_1})\bar{e}_1 + (u_{2,1} - \tfrac{u_1 a_{1,2}}{a_2})\bar{e}_2 + (u_{3,1} - u_1 \tfrac{a_1}{R_1})\bar{e}_3] \cdot \qquad \text{(I.2)}$$
$$[(u_{1,1} + u_2 \tfrac{a_{1,2}}{a_2} + u_3 \tfrac{a_1}{R_1})\bar{e}_1 + (u_{2,1} - \tfrac{u_1 a_{1,2}}{a_2})\bar{e}_2 + (u_{3,1} - u_1 \tfrac{a_1}{R_1})\bar{e}_3]\}$$

$$\boxed{\gamma_{11} = a_1(1 + y_3/R_1)(u_{1,1} + u_2 \tfrac{a_{1,2}}{a_2} + u_3 \tfrac{a_1}{R_1}) +}$$
$$\boxed{\tfrac{1}{2}\{(u_{1,1} + u_2 \tfrac{a_{1,2}}{a_2} + u_3 \tfrac{a_1}{R_1})^2 + (u_{2,1} - u_1 \tfrac{a_{1,2}}{a_2})^2 + (u_{3,1} - u_1 \tfrac{a_1}{R_1})^2\}} \qquad \text{(I.3)}$$

$$\gamma_{22} = h_2 \bar{e}_2 \cdot (u_{1,2}\bar{e}_1 + u_1 \bar{e}_{1,2} + u_{2,2}\bar{e}_2 + u_2 \bar{e}_{2,2} + u_{3,2}\bar{e}_3 + u_3 \bar{e}_{3,2}) +$$
$$\tfrac{1}{2}\{(u_{1,2}\bar{e}_1 + u_1 \bar{e}_{1,2} + u_{2,2}\bar{e}_2 + u_2 \bar{e}_{2,2} + u_{3,2}\bar{e}_3 + u_3 \bar{e}_{3,2}) \cdot \qquad \text{(I.4)}$$
$$(u_{1,2}\bar{e}_1 + u_1 \bar{e}_{1,2} + u_{2,2}\bar{e}_2 + u_2 \bar{e}_{2,2} + u_{3,2}\bar{e}_3 + u_3 \bar{e}_{3,2})\}$$

$$\gamma_{22} = a_2\left(1 + y_3/R_2\right)\bar{e}_2 \cdot \begin{bmatrix} \left(u_{1,2} - u_2 \frac{a_{2,1}}{a_1}\right)\bar{e}_1 + \\ \left(u_{2,2} + u_1 \frac{a_{2,1}}{a_1} + u_3 \frac{a_2}{R_2}\right)\bar{e}_2 + \\ \left(u_{3,2} - u_2 \frac{a_2}{R_2}\right)\bar{e}_3 \end{bmatrix} +$$

$$\frac{1}{2}\begin{bmatrix} \left(u_{1,2} - u_2 \frac{a_{2,1}}{a_1}\right)\bar{e}_1 + \\ \left(u_{2,2} + u_1 \frac{a_{2,1}}{a_1} + u_3 \frac{a_2}{R_2}\right)\bar{e}_2 + \\ \left(u_{3,2} - u_2 \frac{a_2}{R_2}\right)\bar{e}_3 \end{bmatrix} \cdot \begin{bmatrix} \left(u_{1,2} - u_2 \frac{a_{2,1}}{a_1}\right)\bar{e}_1 + \\ \left(u_{2,2} + u_1 \frac{a_{2,1}}{a_1} + u_3 \frac{a_2}{R_2}\right)\bar{e}_2 + \\ \left(u_{3,2} - u_2 \frac{a_2}{R_2}\right)\bar{e}_3 \end{bmatrix} \qquad \text{(I.5)}$$

$$\boxed{\gamma_{22} = a_2\left(1 + \frac{y_3}{R_2}\right)\left(u_{2,2} + u_1 \frac{a_{2,1}}{a_1} + u_3 \frac{a_2}{R_2}\right) + \frac{1}{2}\left\{\left(u_{1,2} - u_2 \frac{a_{2,1}}{a_1}\right)^2 + \left(u_{2,2} + u_1 \frac{a_{2,1}}{a_1} + u_3 \frac{a_2}{R_2}\right)^2 + \left(u_{3,2} - u_2 \frac{a_2}{R_2}\right)^2\right\}} \qquad \text{(I.6)}$$

$$\gamma_{33} = h_3\bar{e}_3 \cdot \left(u_{1,3}\bar{e}_1 + u_1\bar{e}_{1,3} + u_{2,3}\bar{e}_2 + u_2\bar{e}_{2,3} + u_{3,3}\bar{e}_3 + u_3\bar{e}_{3,3}\right) +$$
$$\frac{1}{2}\left\{\left(u_{1,3}\bar{e}_1 + u_1\bar{e}_{1,3} + u_{2,3}\bar{e}_2 + u_2\bar{e}_{2,3} + u_{3,3}\bar{e}_3 + u_3\bar{e}_{3,3}\right) \cdot \left(u_{1,3}\bar{e}_1 + u_1\bar{e}_{1,3} + u_{2,3}\bar{e}_2 + u_2\bar{e}_{2,3} + u_{3,3}\bar{e}_3 + u_3\bar{e}_{3,3}\right)\right\} \qquad \text{(I.7)}$$

$$\boxed{\gamma_{33} = u_{3,3} + \frac{1}{2}\left\{u_{1,3}^2 + u_{2,3}^2 + u_{3,3}^2\right\}} \qquad \text{(I.8)}$$

$$
\begin{aligned}
2\gamma_{12} = {} & h_1\bar{e}_1\cdot\left(u_{1,2}\bar{e}_1 + u_1\bar{e}_{1,2} + u_{2,2}\bar{e}_2 + u_2\bar{e}_{2,2} + u_{3,2}\bar{e}_3 + u_3\bar{e}_{3,2}\right) + \\
& h_2\bar{e}_2\left(u_{1,1}\bar{e}_1 + u_1\bar{e}_{1,1} + u_{2,1}\bar{e}_2 + u_2\bar{e}_{2,1} + u_{3,1}\bar{e}_3 + u_3\bar{e}_{3,1}\right) + \\
& \left(u_{1,2}\bar{e}_1 + u_1\bar{e}_{1,2} + u_{2,2}\bar{e}_2 + u_2\bar{e}_{2,2} + u_{3,2}\bar{e}_3 + u_3\bar{e}_{3,2}\right)\cdot \\
& \left(u_{1,1}\bar{e}_1 + u_1\bar{e}_{1,1} + u_{2,1}\bar{e}_2 + u_2\bar{e}_{2,1} + u_{3,1}\bar{e}_3 + u_3\bar{e}_{3,1}\right)
\end{aligned}
\tag{I.9}
$$

$$
\begin{aligned}
2\gamma_{12} = {} & a_1\left(1+y_3/R_1\right)\bar{e}_1\cdot\begin{bmatrix}\left(u_{1,2} - u_2\frac{a_{2,1}}{a_1}\right)\bar{e}_1 + \\ \left(u_{2,2} + u_1\frac{a_{2,1}}{a_1} + u_3\frac{a_2}{R_2}\right)\bar{e}_2 + \\ \left(u_{3,2} - u_2\frac{a_2}{R_2}\right)\bar{e}_3\end{bmatrix} + \\
& a_2\left(1+y_3/R_2\right)\bar{e}_2\cdot\begin{bmatrix}\left(u_{1,1} + u_2\frac{a_{1,2}}{a_2} + u_3\frac{a_1}{R_1}\right)\bar{e}_1 + \\ \left(u_{2,1} - u_1\frac{a_{1,2}}{a_2}\right)\bar{e}_2 + \\ \left(u_{3,1} - u_1\frac{a_1}{R_1}\right)\bar{e}_3\end{bmatrix} + \\
& \begin{bmatrix}\left(u_{1,2} - u_2\frac{a_{2,1}}{a_1}\right)\bar{e}_1 + \\ \left(u_{2,2} + u_1\frac{a_{2,1}}{a_1} + u_3\frac{a_2}{R_2}\right)\bar{e}_2 + \\ \left(u_{3,2} - u_2\frac{a_2}{R_2}\right)\bar{e}_3\end{bmatrix}\cdot\begin{bmatrix}\left(u_{1,1} + u_2\frac{a_{1,2}}{a_2} + u_3\frac{a_1}{R_1}\right)\bar{e}_1 + \\ \left(u_{2,1} - u_1\frac{a_{1,2}}{a_2}\right)\bar{e}_2 + \\ \left(u_{3,1} - u_1\frac{a_1}{R_1}\right)\bar{e}_3\end{bmatrix}
\end{aligned}
\tag{I.10}
$$

$$
\boxed{
\begin{aligned}
2\gamma_{12} = {} & a_1\left(1+y_3/R_1\right)\left(u_{1,2} - u_2\frac{a_{2,1}}{a_1}\right) + \\
& a_2\left(1+y_3/R_2\right)\left(u_{2,1} - u_1\frac{a_{1,2}}{a_2}\right) + \\
& \left(u_{1,2} - u_2\frac{a_{2,1}}{a_1}\right)\left(u_{1,1} + u_2\frac{a_{1,2}}{a_2} + u_3\frac{a_1}{R_1}\right) + \\
& \left(u_{2,2} + u_1\frac{a_{2,1}}{a_1} + u_3\frac{a_2}{R_2}\right)\left(u_{2,1} - u_1\frac{a_{1,2}}{a_2}\right) + \\
& \left(u_{3,2} - u_2\frac{a_2}{R_2}\right)\left(u_{3,1} - u_1\frac{a_1}{R_1}\right)
\end{aligned}
}
\tag{I.11}
$$

$$
\begin{aligned}
2\gamma_{13} = {} & h_1\bar{e}_1\cdot\left(u_{1,3}\bar{e}_1 + u_1\bar{e}_{1,3}^{\,0} + u_{2,3}\bar{e}_2 + u_2\bar{e}_{2,3}^{\,0} + u_{3,3}\bar{e}_3 + u_3\bar{e}_{3,3}^{\,0}\right) + \\
& h_3\bar{e}_3\cdot\left(u_{1,1}\bar{e}_1 + u_1\bar{e}_{1,1} + u_{2,1}\bar{e}_2 + u_2\bar{e}_{2,1} + u_{3,1}\bar{e}_3 + u_3\bar{e}_{3,1}\right) + \\
& \left(u_{1,1}\bar{e}_1 + u_1\bar{e}_{1,1} + u_{2,1}\bar{e}_2 + u_2\bar{e}_{2,1} + u_{3,1}\bar{e}_3 + u_3\bar{e}_{3,1}\right)\cdot \\
& \left(u_{1,3}\bar{e}_1 + u_1\bar{e}_{1,3}^{\,0} + u_{2,3}\bar{e}_2 + u_2\bar{e}_{2,3}^{\,0} + u_{3,3}\bar{e}_3 + u_3\bar{e}_{3,3}^{\,0}\right)
\end{aligned}
\qquad \text{(I.12)}
$$

$$
\begin{aligned}
2\gamma_{13} = {} & a_1\left(1+y_3/R_1\right)\bar{e}_1\cdot\left(u_{1,3}\,\bar{e}_1 + u_{2,3}\,\bar{e}_2 + u_{3,3}\,\bar{e}_3\right) + \\
& \bar{e}_3\cdot\begin{bmatrix}\left(u_{1,1} + u_2\,\frac{a_{1,2}}{a_2} + u_3\,a_1/R_1\right)\bar{e}_1 + \\ \left(u_{2,1} - u_1\,\frac{a_{1,2}}{a_2}\right)\bar{e}_2 + \\ \left(u_{3,1} - u_1\,\frac{a_1}{R_1}\right)\bar{e}_3\end{bmatrix} + \\
& \begin{bmatrix}\left(u_{1,1} + u_2\,\frac{a_{1,2}}{a_2} + u_3\,\frac{a_1}{R_1}\right)\bar{e}_1 + \\ \left(u_{2,1} - u_1\,\frac{a_{1,2}}{a_2}\right)\bar{e}_2 + \\ \left(u_{3,1} - u_1\,\frac{a_1}{R_1}\right)\bar{e}_3\end{bmatrix}\cdot\begin{bmatrix}u_{1,3}\,\bar{e}_1 + \\ u_{2,3}\,\bar{e}_2 + \\ u_{3,3}\,\bar{e}_3\end{bmatrix}
\end{aligned}
\qquad \text{(I.13)}
$$

$$
\boxed{
\begin{aligned}
2\gamma_{13} = {} & a_1\left(1+y_3/R_1\right)u_{1,3} + \left(u_{3,1} - u_1\,\frac{a_1}{R_1}\right) + \\
& u_{1,3}\left(u_{1,1} + u_2\,\frac{a_{1,2}}{a_2} + u_3\,\frac{a_1}{R_1}\right) + \\
& u_{2,3}\left(u_{2,1} - u_1\,\frac{a_{1,2}}{a_2}\right) + \\
& u_{3,3}\left(u_{3,1} - u_1\,\frac{a_1}{R_1}\right)
\end{aligned}
}
\qquad \text{(I.14)}
$$

$$
\begin{aligned}
2\gamma_{23} = {} & h_2\bar{e}_2\cdot\left(u_{1,3}\bar{e}_1 + u_1\bar{e}_{1,3} + u_{2,3}\bar{e}_2 + u_2\bar{e}_{2,3} + u_{3,3}\bar{e}_3 + u_3\bar{e}_{3,3}\right) + \\
& h_3\bar{e}_3\cdot\left(u_{1,2}\bar{e}_1 + u_1\bar{e}_{1,2} + u_{2,2}\bar{e}_2 + u_2\bar{e}_{2,2} + u_{3,2}\bar{e}_3 + u_3\bar{e}_{3,2}\right) + \\
& \left(u_{1,2}\bar{e}_1 + u_1\bar{e}_{1,2} + u_{2,2}\bar{e}_2 + u_2\bar{e}_{2,2} + u_{3,2}\bar{e}_3 + u_3\bar{e}_{3,2}\right)\cdot \\
& \left(u_{1,3}\bar{e}_1 + u_1\bar{e}_{1,3} + u_{2,3}\bar{e}_2 + u_2\bar{e}_{2,3} + u_{3,3}\bar{e}_3 + u_3\bar{e}_{3,3}\right)
\end{aligned}
\tag{I.15}
$$

$$
\begin{aligned}
2\gamma_{23} = {} & a_2\left(1 + y_3/R_2\right)\bar{e}_2\cdot\left(u_{1,3}\bar{e}_1 + u_{2,3}\bar{e}_2 + u_{3,3}\bar{e}_3\right) + \\
& \bar{e}_3\cdot\begin{bmatrix} \left(u_{1,2} - u_2\frac{a_{2,1}}{a_1}\right)\bar{e}_1 + \\ \left(u_{2,2} + u_1\frac{a_{2,1}}{a_1} + u_3\frac{a_2}{R_2}\right)\bar{e}_2 + \\ \left(u_{3,2} - u_2\frac{a_2}{R_2}\right)\bar{e}_3 \end{bmatrix} + \\
& \begin{bmatrix} \left(u_{1,2} - u_2\frac{a_{2,1}}{a_1}\right)\bar{e}_1 + \\ \left(u_{2,2} + u_1\frac{a_{2,1}}{a_1} + u_3\frac{a_2}{R_2}\right)\bar{e}_2 + \\ \left(u_{3,2} - u_2\frac{a_2}{R_2}\right)\bar{e}_3 \end{bmatrix}\cdot\begin{bmatrix} u_{1,3}\bar{e}_1 + \\ u_{2,3}\bar{e}_2 + \\ u_{3,3}\bar{e}_3 \end{bmatrix}
\end{aligned}
\tag{I.16}
$$

$$
\boxed{
\begin{aligned}
2\gamma_{23} = {} & a_2\left(1 + y_3/R_2\right)u_{2,3} + \left(u_{3,2} - u_2\frac{a_2}{R_2}\right) + \\
& u_{1,3}\left(u_{1,2} - u_2\frac{a_{2,1}}{a_1}\right) + \\
& u_{2,3}\left(u_{2,2} + u_1\frac{a_{2,1}}{a_1} + u_3\frac{a_2}{R_2}\right) + \\
& u_{3,3}\left(u_{3,2} - u_2\frac{a_2}{R_2}\right)
\end{aligned}
}
\tag{I.17}
$$

APPENDIX II

The expressions for [L0], [L1], and [L2] are presented here for completeness:

$$L_0 = \begin{bmatrix} \dfrac{(\ )_{,1}}{a_1(1+y_3/R_1)} & \dfrac{a_{1,2}}{a_1 a_2(1+y_3/R_1)} & \dfrac{1}{R_1+y_3} \\ \dfrac{a_{2,1}}{a_1 a_2(1+y_3/R_2)} & \dfrac{(\ )_{,2}}{a_2(1+y_3/R_2)} & \dfrac{1}{R_2+y_3} \\ 0 & 0 & 0 \\ 0 & (\ )_{,3} - \dfrac{1}{R_2+y_3} & \dfrac{(\ )_{,2}}{a_2(1+y_3/R_2)} \\ (\ )_{,3} - \dfrac{1}{R_1+y_3} & 0 & \dfrac{(\ )_{,1}}{a_1(1+y_3/R_1)} \\ \dfrac{(\ )_{,2}}{a_2(1+y_3/R_2)} - \dfrac{a_{1,2}}{a_1 a_2(1+y_3/R_1)} & \dfrac{(\ )_{,1}}{a_1(1+y_3/R_1)} - \dfrac{a_{2,1}}{a_1 a_2(1+y_3/R_2)} & 0 \end{bmatrix} \qquad \text{(II.1)}$$

$$L1 = \begin{bmatrix} \tilde{\ell}_{11} & \tilde{\ell}_{12} & \tilde{\ell}_{13} \\ \tilde{\ell}_{21} & \tilde{\ell}_{22} & \tilde{\ell}_{23} \\ \tilde{\ell}_{31} & \tilde{\ell}_{32} & \tilde{\ell}_{33} \\ \tilde{\ell}_{41} & \tilde{\ell}_{42} & \tilde{\ell}_{43} \\ \tilde{\ell}_{51} & \tilde{\ell}_{52} & \tilde{\ell}_{53} \\ \tilde{\ell}_{61} & \tilde{\ell}_{62} & \tilde{\ell}_{63} \end{bmatrix} \qquad \text{(II.1)}$$

$$L2 = \begin{bmatrix} \hat{\ell}_{11} & \hat{\ell}_{12} & \hat{\ell}_{13} \\ \hat{\ell}_{21} & \hat{\ell}_{22} & \hat{\ell}_{23} \\ \hat{\ell}_{31} & \hat{\ell}_{32} & \hat{\ell}_{33} \\ \hat{\ell}_{41} & \hat{\ell}_{42} & \hat{\ell}_{43} \\ \hat{\ell}_{51} & \hat{\ell}_{52} & \hat{\ell}_{53} \\ \hat{\ell}_{61} & \hat{\ell}_{62} & \hat{\ell}_{63} \end{bmatrix} \qquad \text{(II.2)}$$

$$\tilde{\ell}_{11}=\left\{\frac{1}{2a_1^2(1+y_3/R_1)^2}\left[\left(\tilde{u}_{1,1}+\frac{a_{1,2}}{a_2}\tilde{u}_2+\frac{a_1}{R_1}u_3\right)(\ )_{,1}-\left(\tilde{u}_{2,1}-\frac{a_{1,2}}{a_2}\tilde{u}_1\right)\frac{a_{1,2}}{a_1}+\left(\frac{a_1}{R_1}\tilde{u}_1-u_{3,1}\right)\frac{a_1}{R_1}\right]\right\} \tag{II.3}$$

$$\tilde{\ell}_{21}=\left\{\frac{1}{2a_2^2(1+y_3/R_2)^2}\left[\left(\tilde{u}_{1,2}-\tilde{u}_2\frac{a_{2,1}}{a_1}\right)(\ )_{,2}+\left(\tilde{u}_{2,2}+\frac{a_{2,1}}{a_{11}}\tilde{u}_1+\frac{a_2u_3}{R_2}\right)\right]\right\} \tag{II.4}$$

$$\tilde{\ell}_{31}=\left\{\ \tfrac{1}{2}\ \tilde{u}_{1,3}(\ )_{,3}\right\} \tag{II.5}$$

$$\tilde{\ell}_{41}=\left\{\frac{1}{a_2(1+y_3/R_2)}\left[\left(\tilde{u}_{1,2}-\tilde{u}_2\frac{a_{2,1}}{a_2}\right)(\ )_{,3}\right]\right\} \tag{II.6}$$

$$\tilde{\ell}_{51}=\left\{\frac{1}{a_1(1+y_3/R_1)}\left[\left(\tilde{u}_{1,1}+\frac{a_{1,2}}{a_2}\tilde{u}_2+\frac{a_1}{R_1}u_3\right)(\ )_{,3}\right]\right\} \tag{II.7}$$

$$\tilde{\ell}_{61}=\left\{\frac{1}{a_1a_2(1+y_3/R_1)(1+y_3/R_2)}\left[\left(\tilde{u}_{1,1}+\frac{a_{1,2}}{a_2}\tilde{u}_2+\frac{a_1}{R_1}u_3\right)(\ )_{,2}-\frac{a_{1,2}}{a_2}\left(\tilde{u}_{2,2}+\frac{a_{2,1}}{a_1}\tilde{u}_1+\frac{a_2}{R_2}u_3\right)\right]\right\} \tag{II.8}$$

$$\tilde{\ell}_{12}=\left\{\frac{1}{2a_1^2(1+y_3/R_1)^2}\left[\frac{a_{1,2}}{a_2}\left(\tilde{u}_{1,1}+\frac{a_{1,2}}{a_2}\tilde{u}_2+\frac{a_1}{R_1}u_3\right)+\left(\tilde{u}_{2,1}-\frac{a_{1,2}}{a_2}\tilde{u}_1\right)(\ )_{,1}\right]\right\} \tag{II.9}$$

$$\tilde{\ell}_{22}=\left\{\frac{1}{2a_2^2(1+y_3/R_2)^2}\left[\frac{a_{2,1}}{a_1}\left(\frac{a_{2,1}}{a_1}\tilde{u}_2-\tilde{u}_{1,2}\right)+\left(\tilde{u}_{2,2}+\frac{a_{2,1}}{a_1}\tilde{u}_1+\frac{a_2}{R_2}u_3\right)(\ )_{,2}+\frac{a_2}{R_2}\left(\frac{a_2}{R_2}\tilde{u}_2-u_{3,2}\right)\right]\right\} \tag{II.10}$$

$$\tilde{\ell}_{32}=\left\{\frac{1}{2}\tilde{u}_{2,3}(\ )_{,3}\right\} \tag{II.11}$$

$$\tilde{\ell}_{42}=\left\{\frac{1}{a_2(1+y_3/R_2)}\left[\left(\tilde{u}_{2,2}+\frac{a_{2,1}}{a_1}\tilde{u}_1+\frac{a_2}{R_2}u_3\right)(\ )_{,3}\right]\right\} \tag{II.12}$$

$$\tilde{\ell}_{52}=\left\{\frac{1}{a_1(1+y_3/R_1)}\left[\left(\tilde{u}_{2,1}-\tilde{u}_1\frac{a_{1,2}}{a_2}\right)(\ )_{,3}\right]\right\} \tag{II.13}$$

$$\tilde{\ell}_{62}=\left\{\frac{1}{a_1a_2(1+y_3/R_1)(1+y_3/R_2)}\left[\left(\tilde{u}_{2,2}+\frac{a_{2,1}}{a_1}\tilde{u}_1+\frac{a_2}{R_2}u_3\right)(\ )_{,1}-\frac{a_{2,1}}{a_1}\left(\tilde{u}_{1,1}+\frac{a_{1,2}}{a_2}\tilde{u}_2+\frac{a_1}{R_1}u_3\right)-\frac{a_2}{R_2}\left(u_{3,1}-\frac{a_1}{R_1}\tilde{u}_1\right)\right]\right\} \tag{II.14}$$

$$\tilde{\ell}_{13} = \left\{ \frac{1}{2a_1^2\left(1+y_3/R_1\right)^2} \left[\frac{a_1}{R_1}\left(\tilde{u}_{1,1} + \frac{a_{1,2}}{a_2}\tilde{u}_2 + \frac{a_1}{R_1}u_3\right) + \left(u_{3,1} - \tilde{u}_1\frac{a_1}{R_1}\right)(\ )_{,1} \right] \right\} \tag{II.15}$$

$$\tilde{\ell}_{23} = \left\{ \frac{1}{2a_2^2\left(1+y_3/R_2\right)^2} \left[\frac{a_2}{R_2}\left(\tilde{u}_{2,2} + \frac{a_{2,1}}{a_1}\tilde{u}_1 + \frac{a_2}{R_2}u_3\right) + \left(u_{3,2} - \tilde{u}_2\frac{a_2}{R_2}\right)(\ )_{,2} \right] \right\} \tag{II.16}$$

$$\tilde{\ell}_{33} = \tilde{\ell}_{43} = \tilde{\ell}_{53} = 0 \tag{II.17}$$

$$\tilde{\ell}_{63} = \left\{ \frac{1}{a_1 a_2\left(1+y_3/R_1\right)\left(1+y_3/R_2\right)} \left[\left(u_{3,1} - \tilde{u}_1\frac{a_1}{R_1}\right)(\ )_{,2} \right] \right\} \tag{II.18}$$

$$\hat{\lambda}_{11} = \left\{ \frac{1}{2a_1^2(1+y_3/R_1)^2} \left[\left(\hat{u}_{1,1} + \hat{u}_2 \frac{a_{1,2}}{a_2} \right)( )_{,1} + \frac{a_{1,2}}{a_2} \left(\frac{a_{1,2}}{a_2} \hat{u}_1 - \hat{u}_{2,1} \right) + \left(\frac{a_1}{R_1} \right)^2 \hat{u}_1 \right] \right\} \tag{II.19}$$

$$\hat{\lambda}_{21} = \left\{ \frac{1}{2a_2^2(1+y_3/R_2)^2} \left[\left(\hat{u}_{1,2} - \hat{u}_2 \frac{a_{2,1}}{a_1} \right)( )_{,2} + \frac{a_{2,1}}{a_1} \left(\frac{a_{2,1}}{a_1} \hat{u}_1 + \hat{u}_{2,2} \right) \right] \right\} \tag{II.20}$$

$$\hat{\lambda}_{31} = \left\{ \tfrac{1}{2} \hat{u}_{1,3} ( )_{,3} \right\} \tag{II.21}$$

$$\hat{\lambda}_{41} = \left\{ \frac{1}{a_2(1+y_3/R_2)} \left[\left(\hat{u}_{1,2} - \hat{u}_2 \frac{a_{2,1}}{a_1} \right)( )_{,3} \right] \right\} \tag{II.22}$$

$$\hat{\lambda}_{51} = \left\{ \frac{1}{a_1(1+y_3/R_1)} \left[\left(\hat{u}_{1,1} + \hat{u}_2 \frac{a_{1,2}}{a_2} \right)( )_{,3} \right] \right\} \tag{II.23}$$

$$\hat{\lambda}_{61} = \left\{ \frac{1}{a_1 a_2 (1+y_3/R_1)(1+y_3/R_2)} \left[\left(\hat{u}_{1,1} + \hat{u}_2 \frac{a_{1,2}}{a_2} \right)( )_{,2} - \frac{a_{1,2}}{a_2} \left(\hat{u}_{2,2} + \hat{u}_1 \frac{a_{2,1}}{a_1} \right) \right] \right\} \tag{II.24}$$

$$\hat{\ell}_{12} = \left\{ \frac{1}{2a_1^2(1+y_3/R_1)^2} \left[\frac{a_{1,2}}{a_2} \left(\frac{a_{1,2}}{a_2} \hat{u}_2 + \hat{u}_{1,1} \right) + \left(\hat{u}_{2,1} - \hat{u}_1 \frac{a_{1,2}}{a_2} \right) (\ )_{,1} \right] \right\} \tag{II.25}$$

$$\hat{\ell}_{22} = \left\{ \frac{1}{2a_2^2(1+y_3/R_2)^2} \left[\frac{a_{2,1}}{a_1} \left(\frac{a_{2,1}}{a_1} \hat{u}_2 - u_{1,2} \right) + \left(\hat{u}_{2,2} + \hat{u}_1 \frac{a_{2,1}}{a_1} \right) (\ )_{,2} + \hat{u}_3 \left(\frac{a_2}{R_2} \right)^2 \right] \right\} \tag{II.26}$$

$$\hat{\ell}_{32} = \left\{ \frac{1}{2} \hat{u}_{2,3} (\ )_{,3} \right\} \tag{II.27}$$

$$\hat{\ell}_{42} = \left\{ \frac{1}{a_2(1+y_3/R_2)} \left[\left(\hat{u}_{2,2} + \hat{u}_1 \frac{a_{2,1}}{a_1} \right) (\ )_{,3} \right] \right\} \tag{II.28}$$

$$\hat{\ell}_{52} = \left\{ \frac{1}{a_1(1+y_3/R_1)} \left[\left(\hat{u}_{2,1} - \hat{u}_1 \frac{a_{1,2}}{a_2} \right) (\ )_{,3} \right] \right\} \tag{II.29}$$

$$\hat{\ell}_{62} = \left\{ \frac{1}{a_1 a_2 (1+y_3/R_1)(1+y_3/R_2)} \left[\left(\hat{u}_{2,2} + \hat{u}_1 \frac{a_{2,1}}{a_1} \right) (\ )_{,1} - \frac{a_{2,1}}{a_1} \left(\hat{u}_{1,1} + \hat{u}_2 \frac{a_{1,2}}{a_2} \right) + \hat{u}_1 \frac{a_1 a_2}{R_1 R_2} \right] \right\} \tag{II.30}$$

$$\hat{\ell}_{13} = \left\{ \frac{1}{2a_1^2(1+y_3/R_1)^2} \left[\frac{a_1}{R_1} \left(\hat{u}_{1,11} + \frac{a_{1,2}}{a_2} \hat{u}_2 - \hat{u}_1 (\,)_{,11} \right) \right] \right\} \tag{II.31}$$

$$\hat{\ell}_{23} = \left\{ \frac{1}{2a_2^2(1+y_3/R_2)^2} \left[\frac{a_2}{R_2} \left(\hat{u}_{2,12} + \frac{a_{2,1}}{a_1} \hat{u}_1 - \hat{u}_2 (\,)_{,12} \right) \right] \right\} \tag{II.32}$$

$$\hat{\ell}_{33} = \hat{\ell}_{43} = \hat{\ell}_{53} = 0 \tag{II.33}$$

$$\hat{\ell}_{63} = \left\{ \frac{1}{a_1 a_2 (1+y_3/R_1)(1+y_3/R_2)} \left[-\hat{u}_1 \frac{a_1}{R_1} (\,)_{,12} \right] \right\} \tag{II.34}$$

APPENDIX III

This appendix is devoted to a more detailed description of the element as well as a more thorough discussion of the computer times and techniques used to solve the nonlinear problems.

As discussed in the body of the text, the finite element can be considered to be a quasi-3D element. That is, it consists of a 2-D isoparametric element containing degrees of freedom of u, v, and w at each of its nodes. This 2-D element is used to discretize the reference surface. The effects of the deformations through the thickness are accounted for by including rotational degrees of freedom at the reference surface, the outer surface of the structure, and at each of the interlaminar boundaries. This leads to an element which has 2M+5 degrees of freedom per node as can be seen in Fig. 42.

The test problems discussed in Chapter IV were solved on the CDC CYBER 175. Each of the nonlinear problems presented were solved by using the Newton-Raphson method. This was accomplished by an incremental load method followed by the Newton-Raphson iteration between each load level to obtain equilibrium. This incremental-iterative technique was used mainly so that the solution process

$$\theta_{ij} = \frac{\partial \hat{v}}{\partial z} \quad \text{(ith node; jth interface)}$$

$$\phi_{ij} = \frac{\partial \hat{u}}{\partial z} \quad \text{(ith node; jth interface)}$$

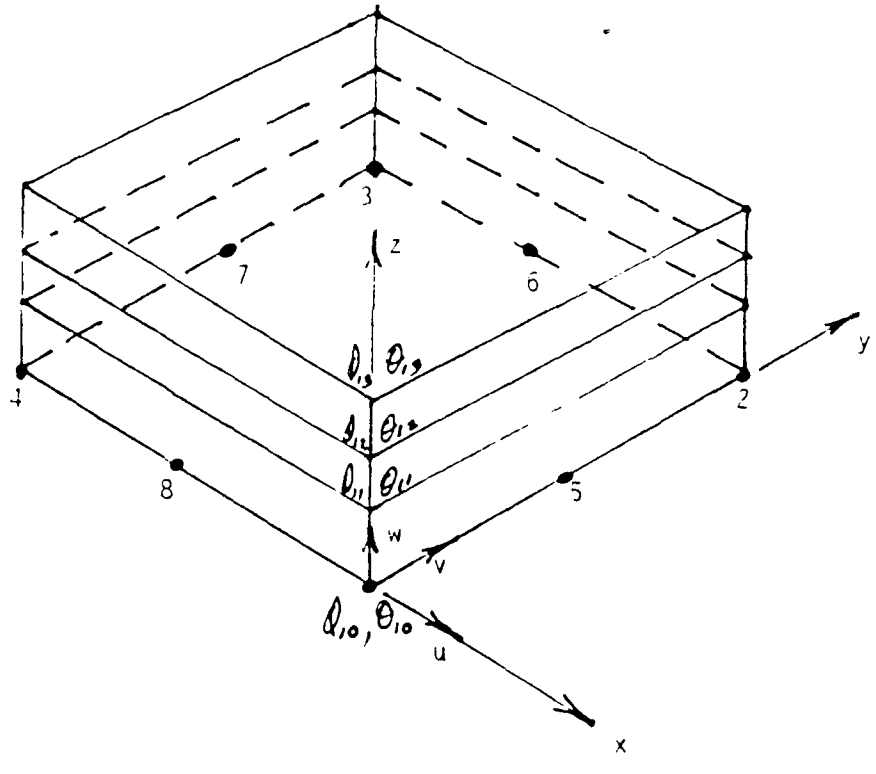

Fig.42 8-noded Finite Element

could be observed and the plots generated.

The solutions were generated by first solving the linear problem, i.e. using [K0] terms only. The load was then incremented by the amount which is indicated by the graphical symbols of Figs. 36 and 39. For Pagano's problem using a (0,0) ply lay-up, the incremental load factor was 25. For the same problem but with a (0,90) ply lay-up, the incremental load factor was chosen to be 10. The incremental load factor used in Chia's problem was chosen to be 50. These choices were made based on observation of the linear solution at the maximum load level desired and selected so as to give favorable graphical points for the curves.

To illustrate the rate of convergence of the solutions for each of the load levels, Table III.1 is presented. This table shows how the solution progressed for Pagano's (0,0) ply lay-up problem. Note that the inclusion of the full nonlinear stiffness matrix terms [K2] did not result in a drastic increase in the number of iterations required to reach equillibrium at each load level. There was only a nominal increase. These solutions were obtained in nearly the same computer time as well. The [K1] solution was obtained in 1085 CP seconds while the [K2] solution was obtained in 1107 CP seconds.

TABLE III.1

Comparison of Iterations Required for Convergence

Load Level	Using [K1]	Using [K2]
25	8	8
50	12	10
75	14	12
100	16	14
125	17	18
150	21	22
175	24	25
200	26	27

The convergence criteria which was used to determine equilibrium was suggested by Zienkiewicz (48). Iteration was continued until the norm of the force imbalance vector was less than some tolerance times the maximum observed norm for previous iterations. For the nonlinear problems shown in this work, the tolerance was set at .0001.

Table III.2 shows the progression of the solution for Chia's problem. Again, there was no large increase in computer resources required to include the [K2] terms. The [K1] solution (which was solved to a load level of 200) was obtained using 62 CP seconds while the [K2] solution (which was solved to a load level of 300) was obtained using 318 CP seconds.

Since Pagano's problems were worked using 5 8-noded elements (2x2 integration) and Chia-s problem was worked using 16 4-noded elements (1x1 integration), one readily observes (from the computer time required for the solutions) the savings which was realized by using the 4-noded elements with 1x1 integration.

TABLE III.2

Comparison of Iterations Required for Convergence

Load Level	Using [K1]	Using [K2]
50	4	5
100	9	11
150	13	17
200	20	27
250	-	44
300	-	68

VITA

Ronald L Hinrichsen was born on 6 June 1949 at Great Falls, Montana. He graduated from C.M. Russell High School in Great Falls in 1967. He enlisted in the Air Force in 1969 and worked as a Minuteman Missile Mechanic at Ellsworth AFB, South Dakota. In June 1973, he was accepted into the Airman Education and Commissioning Program, and attended the University of Arizona in Tucson, where he graduated with high distinction with a B.S. in Aeronautical Engineering in 1975. Following attendance at Officer Training School at Lackland AFB, Texas, he was stationed at Lowry AFB, Colorado where he served as a data analyst for the Foreign Technology Division. In June 1979 he came to the Air Force Institute of Technology to pursue a M.S. Degree in Aerospace Engineering.

He married Miss Kay Lynn Smith in 1967 and they have six children Peter, Renae, Kristen, Ronald, Jarrod, and Heather.

UNCLASSIFIED

SECURITY CLASSIFICATION OF THIS PAGE

REPORT DOCUMENTATION PAGE

1a. REPORT SECURITY CLASSIFICATION: UNCLASSIFIED	1b. RESTRICTIVE MARKINGS
2a. SECURITY CLASSIFICATION AUTHORITY	3. DISTRIBUTION/AVAILABILITY OF REPORT: Approved for public release; distribution unlimited.
2b. DECLASSIFICATION/DOWNGRADING SCHEDULE	
4. PERFORMING ORGANIZATION REPORT NUMBER(S): AFIT/DS/AE/84-2	5. MONITORING ORGANIZATION REPORT NUMBER(S)
6a. NAME OF PERFORMING ORGANIZATION: School of Engineering; 6b. OFFICE SYMBOL (If applicable): AFIT/ENY	7a. NAME OF MONITORING ORGANIZATION
6c. ADDRESS (City, State and ZIP Code): Air Force Institute of Technology, Wright-Patterson AFB, Ohio 45433	7b. ADDRESS (City, State and ZIP Code)
8a. NAME OF FUNDING/SPONSORING ORGANIZATION; 8b. OFFICE SYMBOL (If applicable)	9. PROCUREMENT INSTRUMENT IDENTIFICATION NUMBER
8c. ADDRESS (City, State and ZIP Code)	10. SOURCE OF FUNDING NOS. — PROGRAM ELEMENT NO.; PROJECT NO.; TASK NO.; WORK UNIT NO.
11. TITLE (Include Security Classification): See Box 19	
12. PERSONAL AUTHOR(S): Ronald L. Hinrichsen, M.S., Capt., USAF	
13a. TYPE OF REPORT: PhD Dissertation; 13b. TIME COVERED: FROM _____ TO _____; 14. DATE OF REPORT (Yr., Mo., Day): 1984, September; 15. PAGE COUNT: 156	
16. SUPPLEMENTARY NOTATION	

17. COSATI CODES		
FIELD	GROUP	SUB. GR.
11	04	

18. SUBJECT TERMS (Continue on reverse if necessary and identify by block number): Finite Element Analysis; Composite Materials; Laminates; Cubic Spline Technique; Nonlinear Analysis

19. ABSTRACT (Continue on reverse if necessary and identify by block number)

Title: THE NONLINEAR ANALYSIS OF THICK COMPOSITE PLATES USING A CUBIC SPLINE FUNCTION

Dissertation Chairman: Anthony N. Palazotto
Professor of Aeronautical Engineering

Approved for public release: IAW AFR 190-17

[illegible]
Dean for Research and Professional Development
Air Force Institute of Technology (AU)
Wright-Patterson AFB OH 45433

20. DISTRIBUTION/AVAILABILITY OF ABSTRACT	21. ABSTRACT SECURITY CLASSIFICATION
UNCLASSIFIED/UNLIMITED ☒ SAME AS RPT. ☐ OTIC USERS ☐	UNCLASSIFIED

22a. NAME OF RESPONSIBLE INDIVIDUAL	22b. TELEPHONE NUMBER (Include Area Code)	22c. OFFICE SYMBOL
Anthony N. Palazotto	513-255-2998	AFIT/ENY

DD FORM 1473, 83 APR — EDITION OF 1 JAN 73 IS OBSOLETE.

UNCLASSIFIED

SECURITY CLASSIFICATION OF THIS PAGE

ABSTRACT

A non-linear thick composite shell theory is presented in which the through-the-thickness displacements are modelled using a variation of a cubic spline. The theory is developed by considering the Lagrangian strains in conjunction with the 2nd Piola-Kirchhoff stress. This formulation leads to a theory which encompasses large displacements with moderately large rotations but is restricted to small strains. The imposition of the cubic distribution through-the-thickness insures that the compatability of the displacements and their first and second derivatives and thus the shear strains are maintained from lamina to lamina. The cubic distribution is seen as a higher order approximation than has been previously employed, but because of the nature of the spline, the theory is less cumbersome and more easily implemented than the parabolic theory. In addition, there is no introduction of additional degrees of freedom with the cubic theory. A family of 2-D isoparametric elements is employed in conjunction with the theory to solve a class of 3-D thick plate problems. Results are presented showing comparisons which are in good agreement with previous work.

END

FILMED

5-85

DTIC